Functionalization and Characterization of Magnetic Nanoparticles for Biomedical Applications

Dissertation zur Erlangung des Grades
"Doktor der Naturwissenschaften"

im Fachbereich Chemie, Pharmazie und Geowissenschaften
der Johannes Gutenberg-Universität Mainz
vorgelegt von

Kerstin Koll (geb. Schneider)
geboren in Mainz

Mainz, 2011

Dekan: [redacted]
Erster Berichterstatter: [redacted]
Zweiter Berichterstatter: [redacted]
Datum der mündlichen Prüfung:

Erklärung

Die vorliegende Arbeit wurde in der Zeit von Juli 2008 bis Mai 2011 unter Anleitung von [redacted] an der Johannes-Gutenberg-Universität Mainz, Institut für anorganische Chemie und analytische Chemie angefertigt.

Ich erkläre hiermit, dass ich die vorliegende Arbeit selbständig und ohne fremde Hilfe verfasst habe. Alle verwendeten Quellen und Hilfsmittel sind vollständig angegeben.

Mainz, im Mai 2011

Für meine Mutter

Acknowledgments

During three years of working for a PhD thesis, the number of people that will influence the final product are immense. While some will help on the professional level by discussing and re-discussing results, others are part of this grand undertaking by listening when times are not as rosy.

I sincerely thank [redacted] for giving me the opportunity of working on such an interesting field of research. For allowing me to introduce a little bit of Bio into the Inorganic world of his lab. For letting me work on my pace and finally to allow me to travel the world, broadening my mind.

[redacted] jumped right into the idea of becoming my second advisor and for that I am thankful. During different meetings, he was never short of new ideas.

[redacted] was not only the first person who agreed to be part of my PhD defense committee, she also sat through one hour of my PI defense. I am aware that quite a lot of Bio was present. My gratitutes for this great new ideas and insides.

I would also like to thank [redacted] for being on my PhD defence committee.

Already during my Diplomathesis, [redacted] was a great and inspiring source for new ideas. During my PI defense he did not only offer his knowledge, but further he offered his lab in order to help with the scFvp53 project. Thank you for the opportunity to come back to the [redacted]-Group.

During my PhD thesis, I had the opportunity to stay in Toledo, OH, for three months. During this time, [redacted] helped me not only with starting the expression of scFvp53. He also made sure that I did not run out of microbiology practice. Thank you for letting me be in your team once again.

In this context I absolutely have to thank [redacted] and, of course, [redacted] for making sure to never ever have a boring weekend during my stay in Toledo. The final weekend is still the memory I keep dear. Although I have to say that not waking up with a cat trying to catch my feet with

its claws is kind of refreshing.

We had our discrepancies, but without the help of [redacted], the cell lab would not shine in its momentory glory. So thanks for all the benefitial tipps.

[redacted], well, what can I say. Thanks for showing the biologist all the work you can do using a Schlenk line. Thanks for letting me be a part of your research. Thanks for listening to all my whining. Thanks for being such a great collegue and even better friend. You provided me with so much more than just nanoparticles.

[redacted], thank you for great team work, for showing me the necessary twist in my thesis and for stopping me, when necessary.

I would also like to thank [redacted] for its work, thank you **(President)** [redacted] for sharing the bench (and restocking all the things I broke). Further I would like to thank all members of the Bio-Nano small group and especially [redacted] and [redacted]. Are there any nanoparticles left?

I have once been told that my typing is rather loud, so sorry again. Thanks all members of the old office team for still being able to finish their work. And thanks to the new office team for all the great new ideas. I specially thank [redacted] and **(**[redacted]**)** [redacted] for readily taking up the new office responsibility team.

A huge thank you goes to the TEX-Team [redacted] and possibly the greatest thanks goes to [redacted] (who is going to kill me now...) who sat with me during hours of utter frustration when the references would not want to be accepted by this loverly program.

Further, I thank [redacted] and [redacted] for all their help in the cell-lab. I hope you will have just as inspiring results in there as I had. I also thank all collaborators who helped my with my thesis.

I promised her a long thank you, well, here it comes: [redacted], you have helped me tremendously with my work at the scFvp53. You did not only bring in new ideas,

you further answered my mails full of questions promptly and always with good ideas. You always had great and awesome storys on hold and made sure I never got bored. Thank you!

I would also like to take this opportunity to thank the Birkel-Sisters [redacted] for being such good friends, for all the lovely discussions at the evenings and weekends and for organizing all the fun stuff. Thanks for organizing our talks and for letting us stay on your couch!

"Zwei Dinge sollte ein Kind von seinen Eltern bekommen: Wurzeln und Flügel!" (J.W. Goethe). I thank my family for their support during these three years. I am aware that it was not always easy to be around. But still, you were there to help me every step of the way. Thank you for grounding me when I needed it (just remeber my first day at the university) and for giving me wings to follow my dreams. Thank you [redacted]

Finally, all my thanks go to [redacted]. Thank you for being there for me!

Abstract

Abstract in english:

This thesis addresses, describes and discusses the surface functionalization of MnO nanoparticles (NPs) to enhance their solubility and their applicability as MRI contrast agents. Thereby, different polymers were modified and tested. Briefly, silica coating will further be discussed. It will be proven that the introduction of poly (ethylene glycol) (PEG) into the originally used backbone polymer will enhance the stability of the MnO NPs in body fluids as well as it will greatly improve the applicability of sterile filtration. Different strategies were then applied in order to estimate the concentration of bound bioactive groups to the surface these NPs. Therefore, different techniques such as SDS-PAGE, Bradford assay, Northern- and Western blot as well as different fluorescence measurements will be addressed. Extensive in vitro assays of those and additional NPs will show that MnO NPs feature low toxicity when tested on Caki1 and HeLa cells and do not enhance or lower cell proliferation. Different cupper oxide NPs thereby clearly showed toxic behavior. Further, the binding of a fluorescent dye, protoporphyrin IX, to PEG was achieved and such functionalized MnO NPs could be successfully used as contrasting agents for MRI and additionally showed promising results when tested for their applicability for the photodynamic therapy. Finally, the synthesis of an antibody against p53 will be discussed. This antibody therefore was designed in such a way that it can be further applied to the surface of MnO NPs.

Auszug in deutscher Sprache:

Die vorliegende Arbeit beschäftigt sich mit der Oberflächenfunktionalisierung von MnO Nanopartikeln (NP). Durch die Verwendung und Verbesserung verschiedener Polymere durch die Einbindung von Poly (Ethylen Glycol) (PEG), gelang es, die Löslichkeit dieser Nanopartikel in wässrigen Lösungen sowie in Körperflüssigkeiten zu erhöhen. Zusätzlich konnten diese Nanopartikel deutlich besser steril filtriert werden und zeigten eine erhöhte Aktivität als Kontrastmittel im MRT. Vorläufige Ergebnisse für die Verwendung von Silika als Schutzhülle für MnO NP werden ebenfalls kurz erläutert. Die verwendeten Polymere besaßen dabei zugängliche Aminogruppen, die eine weitere Funktionalisierung durch Bio-aktiver Gruppen ermöglichte. Der Nachweis einer erfolgreichen Bindung durch verschiedene Methoden wie SDS-PAGE, Western- und Northern Blot sowie die Verwendung unterschiedlicher Fluoreszenz-Messungen wird ebenfalls diskutiert. MnO NP und anderer magnetischer NP werden weiterhin auf ihr toxisches Verhalten gegenüber Caki1 und HeLa Zellen getestet. Dabei zeigte sich, dass MnO NP, im Gegensatz zu einigen Kupferoxiden, quasi nicht toxisch waren und das Proliferationsverhalten dieser Zellen quasi nicht beeinflussten. Weiterhin wurde ein Fluoreszenzfarbstoff, konkret Protoporphyrin IX, an die Oberfläche von MnO NP angebracht. Diese konnten dann erfolgreich als Kontrastmittel in der MRT verwendet werden und zeigten vielversprechende Ergebnisse für die Photodynamische Therapie. Desweiteren wird die Synthese des Antikörpers gegen p53 ausführlich erläutert. Dabei wurde genau darauf geachtet, dass dieser Antikörper dann an MnO NP gebunden werden kann.

Contents

List of Figures

List of Tables

CHAPTER 1

Applications of nanoparticles in medicine, an introduction

The human body is remarkable. The skeletal enables us to walk, jump, or cary heavy items. Different organs allow the uptake of nutritients, sort out necessary minerals from those which are not needed anymore. Small nerves within the body are connected to the central control organ, the brain, giving warning signs such as goose bumps when it gets too cold, or enables sweating when the temperature is too high. Every day, the complete blood volume will pass the kidneys roughly 300 times in order to clean it. We breathe approximatly 10-15 times a minute, blink even more often. [1] Our brain catalogues every image, sound, touch or smell, deciding within seconds if this is a necesarry information or if it can be deleted. Our heart beats sometimes faster for no appearend reason. And all of this happens, mostly without our active control. And usually, the every day mechanisms work without any side effects. The human body, or more precisely each human cell, checks and double checks itself and neighbouring cells for any wrong doing. Cells of the immune system circle the human body, helping to clear everything that is non-self or help destroy cells which do not work like they are supposed to. And still, sometimes one small step might go wrong, one protein within the cell might lose its function or might be expressed in such quantities, that it works just too well. Usually, these cells have lost the ability to undergo apoptosis and they will continue to split, grow and grow without reacting to the stop signals of their healthy neighbours. Cancer has evolved. Since these cells are not regognized by the immune system, their growth is not inhibited and will finally lead to the death of the host system. [2]

Numerous methods are known today to fight cancer. The four dominant are chemotherapy, photodynamic therapy, radiation and surgery. [3] The problem which arises is that the immune system of the host usually does not help to fight this desease. In addition, in some cases, the time of when cancer is regognized might be too late for an efficient therapy. Cancer tissue is prone to form metastases, thereby spreading throughout the whole system. Finally, drugs used against cancer usually attack all rapid growing tissues, resulting in loss of hair and immuno efficiency. The prospect of today is the application of intelligent transport vehicles which transport the drug to the target tissue without harming non cancerous organs of the patient.

Examples for such vehicles are nanoparticles (NPs). Already in the 70's, Ringsdorf proposed that the development of those will be a very benefitial tool to fight cancer. [4, 5] Usually, the term nanoparticle desribes organic or inorganic particles with the size-range of 5-100 nm. This particlular size is generally accepted, since nanoparticles smaller than 5 nm will be cleared by the renal system too fast to allow a reasonable use as transport vehicles. Nanoparticles which are larger than 200 nm are rapidly attacked by the reticuendothelial system (RES) and will agglomerate within those organs (liver and spleen). [4, 6, 7, 8] The term nanoparticle does not refer to the shape or the chemical nature thereof. [9] In the inorganic world, spheres, rods, flower-like systems and many more are known. [10, 11, 12, 13, 14] The applications of those nanoparticular systems are thereby not concentrated on biomedicine alone. The use as catalysts or mass data storage are just a few examples. [15, 16] The current thesis however, focusses on the use of metal oxide nanoparticles for the use as markers in the biomedical field.

Metal oxide nanoparticles have different magnetical behaviors than the bulk material. This holds especially true for MnO NPs. MnO as bulk material is a typical antiferromagnet. With dicrease in size however, the number of unsaturated surface spins increase in comparison to the overall size of the NP. Other physical properties such as the single-domain limit as well was the superparamagentic limit further contribute to the formation of a superparamagnet. [17] Such materials are of special interest as contrast agents in the magnetic resonance imaging (MRI). This method is a very poweful non-invasive imaging technique which is based on measuring the proton relaxation in an externally applied magnetic field after being excited with a radio frequency pulse. [15] It should be stated here that two different contrasts can be addressed. The T_1 contrast leads to a brightening (positive) in the signal, wherease T_2 leads to darker (negativ) images. So far, Gd^{3+}-complexes are in routine use as T_1 contrasts, wherease iron oxide nanoparticles, so called SPIONS in particular, are used for an increase in the

latter contrast. [15, 18, 19] When this technique was first described in the 1960's, Mn based contrasting agents were tested as well as promising candidates for T_1 contrasting agents. However, due to toxic effects, the idea was abstained from.[20, 21] Recently however, due to the increase in nanotechnology, MnO NPs came again into focus for MRI application. [22, 23, 24]

Nanoparticles have shown very promising results for bio-medical application so far and will possibly play a tremendous role for future applications. This is due to the fact that the surface of those nanoparticles can be modified to fit perfectly for the needs at hand. The obstacle that metal oxide nanoparticles need to be surface protected and altered to allow the use in biomedical applications can be seen as a great benefit and can be used as an advantage. Since these hydrophobic nanoparticles have to be functionalized with a hydrophilic and biocompatible coating, this layer can be chemically designed in such a way that further functionalities are added. There are different techniques that fit the purpose. Either using inorganic coatings such as carbon or silica, or organic coatings such as lipids, proteins or polymers. [15] To address all examples would clearly go beyond the scope of this thesis. Here, the use of polydentate polymers, bi-functional ligands and silica coatings will be discussed.

One of the most applied surface protectors are polymers, poly (ethylene glycol) (PEG) thereby has a exceptional possition due to its non-fouling properties and the fact that drugs, modified with this compound show enhanced body circulation times. [15, 5] PEG was bound to a reactive ester backbone polymer, which additionally featured fluorescent dyes, an anchor group as well as 1,4 diaminobutane. In general, different anchor groups can be used such as carboxylates, phosphates, phosphonates and thiols.[15] The focus of this thesis however, was the use of dopamine (DA) which has gained general attention. The catchol group of this molecule allows very effective binding to the surface of oxides such as Fe_3O_4, γ-Fe_2O_3 or MnO. [25, 26, 27] Generally, when metal oxide nanoparticles are designed, adding of a capping agent within the synthesis solution is of utter importance to hinder agglomerations and to allow growth of single nanoparticular systems. [17] Using ligand exchange techniques, the capping agent was succesfully replaced by the corresponding polymer. Previous studies have shown that the use of a poly-functional polymer is applicable and succesfully stabilizes metal oxide nanoparticles within the aqueous phase. [28, 29, 30]

In additon, a bi-functional ligand was designed using dopamine and PEG. This system was used in order to simplify the general setup and in order to circumvent any cross linking between single nanoparticles. Finally, all results for polymeric functionalized nanoparticles were

compared to those, functionalized with a silica shell. All results will be discussed in **chapter 2**.

Polymers or silica shells further contribute to the functionality of the NPs. By introducing functional groups such as amino- or carboxylic groups, further molecules such as fluorophores, drugs or even other metal oxide NPs can be attached. This makes the applicability of NPs for cancer treatment or treamtent of other fatal diseases so interresting. The polymers which were designed in the course of this thesis all featured amino groups which were oriented on the surface of the final nanoparticles. Using specific coupling reactants, the covalent binding of proteins, RNA and DNA were tested and are addressed in **chapter 3**.

Today, the issue of toxic side effects is observed critically througout the scientific community. Especially, since the development in nanoscience is comparatively fast, scepsis has replaced the initial optimism. TiO_2 NPs for example, are extensively used for tissue engeneering, in cosmetics and sunscreens. However, recent studies have shown that cells do react to these NPs by increased inflammatory responses.[31, 32] Furthermore, a number of studies indicate that iron oxide NPs, which are generally considered to be exceedingly safe, may be responsible for the occureance of artheriosclerosis, rheumatic arthritis or neuroinflammation [6] and are able to bypass the the blood brain barrier (BBB). [9] Since MnO or manganese oxide NPs in general are relatively new in this field, less is known about their effect on the human system. The issue of *in vitro* applicability will be discussed in **chapter 4**.

Nanoparticles in general can be used to deliver numerous drugs to the target site and allow additional tracking *in vivo*. These theranostic nanoparticles can further be used for applications in therapies such as the phytodynamic therapy (PDT). This methods uses the ability of certain fluorescent dyes (so-called photosensitizers), such as protoporphyrin IX, to be excited upon radiation. This excitation can lead directly or indirectly to the formation of reactive oxygen species (ROS) and ultimatively to cell death. In fact, this method showed such promising results that it is in routine clinical use, especially to treat skin cancer. [3, 33] To combine the contrast enhancement of MnO NPs in MRI with photodynamic therapy, a bifunctional ligand consisiting of dopamine and PEG was covalently attached to protoporphyrin IX. Upon ligand exchange of the capping agent of MnO NPs with this polymer, MnO NPs were created which showed promising results in *in vitro* assays for PDT. This issue which will be adressed in **chapter 5**.

Finally, single chains of different antibodies also gained recent attention in the medical appli-

cability of NPs. In numerous publications, it was proven that the protein p53 is overexpressed in numerous cancers. [34, 35, 36] Upon addition of the antibody against p53, the loss of function could be reversed, the tumor did not increase in size or even showed signs of shrinking. [34, 37, 38] In cooperation with the group of assistant Prof. Dr. D. Ronning (Toledo, Ohio), the antibody fragment scFvp53 against p53 was designed exclusively to bind to surface functionalized NPs. A prescission protease cut site and a cystein C-terminus, allowing direct binding to Au@MnO NPs were two features which were introduced into the peptide structure. The synthetic strategies from the DNA level on, together with the isolation and crystallization setups for additional proteins will be discussed in **chapter 6**.

This thesis should show that the synthesis of highly water soluble MnO NPs was achieved by greatly improving the used polymer; that additional biofunctionalization is possible; that MnO NPs show low toxicity even when kept for longer periods of time and that these NPs show promising results as contrasting agents for MRI as well as promising candidates for the photodynamic therapy.

CHAPTER 2

Synthesis of water soluble magnetic nanoparticles and their improvement

2.1 Introduction

Nanotechnology is no longer a phrase that is used in science fiction novels. It has found numerous applications in modern life and more examples are bound to follow. A subgroup thereby is the field of nanomedicine, letting scientists dream of a future without cancer. Nanomedicine combines biology, chemistry, physics and genetics in order to design systems which might work as biosensors, tissue replacements and many more. [8] Nanoparticles (NPs) typically are between 1-100 nm in size and due to their small size, they feature unique physical protperties coupled with a vast surface to volume ratio. [7, 39] This is what makes them so interesting as nanocarriers in particular. The list of examples for NPs in the literature seem to be endless. There are purely organic systems such as liposomes, dendrimers, micelles and microbubbles [39, 8] or a mixture of organic material and inorganic NPs, such as quantum dots. [7, 40, 41]

Magnetic resonance imaging is a powerful non invasive technique that is in routine clinical use for cancer diagnostic. To be able to take images of the human tissue, the magnetic moments of protons are used. Upon applicaton of an external magentic field, the spins of the protons will aligne in plane to the magnetization M_{xy}. When a radio frequency pulse, oriented perpenticual to the magnetic field is now switched on, the spins of the proton flip, standing

perpendicular to the induced magnetic field as well. After being excited into this state, the pulse is again switched off and as a result, the protons will relax into the original direction M_{xy} upon loss of energy. This relaxation can thereby follow one of two possibilities which is dependent on the tissue of the patient. One possibility is that these spins, after being excited into the frequency pulse magentization M_z, release their energy by transferring it to the surrounding enviroment. Therefore, this effect is known as spin-lattice or longitudinal relaxation, also known as T_1 relaxation. The faster this energy transfer can take place, the faster the protons can be excited again. Therefore, the image gets brighter with decreasing T_1 relaxation time.
A second mechanism is referred to as T_2 or transfer relaxation. Directly after the protons are excited, all spins are in phase. With time, a process of dephasing starts, weakening the MRI signal. Therefore, T_2 weighted iamges are also referred to as negative signals. Dephasing can take place when spins interfere with themselves (spin-spin interaction). The typical T_2 relaxation takes place. However, due to imhomogeneities of the magentic field, such a dephasing will always take place. Inhomogeneities can arise friom the magnetic coils of the MRI scanner or from the patient. Therefore, this effect is referred to as $T_2{}^*$ and is always present as background noise. From the start of MRI in the 1960's, different contrasting agents have been tested and have shown promising results. Today, the most used ones are Gd^{3+}-complexes and different iron oxide NPs. [42, 43] Recently, manganese oxides have joint this group.[24, 44] So far, one Mn containing MRI contrast agent has been approved in clinical trials. [18, 15]

Metal oxide NPs are hydrophobic by nature. For the application in living system however, a water soluble form is favored since then the administration and body distribution is significantly enhanced. Further, agglomerations within small confinments such as the venes of a patients needs to be excluded to not risk embolism. [45] To overcome this obstacle, several possibilities have shown promising results in the past. Examples thereby are surface coating with micellar amphipihiles, bifunctional ligands and their cross-linkable variants thereof. [41, 16]. Another possibility is the use of multidentate polymers and silica coatings. [46, 47] The most promising polymer for surface functionalization thereby is the FDA approved poly (ethylene glycol) (PEG). Numerous studies have shown that NPs or drugs functionalized with PEG have prolonged body distribution times and these systems have the ability to circumvent opzonisation; a reaction of the immune system of the host in order to clear the blood from invading pathogens. [48, 39] In order to be able to bind polymeric systems to the surface if NPs, a ligand transfer is necessary, since magnetic NPs usually feature capping agents. [17] The capping agent and the polymer will compete and only the molecule which binds more

strongly to the NP surface will ultimatively suceed. Catechols have proven to be very promising candidates for strong binding, especially since this molecules allows bidental binding. This molecule can further be found naturally in proteins of certain mussels, enabeling the strong binding to, e.g. the ship hull. [15] Therefore, the use as anchor group towards surface modification of MnO NPs was feasible. This chapter will therefore focus on the characteristics of MnO NPs functionalized with three different polymers. First, a backbone polymer was functionalized with dopamine as an anchour group and 1,4 diaminobutane which allows further functionalization. Finally fluorophore nitro-benzoxotriazol (NBD) was attached. This fluorescent molecule can be used to detect NPs *in vitro* and *in vivo*. This polymer was then further attributed with a PEG chain. The chemical and physical properties of MnO NPs functionalized with a bifunctional ligand was further tested. In addition, preliminary results for SiO_2@MnO NPs are given.

2.2 Experimental Section

Materials: MnO nanoparticles were kindly provided by Dr. Thomas D. Schladt. The backbone polymer was kindly provided by Dr. Florian D. Jochum (Group of Prof. Dr. W. Zentel, organische Chemie, Universität Mainz). NBD piperazin was kindly provided by Jugal Kishore.
NBoc-1,4 diamonobutan; *O,O'*-bis(2-aminopropyl) poly - propylene glycol - block - polyethylene glycol - block - poly - propylene glycol 800 (H_2N-PEG-NH_2), triethylamine, di - tert-butyldicarbonat (boc), ethyl ether, dichloromethane (DCM), 3,4 dihydroxycinnmic acid, dicyclohexylcarbodiimide (DCC), HNO_3 and NH_4OH were purchased from Sigma-Aldrich and were used without further purification. 3 - hydroxy - tyramine hydrochloride, dry DMF, trifluoroacteic acid, $NaHCO_3$ and $MgSO_4$ were purchased from Acros. VWR delivered hexane and NaCl, wherease N-hydroxsuccinimide was purchased from Fluka. Chloroform was purchased from Roth and 1,4 dioaxane from Fisher Scientific. HOBt (N-hydroxybenzotriazol) came from IRIS Biotec. McCoys 5A cell culture medium with phenol red, RPMI 1640 cell culture medium without phenol red, non-essential amino acids (NEA), penicillin-streptomycin (PEST), L-gluthamine, fetal bovine serum (FBS), phosphate buffer saline (PBS, 1x), cell counting kit 8 (CCK8), trypsin (0.25% EDTA solution) and trypan blue solution (0.4%) were purchased from Sigma-Aldrich (Germany). Mycokill was provided by PAA, Germany. Lysotracker DND-22 blue was provided by Invitrogen. Human blood serum was kindly provided from Robert Westphal (Group of Prof. Dr. Dietz).
Equipment used: For cell counting, the counting chamber Fuchs Rosenthal was provided from Marienfeld (depth 0.2 mm, area 0.0625 mm^2). All cell works were done under a laminar flow box (HeraSafe class II, Type HS12, Heraeus Germany) and were incubated in a ShelLab incubator (purchased from Novodirekt Germany) at 37 °C, 95 % relative humidity and 5 % CO_2 (Protador E290). Cells were checked regularly using an invers microscope (Motic AE20, magnification 4 x, 10 x, 20 x, 40 x). For vitality measurements, an ELISA reader Titertek Plus MS 212 (ICN, Eschwege, Germany) was used. Atomic absorption measurments were performed on Perkin-Elmer, 5100 ZL. Magnetic resonance imaging was performed using a clinical 3.0 T MRI scanner (Magnetom Trio, Siemens Medical Solutions, Erlangen, Germany) in collaboration with Stefan Weber in the group of Prof. Dr. L. M. Schreiber, medizinische Physik, Universitätsklinik, Mainz. 300 mesh copper grids covered with a carbon film (Science Services) were used for TEM sample preparation and were measured on a Phillips EM 420 equipped with a LaB_6 cathode and an acceleration voltage of 120 kV. The information limit was 0.2 nm. Slow scan CCD-Camera (2k x 2k) was used for documentation. UV-Vis spectra

were measured using a UV-Vis-NIR spectrophotmeter Cary 5G, Varian. Milli-Q with a conductance of 18 MΩ cm^{-1} was genarated using a Millipore Synergy 185 facility with a Simpak 2 0.22μm Millipore Express filter. The dialysis membrane was purchased from Spectrumlabs with a cut-off size of 3500 g/mol. Syringe filters for sterile filtration were purchased from Millipore, using Millex GS 0.22 μm and Millex HA 0.48 μm pore sizes.

Synthesis of Poly1 and PEG-Poly: Both polymers were synthesized generally in the same way. Difference being that for PEG-Poly a PEG group was further introduced. The poly (active ester) poly(pentafluorophenylacrylate) (PFA) was prepared as reported earlier. [**?** 49, 50] GPC analysis of the obtained polymer (THF, light scattering detection) gave:
M_n = 16,390 g mol^{-1}, PDI = 1.39, with an average of 70 repeating units.
For the synthesis of the multifunctional poly(acrylamides), poly(active ester) poly(pentafluorophenylacrylate) (300 mg, 1.26 mmol repeating units) was dissolved in a mixture of 10 mL dry DMF. After that, 3-hydroxytyramine hydrochloride (50 mg, referred to as DA) dissolved in 1 mL DMF and 0.3 mL triethylamine was added and the reaction mixture was stirred for 2 hours at 50 °C under argon. The fluorescence dye NBD was introduced by mixing 6.3 mg NBD-piperazin with 1 ml DMF and 0.3 ml triethylamine and adding this mixture to the polymer solution. Stirring at 50 °C was continued for 2 h before adding NBoc-PEG$_{800}$-NH$_2$ (synthesis described below) by premixing 366 mg of this compound with DMF and triethylamine as described above (only for PEG-Poly, for Poly1 this step was skipped). Again, the solution was stirred at 50 °C for 2 h. In the final step the remaining active ester groups were substituted using an excess of NBoc-1,4-diaminobutan (dissolved in 2 mL dry DMF and 0.3 ml triethylamine) and the solution was stirred overnight at 50 °C. The solution was concentrated to about 2 mL and the polymeric ligand was precipitated by addition of cold ethyl ether. The precipitated polymer was centrifuged and the solvent was decanted. Upon drying, an orange oil was obtained.

Cleavage of the Boc group: The polymer obtained above was dissolved in CH_2Cl_2 (40 mL). After that, trifluoroacetic acid (2.0 mL) was added and the mixture was stirred at room temperature for 2 h. The solution was concentrated to 10 ml and hexane (30 ml) and water (40 ml) were added. After stirring at room temperature for 30 min, the polymer was completely transferred to the aqueous phase. The organic phase was washed twice with water and the combined aqueous phases were concentrated and dialysed against deionized water for 2 days (cellulose bag, MWCO = 3,500). Finally, the water was evaporated and the product was redissolved in chloroform to make a stock solution which was kept at 4 °C. In case of Poly1, the polymer was redissolved in DMF.

Synthesis of Boc protected bis-amine-PEG (NBoc-PEG-NH$_2$): The synthesis was in accor-

dance to [51]. In a typical reaction, a solution of $(boc)_2O$ (0.02 mol) in 30 mL of anhydrous dioxane was added drop wise to a solution of NH_2-PEG-NH_2 (0.1 mol) in 50 mL anhydrous dioxane. The resulting solution was stirred overnight at room temperature. The solvent was evaporated, and the oily product obtained was dissolved in 50 mL of water and extracted using 50 mL of CH_2Cl_2 (three times). The combined organic phases were washed with a concentrated solution of NaCl and dried over anhydrous Na_2SO_4. The resulting organic phase was concentrated by rotary evaporation to produce a viscous, colourless oil. Further purification was achieved by flash chromatography on silica using a CH_2Cl_2 / ethanol mixture (2:1) as eluent.

Synthesis of DA-PEG: The synthesis of DA-PEG was performed in two steps. First one amino group of *O,O'*-bis(2-aminopropyl) polypropylene glycol-block-polyethylene glycol-block-polypropylene glycol 800 (H_2N-PEG-NH_2) was protected by introducing a Boc group, then dopamine (DA) was covalently attached to the PEG-backbone. Finally the protective group was removed to leave DA-PEG-NH_2 which is referred to as DA-PEG. In a typical reaction, 10 mmol of H_2N-PEG-NH_2 was dissolved in 100 mL of dioxan under standard Schlenk conditions. 10 mmol of triethylamine was added and the solution was allowed to stir vigorously for 30 min at room temperature. 10 mmol di-tert-butyl-dicarbonat ($(Boc)_2O$) were dissolved in 50 mL of 1,4-dioxan and added dropwise to the H_2N-PEG-NH_2 solution (at a constant speed of one drop per second). The reaction was allowed to proceed overnight at room temperature under an inert atmosphere. After removal of the solvent the crude product was transferred into dichloromethane. The organic phase was washed three times with aqueous saturated NaCl solution and subsequently dried over $MgSO_4$. Further purification was achieved by flash chromatography using a silica column and a mixture of dichloromethane and ethanol (ratio 2:1) as eluent. Evaporation of the solvent produced a viscous colorless oil. Conjugation of NBoc-PEG-NH_2 to 3,4-dihydroxyhydrocinnamic acid (DA) was performed by a common DCC coupling reaction under inert conditions. First, 3,4-dihydroxyhydrocinnamic acid (5 mmol) and HOBt (5.1 mmol) were dissolved in 10 mL of dry DMF and stirred at room temperature. After 10 minutes DCC (5.1 mmol in 10 mL of dry DMF) was added, and the solution was stirred for another 10 minutes before NHS (5.1 mmol in 10 mL of dry DMF) was added dropwise over a period of 30 minutes. The reaction was continued for 2 hours. The resulting DA-NHS ester was subsequently added to a stirred solution of NBoc-PEG-NH_2 (5 mmol) in 15 mL of dry DMF over a period of 45 minutes. The solution was stirred overnight at room temperature. After removal of the urea side product by filtration, the crude product was transferred to chloroform. The organic solution was extracted several times with a saturated NaCl solution and washed with Milli-Q water. The solvent was evaporated

and the oily residue redissolved in dichloromethane. Cleavage of the BOC protection group was accomplished by addition of trifluoroacetic acid and stirring at room temperature for two hours. After removal of DCM the product was dissolved in 40 mL of chloroform and washed with a saturated aqueous $NaHCO_3$ solution and Milli-Q water. The organic phase was dried over $MgSO_4$ and the solvent removed *in vacuo* to produce a light brown oil.

Functionalization of the MnO NPs:

MnO@Poly1: In a typical reaction, 30 mg MnO nanoparticles were dispersed in 10 ml dry DMF with the help of an ultrasonic bath and under inert conditions. 30 mg Poly1 was added dropwise using a syringe. Upon complete addition, the solution was stirred vigorously at 60 °C over night. Excess polymer was washed off by centrifugation. MnO@Poly1 were dried and weighed. If not stated otherwise, this sample was then redissolved in water with the help of an ultrasonic bath. The concentration was measured using AAS. If not stated otherwise, all concentrations were referred to the Mn concentration as was measured by AAS.

MnO@DA-PEG and MnO@PEG-Poly: In a typical reaction 30 mg MnO NPs were dissolved in 40 mL of chloroform and added dropwise to a solution of 30 mg DA-PEG or PEG-Poly in 40 mL of chloroform under argon. The solution was stirred overnight at room temperature and subsequently concentrated to 10 mL by rotary evaporation. 30 mL hexane and simultaneously 40 mL Milli-Q water were added under vigorous stirring. Stirring was continued for 30 min after hexane and water were added completely. The aqueous phase containing the MnO NPs was separated and the final Mn concentration was estimated by atomic absorption spectroscopy (AAS).

Filtration of MnO-NP and characterization with AAS: MnO nanoparticles functionalized with different polymers in water were applied to syringe filters with different pore sizes (0.22 μm and 0.45 μm) which were prewashed with 1 ml water. After the solution was filtered, the filter was washed again with 0.5 to 1.5 ml of deionized water. Both flow through fractions were combined. In a typical experiment, 50 μl of each sample was mixed with approx. 4 ml deionized water and 5 drops concentrated HNO_3. Each sample was heated to allow short boiling. After the reaction mixture was cooled down, the pH was raised to 1-3 using NH_4OH (usually 3 drops were added). Each sample was backfilled to 5 ml and the Mn amount was measured using AAS (Perkin-Elmer 5100 ZL). After including all dilution steps, the results were compared to the original sample.

Long-term stability of MnO NP in blood serum: MnO nanoparticles functionlized with DA-PEG, Poly1 or PEG-Poly, were transferred to water and were diluted with blood serum. In a typical experiment, the concentration of MnO-NP was set to 25 μg/ml for MnO@DA-PEG and MnO@PEG-Poly and 91.25 μg/ml for MnO@Poly1 by mixing 250 μl blood serum,

MnO NP and water to gain a final volume of 1 ml. A control sample was prepared by mixing blood serum and water in the same ratio. Additionally, a control sample of MnO@Poly1 was made by diluting this sample in water without further adding blood serum (final concentration 91.25 μg/ml). All samples were checked right after mixing, 24 h later and 120 h later. All samples were kept at room temperature without direct sunlight.

Magnetic resonance imaging: MnO@DA-PEG, MnO@PEG-Poly and MnO@Poly1 as well as water as a control were diluted to 100 μg/ml and were directly applied to MRI measurments in collaboration with Stefan Weber (group of Prof. Dr. L. Schreiber, Institut für medizinische Physik, Klinik und Polyklinik für diagnostische und interventionelle Radiologie, Universitätsklinik Mainz). MR signal enhancement effects were measured on a clinical 3.0 T MRI scanner. Signal reception and radio frequency (RF) excitation was performed using a 8-channel knee coil. For the T_1-measurement, a saturation prepared (SR) snapshot fast low angle shot (SR-TurboFLASH) pulse sequence with repetition time (TR) / echo time / flip angle = 3.0 ms/1.5 ms/20° was used with varying saturation times starting from 20 ms up to 8000 ms. For measuring the T_2 relaxation time, a multi-echo spin-echo pulse sequence with a total of 32 echos and TR = 5000 ms was used, the echo time was varied from 7 ms to 224 ms.

Light scattering experiments: All experiments were done in cooperation with Michael Dietzsch (AK-Tremel) and with kind support of Dr. Karl Fischer, group of Prof. Dr. M. Schmidt (Institut für physikalische Chemie, Universität Mainz). Tested were MnO@PEG-Poly and MnO@DA-PEG. Latter once were tested more extensively and therefore the focus will be on these NPs. All MnO NPs were sterile filtered using a syringe filter with a pore size of 0.22 μm and additionally with a pore size of 0,1 μm (33 mm, Millex VV filter). An aqueous solution of MnO@DA-PEG with the Mn concentration of 134.9 μg/ml was dissolved with a 1.5 M NaCl solution to lead to a final Mn concentration of 45 μg/ml and 1 M NaCl, respectively. This was done in order to exclude any electrostatic or interparticular interactions. 2 mL of this solution was placed in a quartz cuvette (Hellma) with an outer diameter of 20 mm. Measurements were done using multi-angle experiments which were meausured at 20^{circ} C, using a light scattering instrument ALV/CGS-8FDLS/SLS 5022F Goniometer, an ALV-7004 correlator, a 200 mW HeNe-laser (λ= 633 nm) and an APD Avalanche Photodioden Detectorsystem. Multi-angle experiments were further characterized at θ= 30, 47, 64, 81, 98, 115, 132 und 149^{circ} testing 5 measurments every 60 sec. Single-angle measurments were cross correlated at θ = 30^{c}irc. All results were evaluated using a biexponentiol fit.

2.3 Results and Discussion

2.3.1 Surface functionalization of MnO nanoparticles using different polymers

Properties of the used polymers: Due to the synthetic route for MnO nanoparticles (MnO NP), the surface was covered with the capping agent, in this case oleic acid. Capping agents are important during the synthesis since they enable the growth of small seeds and circumvent the formation of agglomerates. That this method is justified in order to create monodispers nanoparticles, was proven previously [17]. Helpful for the synthesis procedure, these capping agents now need to be replaced by other ligands that are water soluble. This thesis based on previous work of Dr. Ibrahim M. Shukoor, who used a special polymer to increase the solubility (Poly1). MnO@Poly1 nanoparticles could then be used to further bind bioactive groups (see 3 and [52, 30, 28]). However, during the course of this thesis, major drawbacks became apparant which resulted in first the alteration of polymer and finally to the synthesis of a simplified polymer that served the purpose of solubilization just as fine. Functionalization procedures and different characterizations with MnO nanoparticles, functionalized with one of the three polymers will be described in this chapter. The chemical structures of the polymers used are sketched in figure 2.1.

The first polymer used in this thesis is given in figure 2.1 a. The backbone polymer as provided featured reactive ester groups (underlined in gray). These active groups were reactive towards amino groups and were stepwise replaced by first the nanoparticle anchoring group dopamine (DA) shown in blue. The fluorescence dye NBD (green) was introduced first by creating a NBD-piperazin derivative which then was coupled to the backbone polymer. Finally, 1,4-diaminobutan (orange) was introduced. All steps were done in an one pot synthesis and were mixed at 50-60 $^{\circ}$ C over night. To avoid cross linking reactions, 1,4-diaminobutan featured a BOC protection group on one side which was cleaved after precipitation in ice cold either and resuspension in dichloromethane by adding trifluoroacetic acid. The final product was dried, weighted and kept in DMF or water prior to use. Note that after the final step, all reactive ester trifluoro-toluene groups were replaced by one of the groups described above.

PEG-Poly (figure 2.1 b) was obtained by further introducing polyethylene glycol (PEG) with an approximate molular weight of 800 mg/ml and an approximate chain length of 12-15 repeating units. The general synthetic setup however, was kept. PEG was also introduced with a single BOC protection group which was pre-synthesized. Different amounts of PEG were tested, first being that 1,4-diaminobutane was replaced completely by PEG. However, it was

observed that possibly not all reactive ester groups could be replaced due to steric hindrance. Therefore 25 % PEG (molar ratio compared to a monomer of the backbone polymer) was used. Excess of 1,4-diamonobutan was then added to replace the remaining reactive ester groups.

Finally, the system was simplified by coupling DA with PEG as is sketched in figure 2.1 c.

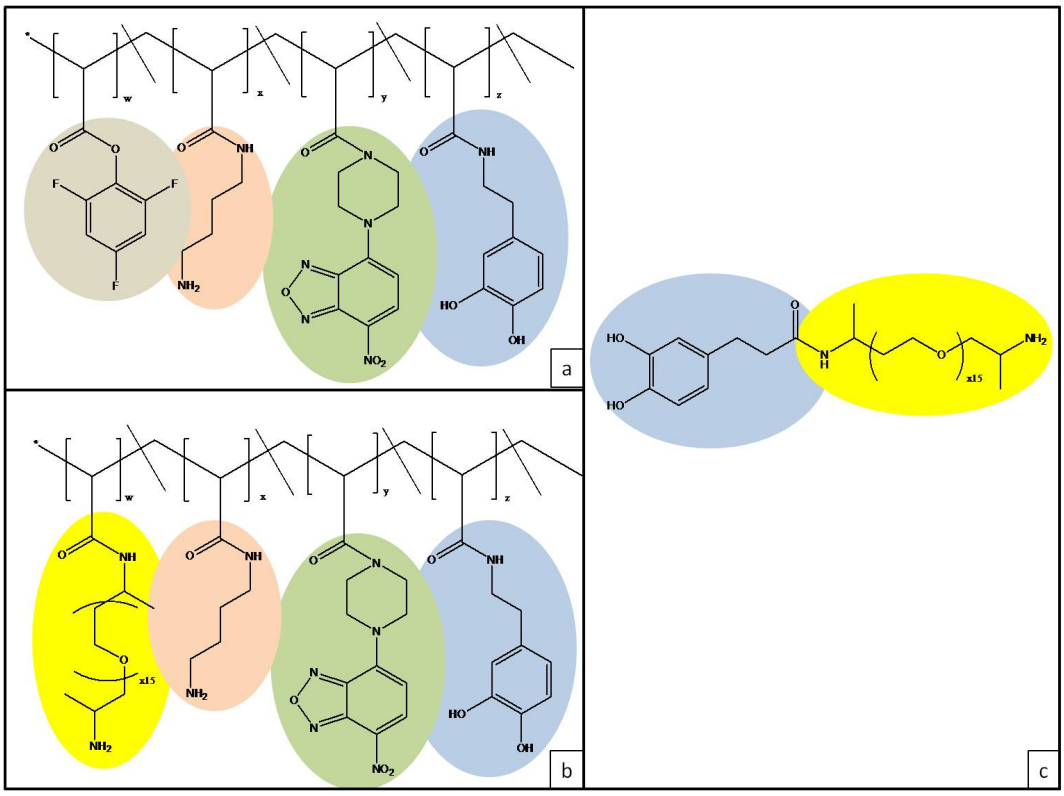

Figure 2.1: **Polymers used for solubilize MnO NP:** Different polymers were used to solubilize magnetic nanoparticles in aqueous solution. a: Poly1, a reactive ester backbone polymer (shown in gray) which was stepwise replaced by the NBD (green), 1.4-diaminobutane (orange) and dopamine (blue). b: PEG-Poly using the same backbone but introducing PEG. c: simplified polymer consisting of the anchoring group dopamine and PEG with chemical accessable amino groups.

The aminogroups were first single protected using BOC. The free amino group was reacted with dicyclohexylcarbodiimid (DCC) and 3,4-dihydroxycinnamic acid, a derivative of DA. As a last step, the Boc group was then again cleaved using trifluoroactic acid.
All polymers and their solubility behavior are described in table 2.1.

Synthetic steps for functionalization: Due to the choice of the capping agent during synthesis, solubility was limited to non-polar solvents such as hexane or chloroform. Poly1 however, was only soluble in polar solvents such as water or DMF. Therefore MnO nanoparticles had

Table 2.1: Polymers with abbreviation used to functionalize MnO nanoparticles

Abbreviation	**Composition**	**Soluble in:**
Poly1	Backbone polymer containing DA, NBD 1,4 diaminobutan	DMF and Water
PEG-Poly	backbone polymer containing DA, NBD, PEG 1,4 diaminobutan	DMF $CHCl_3$ and water
DA-PEG	PEG and DA	water, DMF and $CHCL_3$

to be dispersed in DMF with the help of an ultrasonic bath. Poly1 in DMF (attributed with one drop of water) was added dropwise and the ultrasonic treatment was kept for additional 30 min. Finally, the reaction was stirred at 60 °C over night. The general setup is shown in figure 2.2 a.

When PEG was introduced to the backbone polymer, the resulting PEG-Poly was soluble in chloroform. One monomer of this polymer thereby carried more than one anchoring group which were distributed statistically. To avoid cross linking between single MnO nanoparticles, MnO NPs were added to the polymer rather than the other way around (see figure 2.2 b) by using a dropping funnel. In addition, the concentration of both, polymer and NPs were raised by the factor three. After complete addition, the reaction was stirred over night at room temperature. MnO@PEG-Poly NPs were precipitated with hexane and immediatly redissolved in the same flask by adding water. Due to hexane, the organic phase had a lower density than water. Separation of both phases was achieved by a separatory funnel wiht the organic phase above the water phase(see figure 2.2 c). It can be orbserved that the upper organic phase was colorless, wherease the aqueous phase showed a brown color. AAS measurments as well as TEM confirmed that this phase contained MnO NPs. To allow for better separation between both phases, the aqueous phase was further centrifuged. In all cases, a small pellet was formed which is shown in figure 2.2 d. The origin of this pellet will be discussed later in this chapter. Generally the exact same steps were done when DA-PEG was used. The final product was concentrated to usually 10 ml and the Mn concentration was measured using AAS.

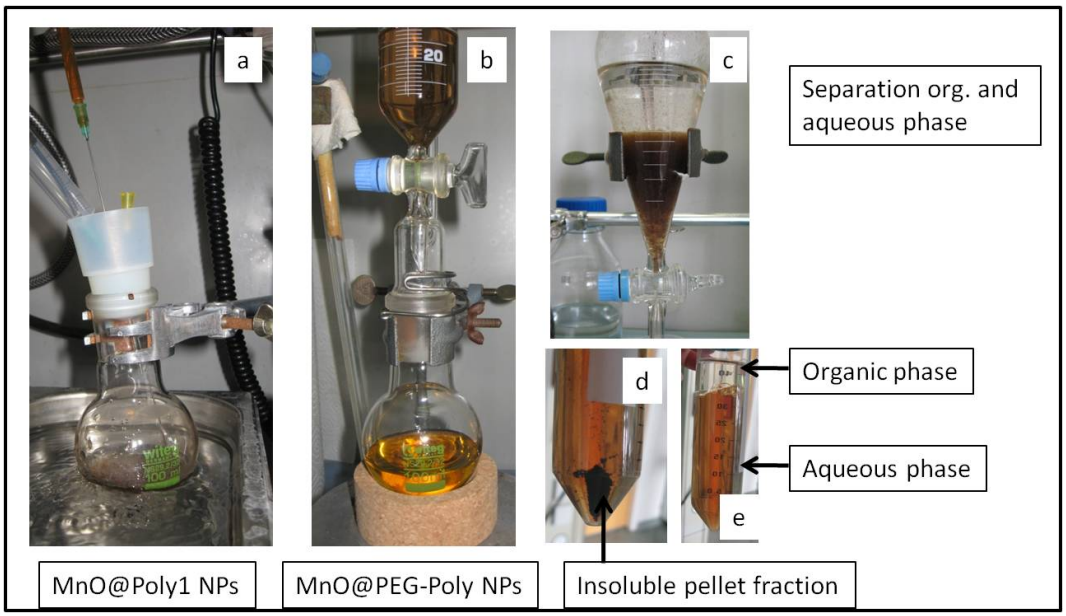

Figure 2.2: **Functionalization setup for MnO NP:** MnO@Poly1 NPs were functionalized by dispersing MnO NPss in an ultrasonic bath (a). Poly1 was added using a syringe. MnO@PEG-Poly and MnO@DA-PEG NPs were synthesized by dropping MnO nanoparticles in $CHCl_3$ to a solution of the corresponding polymer (b). Transfer into the aqueous phase was done by precipitation with hexane and simultaneously adding water (c). The aqueous phase was centrifuged. A small pellet was found (d) but also a colorless organic phase with a brown colored water phase (e).

Sterile filtration applicability: All synthesis steps were done under synthetic lab condition. However, when NPs shall be used for medical purposes, sterility needs to be guaranteed. The easiest method to allow this, is the so called sterile filtration. Fluids are washed through a filter with a defined pore size (e.g. 0.22 μm). Perturbing parts such as bacteria or other parasites are thereby successfully retained in the filter. However, MnO nanoparticles functionalized with different polymers are composite materials and might also be blocked by the filter. To address this issue, different pore sized filters were tested. An aqueous sample of MnO with the corresponding polymer was applied to syringe filter with the pore size of 0.22 μm and 0.45 μm, respectively. The flow through fractions, as well as the original sample, were characterized using atomic absorption spectroscopy (AAS). After including all dilution steps, the final concentration was compared to the original sample and plotted as percent in comparison to the control in figure 2.3 a. MnO NPs were brown in color, a fact that was kept even when surface functionalized using any polymer. Therefore, a visual check of the flow through fraction already gave a hint of the filtration success. In case of MnO@Poly1 NPs, the flow

through was colorless. The nearly complete absence of MnO@Poly1 NPs was confirmed by AAS measurements as is shown in figure 2.3 a. The Mn concetration did not exceed more than 15 % and was independent of the pore size of the used filter. MnO@PEG-Poly NPs on the other han, were only retained to approximatly 6 % compared to the original sample, which was supported by the brown color of the flow through. For MnO@DA-PEG NPs the filter with a pore size of 0.22 μm retained approximately 12 %, wherease the use of the 0.45 μm sized filter showed an increase of approximately 20 % when compared to the original sample. This filter was washed more thoroughly which might be the reason for this outcome. Mistakes in the measurement itself cannot be excluded either.
Due to the successful application of syringe filters, MnO@DA-PEG and MnO@PEG-Poly NP NPs were sterile filtered using a syringe filter with the pore size 0.22 μm prior further use. NPs functionlized with Poly1 were not treated further.

Stability in body fluids: MnO@DA-PEG and MnO@PEG-Poly NPs could be stored in water at 4 °C for months without any agglomeration. However, when particles shall be applied *in vivo*, the stability needs to be confirmed in bodyfluids. Therefore, MnO NPs functionalized with different polymers were incubated with human blood serum and were kept at room temperature for up to 5 days. MnO NPs were diluted in water and 1/4 total volume blood serum. Resulting samples were then photographed and are displayed in figure 2.3 b.
The upper lane shows NPs immediatly after preparation, the following lane shows the same NPs after 24 h and finally after keeping the samples at room temperature for 120 h. MnO@Poly1 NPs without serum (MnO@Poly1-W) immediatly agglomerated, even when freshly prepared. When serum was present (MnO@Poly1), agglomeration occurred within a day. MnO@DA-PEG as well as MnO@PEG-Poly NPs were stable within this time period, independent of whether serum was present or not (latter data not shown). However, every raction tube which contained blood serum, displayed a white precipitate. This observation was made for the control sample as well as samples where blood serum and NPs were co-incubated. Upon loading this precipitate on a 10 % SDS-PAGE, it could be shown that protein degration occured (data not shown).
MnO@PEG-Poly and MnO@DA-PEG NPs were further tested by incubation with FBS, cell media as well different buffers including buffers with a high and a rather low pH. In all cases, the particles were stable throughout the experiment (usually keeping samples at room temperature over night) and no agglomeration occured (data not shown). These results indicate that the use of PEG allows excellent long term stability in different solvents.

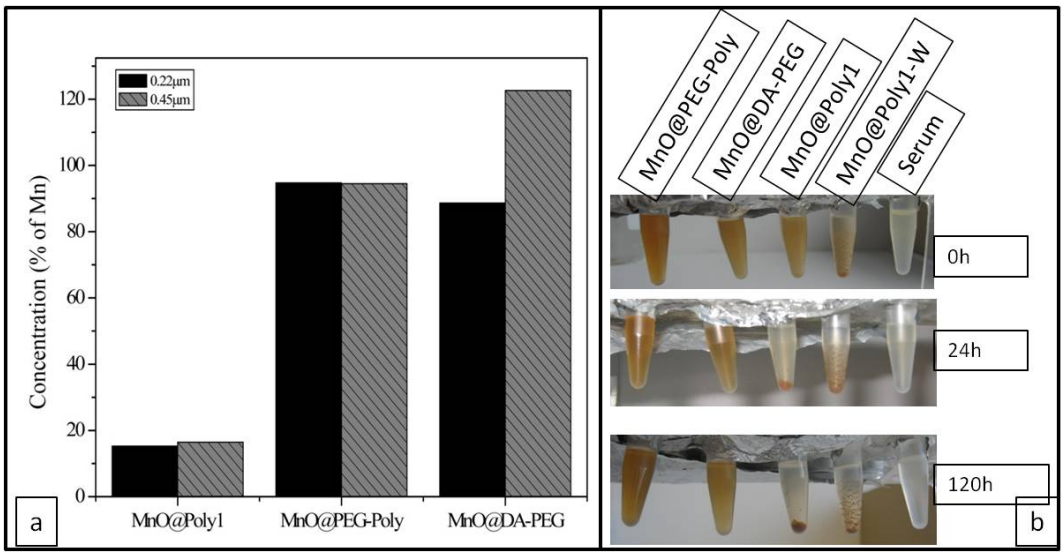

Figure 2.3: **Filtration applicability and long term stability of MnO based nanoparticles:** a: MnO nanoparticles functionlized with the corresponding polymer were filtered using syringe filters with a pore size of 0.22 μm and 0.45 μm, respectively. The flow through was characterized via AAS and the resulting Mn concentration was compared to the original sample before filtration. b: MnO-NP with different polymers were mixed with blood serum and were kept at room temperature for up to 120 h. In addition, serum only and MnO@Poly1 nanoparticles in water (MnO@Poly1-W) were tested.

UV-Vis measurments: MnO nanoparticles functionalized with Poly1 or PEG-Poly were diluted to give a final concentration of 100 μg/ml. Samples were measured between 800 and 260 nm and the results are given in figure 2.4. Both samples show a general increase of the absorption with shorter wavelength which is a general attribute of nanoparticles. For MnO@Poly1 NPs a slight maxima was be observed around 500 nm which is due to bound NBD dye. This maxima was much more pronounced for MnO@PEG-Poly. In addition, a second, much smaller maxima can be seen at around 660 nm. The origin of this peak is unknown. In both cases however, a defined absorption at around 280 , which accounts for the dopamine group, could not be identified.

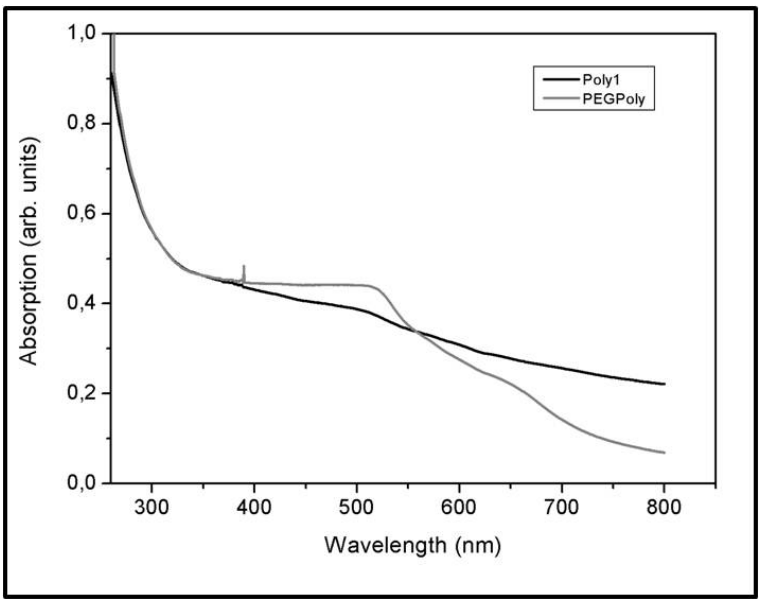

Figure 2.4: **UV-Vis spectra of MnO nanoparticles** functionalized with Poly1 (black) and PEG-Poly (light gray), respectively. All samples were measured in water. Measurments were taken from 800 to 260 nm.

MRI applicability: MnO nanoparticles were tested for their applicability as T_1 contrasting agents in MRI. Therefore, MnO nanoparticles with roughly the same size (8-9 nm MnO core size) were functionalized with Poly1, PEG-Poly and DA-PEG and were diluted with water to a final concentration of 100 μg/ml. Provided in 1.5 ml reaction tubes, these nanoparticles were then measured using a clinical 3 Tesla MRI scanner. The T_1 relaxation times were provided by Stefan Weber (Group of Prof. Dr. L. Schreiber) and are plotted in figure 2.5 b.
Generally, when the T_1 relaxation is measured, tissue with an enhanced T_1 contrast appear brighter in MRI. This also holds true for solutions of T_1 contrasting agents. Images can be taken transversally or saggitally, the latter one meaning horizontally. Figure 2.5 a shows the MnO based samples in both orientations. Generally, these samples either had a round shape or appeared conical which originates from the vessels used. Additionally, MnO@PEG-Poly and MnO@DA-PEG appeared much brighter than MnO@Poly1. Interestingly, although MnO@Poly1 agglomerated during the measurement, the tip of the reaction tube where most of these nanoparticles could be found, did not appear brighter than the supernatant water. For comparison, a sample with water was also applied, however, a difference from the images of water and MnO@Poly1 could not be made. Positiv T_1 contrast can also be shown by the relaxation time. The shorter this time, the better the T_1 contrasting agent. Times were plotted and are displayd in figure 2.5 b. As expected, the T_1 relaxation time was rather short

for MnO@DA-PEG (61.2 ms) and MnO@PEG-Poly (30.8 ms). For MnO@Poly1, this value was 20 times higher than for MnO@DA-PEG (1121.6 ms) but much shorter than water alone (2821.4 ms). A major difference between transversal and saggital measurments could thereby be not observed.

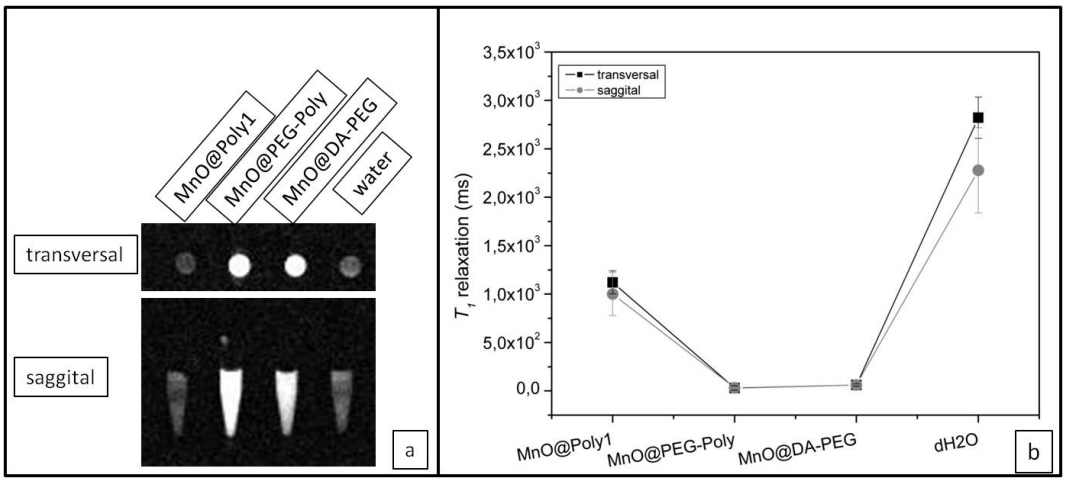

Figure 2.5: T_1 **wheighted MRI images:** MnO NPs were functionalized with either one of the polymers (Poly1, PEG-Poly, DA-PEG) and were diluted to a final concentration of 100 μg/ml with water. The samples were provided in 1.5 ml reaction tubes and were measured on a clinical 3 Tesla MRI scanner. Relaxation times (ms) were then plotted for each sample applied (b). Images of the samples measuring in the transversal and saggital orientation are given in a.

TEM characterization: Transmission electron microscopy is a very helpful technique to characterize inorganic materials. TEM can give insights whether nanoparticles are mono- or polydispers and if agglomeration occurs. Results of MnO nanoparticles functionalized with different polymers are given in figure 2.6. The upper row displays MnO NPs with roughly the same size (core: 8-9 nm) that were functionalized with different polymers. The lower line refers to specially treated nanoparticles and will be described later.
When NPs were functionalized with Poly1, these particles tended to agglomerate with time. Ultrasonification was usually neccesary before further application. The advantage of this system however, was that NPs could be centrifuged and thereby excessive polymer or bioactive groups (see chapter 3) could easily be washed off. However, TEM images revealed, why this agglomeration occurred (see figure 2.6 a). The image shows MnO@Poly1 NPs in DMF. This sample was not transferred to water yet. However, already at this state, single MnO NPs could not be isolated. Rather than this, islands were found, where numerous particles were still

monodisperse themselve but formed bigger agglomerates. This behavior was already seen for MnO NPs dispersed in DMF prior to polymer adding (see figure 2.6 d). When the polymer was extended with PEG (PEG-Poly), a complete different behavior was found (see figure 2.6 b). In this case, MnO@PEG-Poly NPs were stable in water for months when kept at 4 °C. TEM images revealed nicely separated NPs throughout the whole TEM grid. Poly1 could not improve this behavior, since the anchouring DA groups could only access the surface of nanoparticles agglomerates and not each single nanoparticles. When PEG was introduced, the resulting PEG-Poly was soluble in chloroform, as were the MnO NPs which accounts for the excellent monodispers behavior.

When MnO NPs were functionalized with DA-PEG, the same observation as for PEG-Poly was made (see figure 2.6 c). MnO@DA-PEG NPs were nicely separated. And just as the MnO@PEG-Poly NPs, the stability in water was long-termed. Agglomerations that settled at the bottom of the tube were not found.

To confirm this long term stability, MnO@PEG-Poly were kept at 4 °C for 50 days and were then again characterized using TEM. As figure 2.6 e shows, MnO@PEG-Poly NPs were still nicely separated. However, they decreased slightly in size which is in agreement to leaching experiments made for MnO@DA-PEG nanoparticles (unpublished results by Dr. Thomas D. Schladt). Here, MnO@DA-PEG NPs were applied to a dialysis membrane and the amount of Mn^{2+} was measured in certain time intervals for a total of 28 days. The amount of manganese in this sample decreased during this time by roughly 20 $\%$. However, the spherical structure was kept intact.

During the synthesis of MnO@DA-PEG but also MnO@PEG-Poly, NPs were transferred to the aqueous phase by hexane precipitation. During this transfer, a small amount could not be redissolved in water but could be centrifuged or filtered off. This pellet was also applied to TEM and is shown in figure 2.6 f. Au@MnO NPs are exemplarily shown. Small NPs were found in close proximity of denser material which possibly could be attributed to excess of PEG-Poly or DA-PEG polymer. During the synthesis, triple the amount of polymer was used in comparison to MnO NPs. If one calculates the surface atoms of each NP and compares this to the molar amount of polymer, this value is even higher. Different techniques such as dialysis, slow hexane precipitation or different filtration tasks were applied (see also chapter 3. However, a successful separation between unbound and bound polymer was not successful so far. Further titration experiments with less polymer are therefore necessary.

To confirm the monodispersity of MnO@DA-PEG and MnO@PEG-Poly, these NPs were further characterized using dynamic light scattering (DLS), focussing on MnO@DA-PEG. During this curse, measurements showed that the nanoparticles were not as nicely distributed

as TEM images might have revealed. Rather than this, NPs with different hydrodynamic sizes were found, one being roughly 2.5 nm, wherease other NPs showed a hydrodynamic radius of 60 nm. If a closer look is taken at the corresponding TEM images of MnO@DA-PEG NPs, different NPs were found in close proximity to each other(see figure 2.6 c). These NPs might also have formed the polydisperse NPs which could explain the larger NPs found. The concentration of MnO nanoparticles on one grid might have been to low to comfirm the polydispersity. In addition, organic material cannot be observed with TEM, making it impossible to show, if MnO NPs in close proximity to each other where agglomerates with a rather big PEG-Poly or DA-PEG shell, or if their allocation was simply random.The MnO NPs used to functionalized with DA-PEG had an average size of 8 nm. However, as already mentioned, Mn leaking could be obserrved and these NPs shrunk with time. Since MnO@DA-PEG NPs tested with DLS where not freashly prepared, this could explane the samller NPs of 2.5 nm found. If this assumtion us correct, the used polymers improve the solubility but MnO NPs functionalized with thse cannot be stored for a prolonged time.

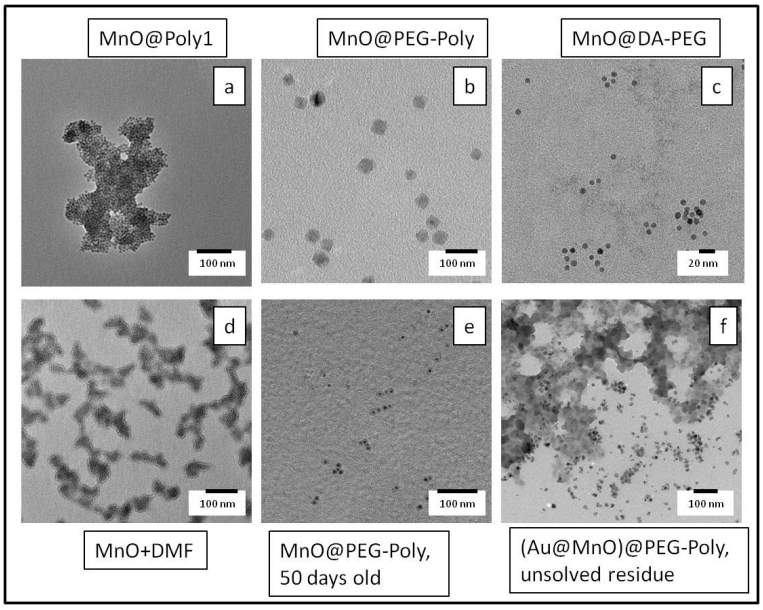

Figure 2.6: **TEM images of MnO NPs:** MnO NPs were dispersed in DMF (d) and functionalized with Poly1 (a). (b) shows the TEM image of MnO NP functionalized with PEG-Poly, whereas (c) shows the image when DA-PEG was used. MnO@PEG-Poly were kept at 4 °C for 50 days (e). Additionally the image of the pellet formed during the synthesis of MnO@DA-PEG and MnO@PEG-Poly, respectively, is shown (f). All samples were prepared by dropping a solution on a TEM grid that was dried at room temperature prior to measurments.

2.3.2 MnO surface functionalization using SiO_2

Without question, the introduction of PEG significantly increased the overall applicability of MnO NPs. PEG improved the short and long-term stability, MRI contrast was enhanced as well as vitality. However, one main obstacle still was present, namely the indication of Mn leaching. To address this issue, MnO NPs were surface protected using a silica shell. Again, numerous tests were done to characterize SiO_2@MnO NPs.

Due to the synthetic procedure, SiO_2@MnO NPs were already provided in an aqueous solution. Thereby, an elaborate transfer to water, as was necessary for MnO@DA-PEG and MnO@PEG-Poly NPs, was redundant. TEM images taken after the synthetic steps show the monodispers behavior of these NPs (see figure 2.7 a), a fact which was confirmed by dynamic light scattering (unpublished results by Heiko Bauer). The average size of a typical SiO_2@MnO NP batch was 12.5 nm and the color was brown. Applicability to steril filtration was thereby only tested visually. Sine flow through sections of SiO_2@MnO NPs after sterile filtration also showed this typical color, no further tests were done. All concentrations described in this chapter are referred to the concentration of Mn in the sample after sterile filtration.

The excellent properties of MnO NPs as T_1 contrast agent thereby were not influenced by

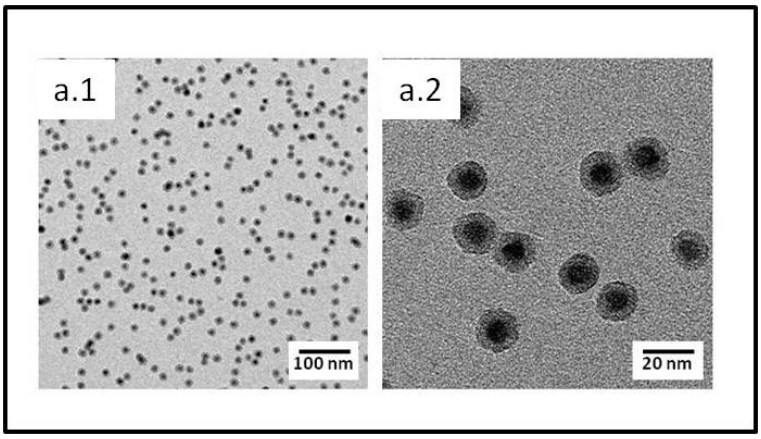

Figure 2.7: **TEM images:** SiO_2@MnO NPs as synthesiszed (a.1) and an enlarged image thereof (a.2).

the silica shell (see figure 2.8 a). Shown are SiO_2@MnO NPs diluted in water and kept in 1.5 ml reaction tubes. Different concentrations in mM Mn were used. It could be observed that with increasing concentration the brightness of the samples increased. These NPs were kept at room temperature and did not show signs of agglomeration. This was further proven by stability assays in blood serum (see figure 2.8 b). As described for MnO NPs functional-

ized with different polymers, a sample was prepared by mixing SiO_2@MnO NPs with human blood serum. During this course, the only precipition observed was white and was seen for all samples were serum was present. This agglomeration was dedicated to protein precipitation which was proven with SDS-PAGE for MnO@DA-PEG samples (see 5, image 2.7 d).
SiO_2@MnO NPs were further mixed with citrate buffer pH 5 and were incubated for one week. After one day however, the low pH of the citrate buffer was sufficient to dissolve the silica shell which protected the MnO cores. The nanoparticles dissolved, which was observed by the diminished color of the sample in comparison to the control sample (see figure 2.8 c). The fact that these NPs are not stable in solutions with a low pH thereby, should not be seen as a disadvantage, since the question of the fate of the MnO nanoparticles *in vivo* arises. If these nanoparticles are unstable at a low pH, they can be degraded by the cell system, e.g. by entering the lysosomes. These cell organelles feature a pH of roughly 5, thereby allowing a way out.
So far, SiO_2@MnO NPs showed very promising results as non-toxic T_1 contrasting agents. Since in this case, a separation between bound and unbound polymer is not necessary, binding of bioactive groups could be thereby greatly improved. However, additional tests are necessary.

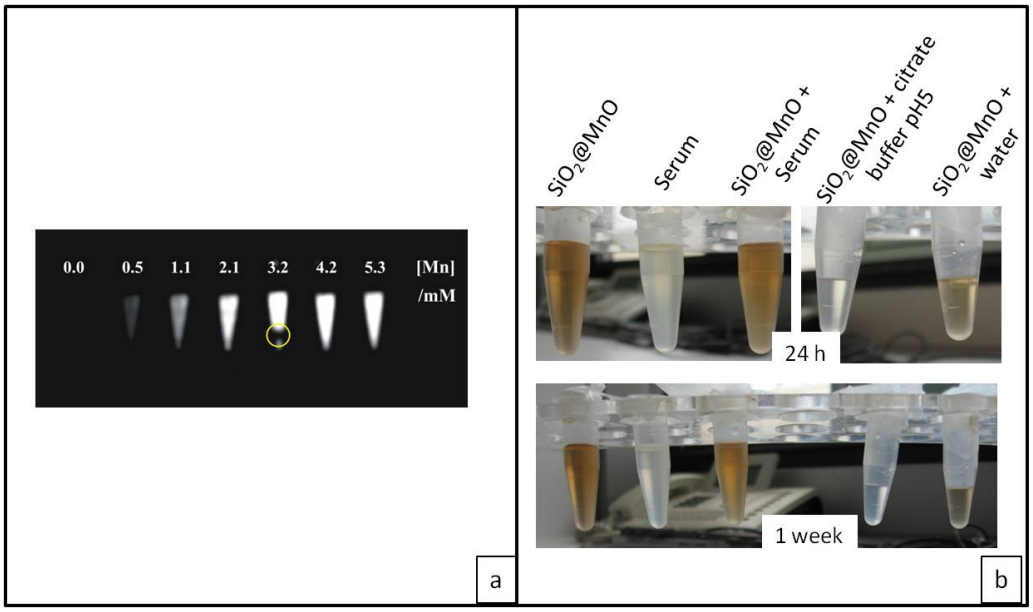

Figure 2.8: **MRI and serum stability of SiO_2@MnO NPs:** Different concentrations of SiO_2@MnO NPs were applied to MRI measurments with T_1 contrast (a). b: Stability of SiO_2@MnO NPs in blood serum after 24 h and one week as well as stability of these NPs in citrate buffer with a pH of 5.

2.4 Summary and Outlook

MnO@Poly1 NPs showed an easy handling when excess polymer should be washed off, since these NPs could be easily centrifuged and resuspended in water or buffer. However, with time, agglomeration occured, making *in vitro* and *in vivo* application difficult. Further, the inabilty in regards to sterile filtration, questiones the use of MnO@Poly1 NPs as *in vivo* contrasting agents. Agglomerations thereby already occurred when MnO NPs were distributed in DMF prior to polymer application and was therefore true throughout the process of MnO@Poly1 synthesis. The agglomerating tendency was greatly improved when an additional group, PEG, was introduced to the backbone polymer. PEG thereby allowed the change of the solvent from DMF to chloroform, thereby making ultrasonic applicatoins redundant. MnO NPs functionalized with PEG-Poly or DA-PEG showed long term stability at 4 °C which was confirmed by TEM. Additionally, this stability was not altered when the temperature was raised or in the presence of blood serum. However, Mn ion leaching was observed by TEM and other techniques, clearly stating that albeit agglomerations do not occur, MnO@DA-PEG and MnO@PEG-Poly NPs cannot be stored for a prolonged time. MnO@DA-PEG as well as MnO@PEG-Poly NPs also shows MRI activity making these NPs suitable as contrasting agents. The only obstacle found is the polydispersity which was confirmed by light scattering but not directly by TEM. Titration experiments with decreased polymer content are therefore necessary to decrease the polymeric content.

MnO NPs were further surface protected using a silica shell. These NPs were not tested extensively but already showed promising results when applied to MRI, TEM and DLS. The long term stability was further guaranteed as was observed when incubated with water or human blood serum and SiO_2@MnO NPs could be dissolved completely at pH 5. It needs to be proven, if stabilization of the silica shell is necessary to allow enhanced stability at lower pH or if these silica coated MnO NPs are able to succesfully transport their target molecule to the site of interest. Currently, numerous tests are done to allow binding of different fluorescence dyes such as FITC and RITC to the SiO_2@MnO NPs. *In vitro* tests are being followed by means of colocalization of NPs and cells using fluorescence microscopy as well as FACS. Finally, it could be shown that mesoporous silica shells are able to incooperate different bioactive groups.[15] Since this shell can be degraded at a low pH, this drug can then be set free once arriving at the target cells. Therefore, such a design is of general interest and is followed momentarily.

CHAPTER 3

Characterization of surface functionalized magnetic nanoparticles

3.1 Introduction

Nanoparticles (NPs) are of special interest for medical applications, since they excibit an increased surface/ weight ratio, can be chemically altered to adress defined issues and further, can be equipped with drugs, making them ideal candidates as drug delivery vehicles. Further, physical, chemical and biological properties can be combined to allow excellent body distribution, enhanced MRI contrast and coupling of molecules which allow targeting of special tissues. [53, 8, 45] After application of NPs *in vivo*, several issues however need to be overcome in order to allow agglomeration at the target site. As a first barrier, host immune system needs to be overcome. In this contest, clearance by opsonization is most inportant barrier. Possibilities to circumvent this, is the size modification of the NPs. A second possibility is the surface modification using different polymers such as PEG. This issue was addressed more extensively in the previous chapter. Once a prolonged body distribution is ensured, NPs need to be carried to their target tissue. Generally, there are two target possibilities. The passive target uses the fact that tumor tissue features leaky capillary endothelium and generally misses a lymphatic drainage. Due to this enhanced permeability and retention (EPR) effect, nutritients but also drugs and NPs agglomerate within these cancer cells. [4, 54] Active targeting refers to NPs equipped with certain biomarkers, which can bind to the surface of cancerous tissue,

allowing a more effective transport. Different examples for such biomarkers, such as carbohydrates, ligands for overexpressed receptors or antibodies, have been tested and have shown promising results. [54, 45, 8]

Some cancer cells are known to express certain receptors that are unusual for these type of cells or which cannot be found in such high concentrations. [55] Such an example are the toll-like receptors (TLR). These receptors play a crucial role in the innate immune system, the first barrier of pathogens upon entering the human host system. [56] TLR are expressed in cells of the innate immune system such as macrophages or dendritic cells. Latter one play an important role upon connecting the innate immune response with B- and T-lymphocytes, cells of the adaptive immune response. [57] This step is of utter importance since this system is much more effective and responsible for long term immunity. The TLR have first been identified in *Drosophila* as toll receptors. [58] In the 1990's, TLR1 and TLR4 were first identified in the human system. [56] Until today, at least 10 different TLR were characterized. [58, 55] TLR are members of the pattern recognition receptors (PRR) and feature a Toll/ Interleukin-1 recepor (IL-1R) homology domain (TIR) which can be found on the intracellular region of the TLRs. Upon ligand binding, activation of the nuclear factor (NF)-κB, cytokine or chemocine expression can follow, leading to an activation of the immune response. TLR are thereby very specific towards their ligands, each subgroup identifies components of the pathogens which cannot be found within the host. These components are called pathogen-specific molecular patterns (PAMPs). [56, 55] TLR3 recognizes double stranded (ds)RNA, which are prominet for different viruses. To activate this receptor under lab conditions, the synthetically available ds polyinosine-polycytidylic acid (Poly(I:C)) has shown promising results. Additionally, different cancer cells are known to express this receptor and undergo direct apoptosis when Poly(I:C) is applied. As a benefitial side effect, the immune system of the host is activated, assisting further in cancer treatment. TLR9 on the other hand, recognizes unmethylated CpG motifs, typically within single stranded (ss) DNA. Again, oligonucleotides, equipped with this motif, are commercially available (CpG) and have shown promising results in increased DC activation, [56] leading to enhanced T-cell activity and ultimately will assist in cancer therapy. This process is thereby most effective, when CpG is administerred directly to the TLR9 expressing tumor site. Since side effects were observed previously, CpG should either be encapsulated, or should otherwise be modified. [55] Finally, nonself proteins can be identified by TLR. Typically, a specific amino acid sequence is thereby recognized. For the chicken egg albumin (Ovalbumin, Ova), this sequence was identified as SIINFERKL sequence. Activation of DC upon presenting SIINFERKL has been proven previously.[59, 60, 61]

This chapter will focus on the coupling of MnO NPs (functionalized with different polymers) with Poly(I:C), CpG or Ova. Since either polymer (Poly1, PEG-Poly or DA-PEG) was synthesized in such a way that amino groups can be found on the surface and can be addressed chemically, the well known EDC coupling was applied. [62, 63] The chemical route is sketched in figure 3.1. EDC thereby reacts with phosphate or carboxylic groups and easily forms an O-acylisourea derivative. Upon NHS addition, and N-succinimidylester (NHS-ester) is formed, which is known to react easily with free amino groups to finally form an amide-/ phosphoramidit binding. The general procedures described described in [64] were thereby followed.

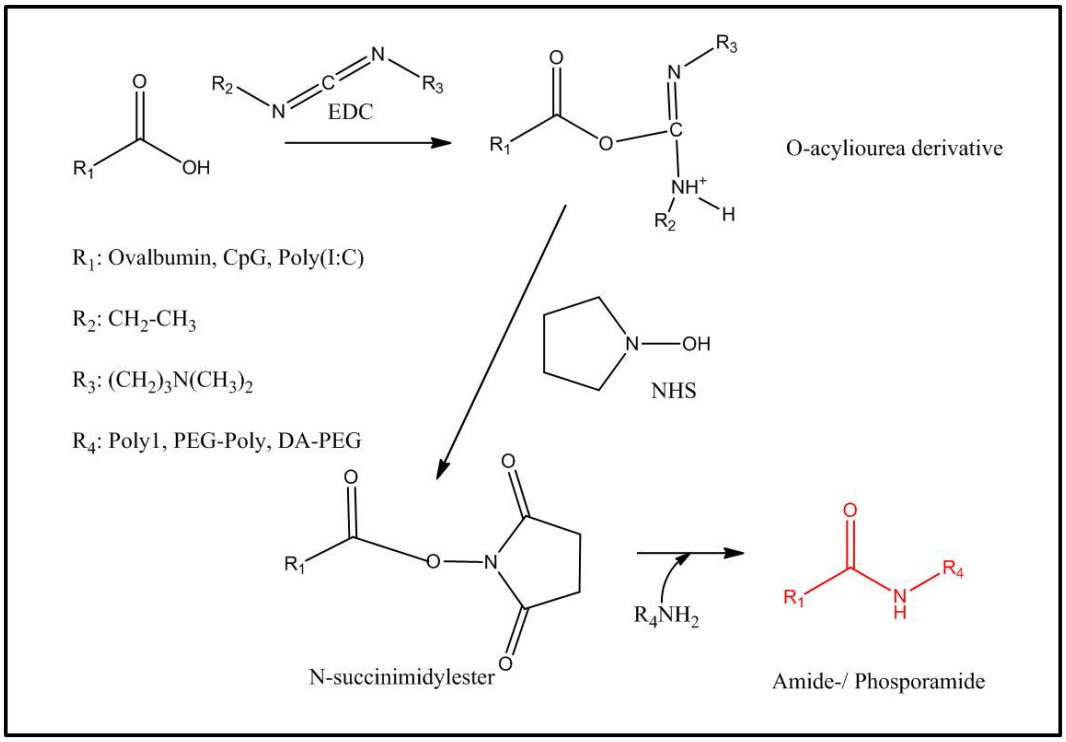

Figure 3.1: **Sketch for EDC coupling using NHS:** Phospate or carboxyl groups react upon EDC addition by forming an O-acylisourea derivative. When NHS is further added, an NHS-ester is formed which reacts easily with free aminogroups.

3.2 Experimental Section

Please not that experimental data which cannot be found here, are described in 2.

Materials: Poly(I:C) and CpG were provided by Invivogen; chicken egg albumin (ovalbumin; Ova) was purchased from Sigma-Aldrich; 1-Ethyl-3 -(3 - dimethylaminopropyl)carbodiimide hydrochloride (EDC) was provided by TCI europe. TEMED, APS, Rotiphorese-Gel 40 (Acrylamid/Bisacrylamid stock solution 19:1), Agarose MEEO, milk powder, PVDF membrane and MOPS were purchased from ROTH, Germany; as well as agarose Roti®garose middle elektroendosmosis (EEO = 0,16-0,19). Sigma Aldrich provided perchloric acid, glycerol, formamide, anti-chicken egg albumin antiserum, imidazol, NaOH and Anti-Rabbit IgG alkaline phosphatase. Coomassie Brilliant Blue G 250 (CBB), SDS, bromophenolblue and β-mercaptoethanol came from AppliChem. Methylenblue was purchased from Acros. Tris was ordered from neolab, acetic acid, sodium acetate and EDTA from Fluka. HCl, methanol and ethanol were ordered from VWR. Trisodium-citrate was purchased from Merck.

Devices: Fluorescence spectrophotometer: FluoroMax-2, Jobin Yvon-Spex using the software FluorEssence; SDS-PAGE: MINI-Vertikal-Double-Electrophoresis-Chamber, Carl Roth, Germany; Agarose Elektrophoresis: Mini Easy Elektrophorese-Chamber, Carl Roth, Germany; Power supply for SDS-PAGE and agarose GE: EV243 4-300 V, Carl Roth, Germany; Scanner: Canon CanoScan 4200F; VersaDoc, Eppendorf

Polymer synthesis: The synthesis of all polymers used in this chapter, as well as the ligand exchange reaction of oleic acid to water soluable polymers and the transfer to water are described in the experimental section of the chapter 2.

Binding RNA/DNA and proteins to polymer functionalized nanoparticles: For DNA and RNA samples, two restrictions occured during this synthetic step. First, the synthesis of polymer functionalized nanoparticles was limited due to the synthetic route. Secondly, the chosen DNA and RNA sample cannot be purchased in a greater abundance. Therefore all binding experiments were limited and using a definit nanoparticle sample was abstained from. In this section, typical reactions are therefore described while the amount of nanoparticles could vary in each experiment. The chicken egg protein Ovalbumin (Ova), single stranded DNA (CpG) and double stranded RNA (Poly(I:C)) were covalently bound. In a typical reaction, 2-(N -morpholino)ethansulfonic acid (MES-buffer) pH 4.5, EDC and N-hydroxysucciniide (NHS) were used. The weight ratio was 10:1:0.25. Ovalbumin was further added in a weight ratio MES:Ovalbumin 1:1 . Poly(I:C) and CpG were used in lower concentrations (Poly(I:C): 1:0.3 and CpG 1:0.16). Milli-Q water was used as a solvent. The reaction was carried out in a 1.5 ml reaction tube at 4-10 ° C overnight. The total volume ranged between 500 μl and 1 ml. Typical

experimental setups are given for each bioactive group in table 3.1. Metallic nanoparticles that carried Poly1 were washed twice by centrifugation, for all other nanoparticles the separation was more diffcult and is desribed in the result section.

Table 3.1: Metallic nanoparticles that were functionalized with Poly1, PEG-Poly or DA-PEG were further functionalized with CpG, Poly(I:C) or Ova.

Bioactive group	**Chemical**	**Amount added (μl)**
Poly(I:C)	nanoparticles	34μl
	MOPS (0.1 M stock)	88-42 μl
	EDC (1 % stock)	22-64 μl
	NHS (1 % stock)	10μl
	Poly(I:C)	20-60 μl
	LAL water	82-36 μl
CpG	nanoparticles	360μl
	MES (1 % stock)	120 μl
	EDC (1 % stock)	12 μl
	NHS (1 % stock)	3μl
	CpG	5 μl
Ova	nanoparticles	90μl
	MES (1 % stock)	240 μl
	EDC (1 % stock)	24 μl
	NHS (1 % stock)	6μl
	Ova (1 % stock)	150-240 μl
	dH_2O	500-330 μl

Bradford-assay: The Bradford assay is a widely used technique to determine how much protein is in a specific sample. The Coomassie Brilliant Blue (CBB) dye thereby binds to cationic amino acids of the target protein, shifting its absoption maxima from 470 nm to 595 nm. The Bradford solution was prepared by mixing 0.06 % CBB and 3 % perchloric acid. In a typical experiment, 100 μl of this solution was mixed with 900 μl of a solution that contained Ova as well as nanoparticles. The incubation time was set to 15 min before the absorbance was measured using a UV-Vis spectrophotometer.

PI measurements: Propidiumiodide can intercalate into DNA or RNA double strands just like ethidiumbromide. But unlike the latter one, PI cannot penetrate living cell membranes and is therefore assumed less toxic. In a typical experiment, Poly(I:C) and PI, respectively, as well as nanoparticles containing Poly(I:C) and PI were mixed in a volume ratio 1:1. The concentra-

tion of PI was 1 mg/ml. After mixing, the samples were applied to a fluorescence spectrometer and the excitation was set to 500 nm and 250 nm, respectively. The emission spectra was then collected 10 nm above the excitation output and up to 350 nm to the longer wavelength (e.g. when the excitation was set to 500 nm, the spectra was collected from 510 nm to 850 nm). In addition, the absorbance of the PI/NP and PI/Poly(I:C) sample was measured on a UV-Vis sprectrometer.

SDS-PAGE: Sodiumdodeculsulfate - polyacrylamide gelelectropheresis (SDS-PAGE) is described in chapter 6. The composition for the self made gels is described in table 3.2. Samples were incubated with 3-4 x sparmix (24 % glycerol; 0.4 mM bromophenolblue; 4 % SDS and 1.4 M β-ME) in a ratio sparmix-sample 1:3 and were heated up to 70 °C for 5 min before loading onto the gel. The running time was set to 50 min at 120 V. Gels were stained by submerging the gels in a coomassie brilliant blue (CBB) solution (0.25 % CBB; 40 % ethanol and 7 % acetic acid) for 15 min. Destaining was 20 min using destaining solution one (10 % acteic acid and 7 % ethanol) and overnight using a 10 % acetic acid solution (destaining solution 2).

Table 3.2: Composition of a 10 % resolving SDS-PAGE with a 6 % stacking gel for protein separation

	Resolving Gel	**Stacking Gel**
H_2O	14.8 ml	5.8 ml
Tris/ HCl 1.5 M pH 8.8	2.5 ml	2.5 ml (pH 6.6)
Acrylamide/ bisacrylamide 40 %	2.5 ml	1.5 ml
Glycerol 100 %	0.2 ml	0.2 ml
SDS 10 %	0.1 ml	0.1 ml
TEMED	0.01 ml	0.01 ml
Ammonium peroxide (APS) 10 %	0.1 ml	0.1 ml

Agarose gelelectrophoresis: Agarose gelelectrophoresis is a method generally used for DNA or RNA samples. The purpose for using it in this context was to separate unbound DNA/RNA from samples that were bound to nanoparticles using EDC coupling beforehand. For the agarose gel, 0.4-2 % (w/v) agarose was mixed with 2 x TAE buffer (40 mM Tris, 16 mM acetic acid, 10 mM EDTA/KOH pH 8). This solution was melted under vigorous stirring. Upon reaching a temperature of roughly 60 °C, the liquid gel was poured into the gel holder and was cooled further to allow polymerisation. Samples (24 μl) were mixed with 4 μl 6 x

gel loading dye (10 mM Tris/HCl; 0.03 % (w/v) bromophenolblue, 60 % (v/v) glycerol and 60 mM EDTA/KOH pH 7) and were loaded onto the gel which was then submerged in 2 TEA buffer. The running time was 1.5 h at 80 V. When DNA or RNA was present, the gel was further stained using an ethidiumbromide solution (0.5 μg/ml). Gels were either scanned using a scanner or were pictured using a Versa-Doc gel documentation system (Eppendorf). In addition, denaturating agarose gels were tested. The general approach was kept, however, the buffer was changed to 1 x MOPS buffer (10 x MOPS buffer: 200 mM morpholinopropansulfonic acid (MOPS); 50 mM sodium acetate, 50 mM EDTA pH 7). Additionally 6 % (v/v) formaldehyde was added to the agarose mixture before melting. Samples were mixed with RNA sample buffer (50 % formamide, 6 % (v/v) formaledhyde, 6 % glycerol, 10 % 10 x MOPS buffer and 0.04 % (w/v) bromphenolblue).

Northern blot: Typically, nitrocellulose or nylon membranes are used for this DNA detection method. For this experiment however, the membrane was switched to PVDF. These membranes need to be activated prior to use by submerging in methanol and washing with water and buffer (SCC; 150 mM sodiumchloride and 15 mM sodium citrate pH 7). All samples were kept on ice prior to mixing with denaturation buffer (ratio sample:buffer 1:1, denat.buffer: 500 mM sodium hydroxide and 1.5 M sodium chloride). After 30 min, neutralizing buffer (500 mM Tris/HCl pH 7 and 1.5 M sodiumchloride, ratio 1:1 with original sample) was added and all samples were again mixed at room temperature for 30 min. Then, each sample was slowly dropped onto the PVDF membrane using a pasteur pipette. Prior to activation, the final spots for the samples were labelled with a pencil. The membrane was kept moist during the process. Finally, the membrane was submerged in an aqueous solution of 0.02 % methylenblue solution for 2 min. Destaining was done with water. The final membrane was pictured using the scanner Canon CanoScan 4200F.

3.3 Results and Discussion

3.3.1 Biofunctionalization of MnO@Poly1 NPs

Biofunctionalization using Poly(I:C):

Trials with imidiazole buffer: Poly1 featured free aminogroups that could be used to further bind biological active groups. The purpose of this was to allow a more specific targeting *in vivo*. The first tests were done with Poly(I:C), a synthetical double stranded (ds) RNA oligonucelotide that can be regognized by toll like receptor 3 (TLR3) of human cells. For this purpose MnO@Poly1 NPs kept in DMF were centrifuged and the NP containing pellet was resuspended in imidazol buffer (20 mmol). The concentration of this sample was estimated after the pellet was dried and weighted before resuspension. In this context, MnO@Poly1 NPs were mixed with water, EDC and Poly(I:C) to give a final concentration of 1.05 mg/ml NPs, 0.06 M EDC and 0.1 mg/ml Poly(I:C). A control sample with water instead of Poly(I:C) was also prepared. These samples were mixed at room temperature for 1 h and were then centrifuged and washed with an imidazol solution. The pellet fraction contained MnO@Poly1 NPs and was resuspended in buffer. Excess Poly(I:C) was washed off by additional washing cycles. The final pellet was again resuspended and labeled MnO@Poly1+Poly(I:C). All supernatants were kept and were, as well as an aliquot of the original sample, applied to a 1 % (w/v) agarose gel. Additionally, all samples were characterized with UV-Vis. The results are given in fig. 3.2.
One characteristic of the synthetically designed Poly(I:C) is that the exact length of the ds RNA is not defined but rather is provided as 2-5 kb sample. Therefore, when only Poly(I:C) was loaded on the agarose gel, no distinct band but rather a smear was observed. This also held true for the supernatant of MnO@Poly1+Poly(I:C). To test whether MnO@Poly1 NPs by themself have the ability to bind ethidiumbromide, a corresponding sample was also applied (MnO@Poly1). However, neither this sample, nor the control or the MnO@Poly1 + Poly(I:C) sample (MnO+Poly(I:C)) showed any increase in the fluorescence. This indicated that Poly1 did not absorb ethidiumbromide but it also showed that the binding of Poly(I:C) was not successful, a fact that was further confirmed by UV-Vis. DNA as well as RNA show an absorption maxima at 260 nm. This is used to determine the amount of DNA/RNA in a given sample. Therefore the control sample, MnO+Poly(I:C) NPs and the corresponding supernatant were applied to a UV-Vis photometer (see left figure in 3.2). Both, the control sample and the nanoparticle sample Mn@Poly(I:C) did not show any specific absorbtion in the region of 228-300 nm. The MnO@Poly1 NP free supernatant however, which was gained after the first of

two washing steps, showed a peak at roughly 270 nm which could be attributed to Poly(I:C). The slight shift from 260 nm might have originated from EDC and imidazole. The UV-Vis spectra further showed that the absorption increased with decreasing wavelength at the UV region. This was accounted for EDC and imidazol, two components of the coupling solution, but also to the backbone of Poly(I:C). The complete absence of a peak for MnO+Poly(I:C) NPs emphasized that the binding between the amino groups of the polymer and the phosphate groups of Poly(I:C) was not successful or simply not effective enough to be detected by ethidiumbromide or UV-Vis. As already mentioned, MnO NPs that were possibly coupled with Poly(I:C) were washed twice. The supernatant of the second step is not shown here, since neither agarose gelectrophoresis nor UV-Vis gave a positiv result. Therefore it was assumed that one washing step was generally sufficient to wash unbound RNA off the particles. However, two washing steps were maintained.

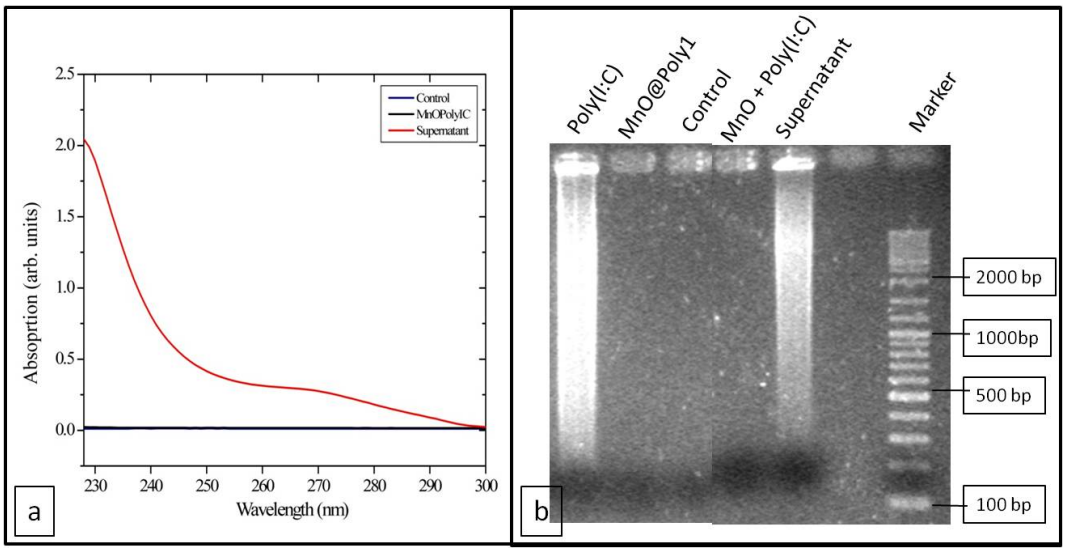

Figure 3.2: **UV-Vis measurements of MnO+Poly(I:C) and agarose gels thereof:** a: UV-Vis measurements of NPs that were either not treated at all (MnO@Poly1) or were surface functionalized with Poly(I:C) (MnO+Poly(I:C)) by applying EDC coupling. The supernatant sample was measured also. These samples were additionally loaded on A 1 % agarose gel (b) together with a control sample. Samples were washed with imidazole after the coupling was completed and the corresponding supernatant was applied as well. The gel was stained with ethidiumbromide and was pictured with the VersaDoc system. As a marker the Generuler DNA-ladder mix (Fermentos) was used.

Results for MOPS and MES buffer; Agarose gel: Following these results, the procedure for EDC coupling was changed. Imidazole was first replaced by MOPS, then by MES buffer. Additionally, NHS was introduced to help form a NHS ester of Poly(I:C) which is much more active towards free amino groups. In additon, the reaction time was increased to over night, shaking all prepared samples at 10 °C. Again, a control sample was prepared. Both samples were washed two to three times by centrifugation and resuspension of the pellet in MES buffer. The original MnO@Poly1 NP sample, the control sample (MnO@Poly1, no Poly(I:C)) as well as the supernatant of the first washing step and MnO@Poly1+Poly(I:C) were loaded on a 1 % agarose gel which was then stained with ethidium bromide (see figure 3.3 a). The control sample as well as the untreated MnO@Poly1 NP sample gave no result with ethidiumbromide as has been observed before. The supernatant fraction was stained, leading to the conclusion that unbound Poly(I:C) could have been washed off. However, the most stained fraction was found for MnO@Poly1+Poly(I:C) NPs. A smear was seen for this sample but also a rather intense bulk close to the pocket of the agarose gel. This was attributed to nanoparticles that were too big to enter the gel in significant amounts. The smear of the band however, also indicated that some part of Poly(I:C) was either not bound to Poly1, or that during the gel run, Poly(I:C) got detached from MnO@Poly1.

Results for MOPS and MES buffer; PI: These tests were repeated, this time bound Poly(I:C) was tried to be visualized with different methods. For this purpose, propidium iodine (PI) was used. Like ethidium bromide, this dye can intercalate into ds DNA or RNA. Thereby the absorption maxima, as well as the emission maxima, is changed. Pretests with Poly(I:C) and PI were done to establish the optimum concentration of PI. It turned out that the best conditions were optained, when an aqueous PI solution (1 mg/ml) was mixed 1:1 with a Poly(I:C) solution. Upon intercalation, the pink color of PI changed immediatly to bright orange. All samples were mixed and then applied to a fluorescence spectrometer. Excitation was set to 500 nm and the spectra was measured from 510 to 800 nm as is shown in figure 3.3 b. The emission of all samples except the supernatant of MnO@Poly1+Poly(I:C) (sample sup1) were comparable, featuring a broad peak with two smaller maxima at 620 and 638 nm. A much higher emission was measured for the supernatant of MnO@Poly1+Poly(I:C). Here, a maxima was observed at 611 nm. As already shown for previous samples, the supernatant contained unbound Poly(I:C), which might have been the source for this emission shift. When the excitation was set to 250 or 270 nm to excite the backbone of Poly(I:C) a general elevated emission at 370 nm was observed. However, a general distinction between the samples could not be made. In addition to fluorescence imaging, the absorption of all samples were measured.

Again, samples were incubated with PI as described above. The absorbance measurements mirrored the fluorescnece results (see figure 3.3 c). The most pronounced shift was visible for the supernatant fraction (samplesup1). The control sample and MnO@Poly1+Poly(I:C) (sample) sample did not differ significantly. The control sample (control) and the second supernatant fraction (samplesup2) also displayed the same maxima, however, the absorption was not as high as for the other two samples. During pretests with Poly(I:C) and PI, it could be observed that the shift seen for supernatant 1 was also true for samples with higher concentrations of Poly(I:C). However, when the content of the RNA was lowered in the PI mixture, the absorption shift was not as significant, but the absorption intensity at 495 nm decreased. This might be a proof that Poly(I:C) was still present in the second supernatant. A reason to why the absorption of the control sample was lower was unclear. To varify whether it is possible that MnO@Poly1 NPs did not bind Poly(I:C), a negative control was set up. For this purpose, MnO nanoparticles were functionalized as described above using the backbone polymer. Instead of dopamine as an anchoring group, a carboxylic group was introduced. Additionally, this polymer did not feature free amino groups, ensuring that a binding of Poly(I:C) via EDC coupling was not possible. However, when these MnO NPs were treated the exact same way as MnO@Poly1 NPs, the absorbance at 495 nm did not shift significantly for either taken sample (also supernatant). The emission when excited at 500 nm showed a slight shift to lower wavelength for the supernatant fraction, however, it was not as pronounced as for MnO@Poly1. In contrast, emission maxima were shifted to the red for all samples (data not shown).

Results for MOPS and MES buffer; Norther Blot: To adress the issue that the concentration of bound Poly(I:C) might not have been high enough to give detectable results, another detection method was used. So called northern blots are systems that are routinely used to detect DNA. Therefore, the sample was blotted onto a specific membrane and was then stained using methylenblue. Again, MnO@Poly1 NPs were coupled with Poly(I:C) using MES buffer, EDC and NHS. The reaction was kept over night at 10 °C and unbound RNA was washed off by centrifugation. Samples of Poly(I:C) (5, figure 3.3 d), MnO@Poly1 NPs (15) which were applied to Poly(I:C) in the presence of EDC (1), supernatants of each washing steps (2; 7; 8) and the corresponding control sample (11) with the supernatant of the washing step (12) were tested. All samples were premixed with denaturation solution and were mixed at room temperature for 30 min prior to neutralization and mixing for half an hour. Then each sample was applied on an activated PVDF membrane. After the samples were dry, the membrane was stained with a methylenblue solution. After destaining with water, samples that contained

Poly(I:C) appeared darker than the background. Positve staining was shown for the samples 2, 5 and 9. All these samples did not contain MnO@Poly1 NPs. Neither the control sample (11) and the untreated MnO@Poly1 NPs that were added (15), nor the Poly1 sample (16) showed signs of positive staining, which indicated that these samples could not bind methylene blue. A rather weak spot was seen for possible MnOPoly1+Poly(I:C) NPs. Since the final washing step was negative (8), this spot needs to have had its origin in bound Poly(I:C) to the surface of MnO@Poly1 NPs.

Taking all results into account, binding of Poly(I:C) to MnO@Poly1 NPs using EDC, NHS and MES or MOPS was successful but could only be detected using agarose gelelectrophoresis with additional ethidiumbromide staining, as well as staining samples with methylenblue using northern blot technique. Both techniques allow the proof of for of present Poly(I:C) but cannot be used to determine how much Poly(I:C) was successfully coupled.Since MnO@Poly1 NPs where abstained from due to agglomeration as was described in the previou section, further testing was not done.

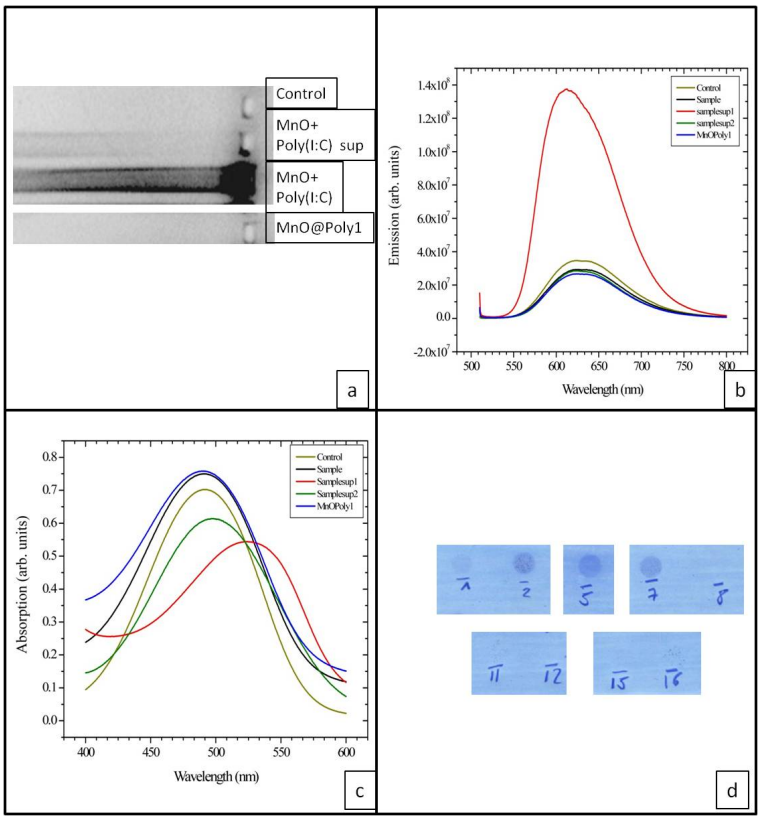

Figure 3.3: **Different techniques were used to characterize MnO@Poly1 NPs:** a: 1 % agarose gel stained with ethidiumbromide. Loaded were MnO@Poly1 NP samples that were functionalized with Poly(I:C) (MnO+Poly(I:C)) or used in the same reaction as control sample (control). Samples were washed and the supernatant of the sample were Poly(I:C) was added was also loaded (MnO+Poly(I:C)sup). b/c: MnO@Poly1 NPs + Poly(I:C) were incubated with PI and the emission at 500 nm (b), as well as the absorbance (c) was measured. Loaded were control samples of MnO@Poly1 NP wihtout Poly(I:C) (control) and NP samples with Poly(I:C) (sample), as well as suparnatants of the washings thereof (sample sup1/2). Untreated MnO@Poly1 NPs were loaded as well (MnO@Poly1). Unlike the control sample, EDC, NHS and MES were not added. Samples were washed twice by centrifugation, supernatants were also measured. The excitation was set to 500 nm. d: northern blot was applied by dot blot technique. The membrane was stained with methylenblue and scanned using a Canon CanoScan 4200F. 1: MnO@Poly1 + Poly(I:C); 2: supernatant of 1, washed by centrifugation; 5: Poly(I:C) sample; 7,8: supernatant 2 and 3 of washing steps of MnO@Poly1 + Poly(I:C); 11/12: control and washing step thereof; 15: MnO@Poly1 untreated, 16-: Poly1.

Biofunctionalization using Ova:

In addition to Poly(I:C), a second bioactive group was used. Chicken egg albumin (Ovalbumin, Ova) is a protein which possibly serves as a nutrient for chicken fetus in eggs. Since it does not have human origin, when co-incubated with human cells of the immune system an immune response is triggered. Responsible for this is a specific sequence (SIINFEKL) within the protein that is recognized by the human host. Goal of this research was to bind ovalbumin to the surface of MnO@Poly1 NPs and then varify a positive binding.

Detection via fluoresence and absorpion measurements: Due to the aromatic amino acid side chains of tryptophan and tyrosin, proteins can be detected at a wavelength of 280 nm. When bound to the polymer that surrounds the MnO NP core, Ova should thereby be detected. MnO@Poly1 NPs were incubated with Ova, MES, NHS and EDC overnight. For the control sample, water was added, otherwise an aqueous solution of Ova was used. MnO@Poly1 NPs were then washed by centrifugation and resuspension in buffer for up to three times. All samples and supernatants of the first washing steps were then characterized by UV-Vis (see figure 3.4 a). The control sample (red) did not show any sign of absorption which was surprising since Poly1 was attached to the nanoparticles via dopamine. This tyrosin derivative should also show a slight absorbance at 280 nm. The supernatant of the control sample (controlsup) as well as of MnO@Poly1+Ova (MnOOvasup) displayed a maxima at approx. 260 nm. This peak was shifted when compared to the Ova sample (Ova, light blue). The pure protein sample might have been too concentrated to give a distinct peak at 280 nm. MnO@Poly1+Ova (MnOOva, dark yellow) also showed a peak at 280 nm. However, the overall absorption was higher than for the control sample and increased from 300 nm to shorter wavelengths. This might have been an indication for a positive binding.
Emission spectra are more sensitive than UV-Vis measurements. Therefore all samples were applied to a fluorescence spectrometer. When excited at 250 nm, all samples but the control sample (control), the supernatant of the control samples (controlsup) as well as untreated MnO@Poly1 NPs (MnOPoly1), showed a maxima at 330 nm (see figure 3.4 b). The highest signal thereby was reached for MnO@Poly1+Ova (MnOOva, dark yellow). Since the pure protein samples (Ova, cyan) also emitted at this region and since the untreated MnO@Poly1 NPs (MnO@Poly1) did not show such a specific maxima, it was feasible to state that this peak derived from bound ovalbumin.

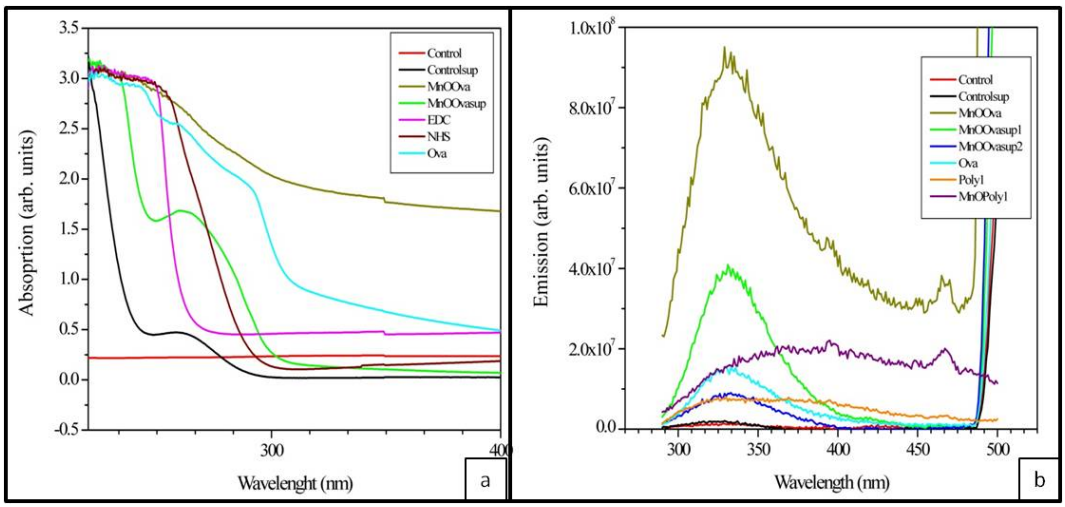

Figure 3.4: **Absorption and Emission spectra for MnO@Poly1+Ova:** MnO@Poly1 NPs incubated with Ova (MnOOva), control samples (control), as well as untreated MnO@Poly1 NPs and Poly1 were characterized via absorption (a) as well as fluorescence imaging (b). Red: MnO@Poly1 NPs used as a control sample during EDC coupling (control), black: supernatant of the control sample (controlsup), dark yellow: MnO@Poly1+Ova NPs (MnOOva), green and blue: washing steps thereof (MnOOvaSup1/2). Light blue: Ovalbumin (Ova), orange: Poly1 (Poly1), purple: untreated MnO@Poly1 NPs (MnOPoly1). Finally EDC and NHS are shown in pink and wine red (a). a: the protein absorption at 280 nm was measured. The proteinspecific fluorescence when excited at 250 nm is shown in b.

Detection via SDS-PAGE and Western Blot: When dealing with proteins, numerous detection methods are routinely used. Poly1 contained DA, which also absorbs at 280 nm and which could have led to false positive results. Additionally, the Bradford assay was applied, an assay that uses the shift of the absorption of Coomassie Brilliant Blue (CBB) when bound to proteins, could not be used, since the NBD dye did interefere with CBB. Untreated MnO@Poly1 NPs thereby also showed the absorption profile of a pure protein solution (data not shown). Therefore, a more specific approach was necessary.

Antibodies are specific proteins that can bind to a single target molecule and will then lead to an immune response. They can, however, also be used to detect their target protein within a protein mixture. Antibodies are thereby very specific and hardly interact with anything else other than their target. Additionally, secondary antibodies can be used. These molecules will bind to the first antibody. When linked to an enzyme, in this case the alkaline phosphatase, the presence of the antobody can be visualized upon incubation with its substrates (5-Brom-4-chlor-3-indolylphosphate (BCIP)) and nitro blue tetrazolium (NBT)). As a result, a reduction

takes place, leading to a blue product. This colorchange is then detected. Usually proteins are directly plottet from SDS-PAGE onto, e.g. a PVDF membrane. However, since MnO@Poly1 NPs do not enter the SDS-PA gel, a dot blot method was chosen. A drop of a control sample (control), samples of MnO@Poly1 NPs (MnO+Ova) which were incubated with EDC, NHS, MES and Ova, samples originating from washing steps as well as an ovalbumin solution were dropped on a PVDF membrane. After drying and blocking steps, the first antibody was incubated at 4 °C overnight. After additional washing steps, the membrane was incubated with the secondary antibody for 1 h at room temperature. BCIP and NBT were added and the reaction was stopped with water after appr. 5 min. Results are shown in figure 3.5 a. A blue discoloration was observed for the pure protein sample (Ova), as well as for MnO@Poly1+Ova NPs (MnO+Ova) and the supernatants of the washing steps thereof. NHS and the control sample also resulted in a light color change, which probably were artefacts. These observations support the assumption that ovalbumin bound to MnO@Poly1 NPs.

Further proof was made using a SDS-PAGE (see figure 3.5 b). The corresponding samples as were used for the western blot were loaded on a 10 % SDS-PA gel. The control sample was negative, as was Poly1. MnO@Poly1+Ova NPs (MnO+Ova) however, could be positivly stained using CCB. It has to be noted that a broad band was observed in the well, however, the gel itself gave some sort of smear with two additional lanes which could be attributed to Ova. The supernatant samples as well as the pure protein sample (Ova) also showed these two bands, with an additonal band in the higher molecular region (possible dimer of Ova). The second washing step was also applied (MnO+Ovasup2), however, the signal that was produced in the gel was comparatively weak. Most of the unbound sample thereby was washed off after the first washing step.

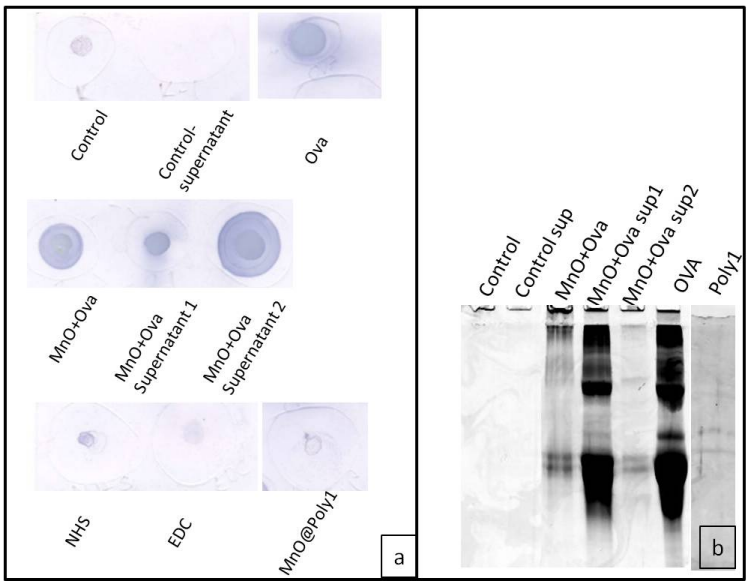

Figure 3.5: **SDS-PAGE and Western blot for MnO@Poly1:** MnO@Poly+Ova NPs were applied to a PVDF membrane (a) and a 10 % SDS-PAGE (b). Additonally control samples of MnO@Poly1 were added (Control). The supernatant fractions were collected and also applied as well as a solution of Ova, NHS and EDC together with untreated MnO@Poly1 NPs. SDS-PAGE was stained with CBB, the PVDF membrane was incubated with chicken egg albumin antiserum and a secondary anibody with alkaline peroxidase activity.

Infuence of EDC and DCC as coupling agents: The positive staining of supernatant fractions of MnO@Poly1+Ova NPs implied that a rather big amount of protein could not be attached to Poly1. EDC is known to hydrolyse in water, thereby its reactivity might have been significantly reduced. DCC works just like EDC but might be more efficient. MnO@Poly1 NPs were incubated with EDC or DCC, respectively, but were otherwise treated equally. Distinguishing what method was more effctive was thereby difficult. The Bradford assay could not be used since Poly1 also absorbs CBB. A reproducable detection of the amount which was bound to the NP surface could not be established. Therefore all samples were applied to SDS-PAGE and UV-Vis photometer. The results are shown in figure 3.6.
For each approach a corresponding control sample was prepared (DCC-control1; EDC-control2). The specifics of each sample will not be adressed here since it was already discussed above. The main focus will therefore be on the MnO@Poly1+Ova NP samples that were functionalized with EDC and DCC and the supernatants of the washing steps thereof. Both supernatants (DCC sup1/2, EDC Sup 1/2) showed bands in the SDS-PAGE which could be attributed to Ovalbumin. Corresponding absorption was also visible in the UV-Vis spectra.

MnO@Poly1+Ova NPs was only successful for DCC (see sample DCC) not for EDC as coupling reagent (see band labelled EDC). This lane was surprisingly completely empty and this sample also did not lead to any significant absorption when used in UV-Vis (see EDC, orange line in figure 3.6 b). Supernatants for EDC and DCC coupling showed a specific absorption band with can be attributed to Ova and is higher when EDC was used as coupling agent (EDC). An absorption pattern was also seen for MnO@Poly1+Ova NPs which were incubated with DCC (see DCC, dark yellow line). All results taken into account, the observation that MnO@Poly1 NPs that were incubated with DCC showed distinct peaks in UV-Vis and lanes in the SDS-PAGE, do underline that in this particular experiment DCC was the more efficient coupling agent. A reason why EDC might not have worked at all is not clear.
Western blot, SDS-PAGE, UV-Vis and emission analysis all reveiled that the binding of Ova to MnO@Poly1 was successful. However, it might not have been a covalent binding but rather due to interaction between the polymer and the protein. When unbound protein was tried to be washed off using detergents such as SDS, UV-Vis indicated that not only unbound protein but rather the complete polymer was washed off. Harsh methods were not possible to be used. Rather than using harsh methods, repeating the washing steps more often might have helped to wash off excessiv ovalbumin. Again, since MnO@Poly1 showed extended signs of agglomeration, further tests were not made using these NPs.

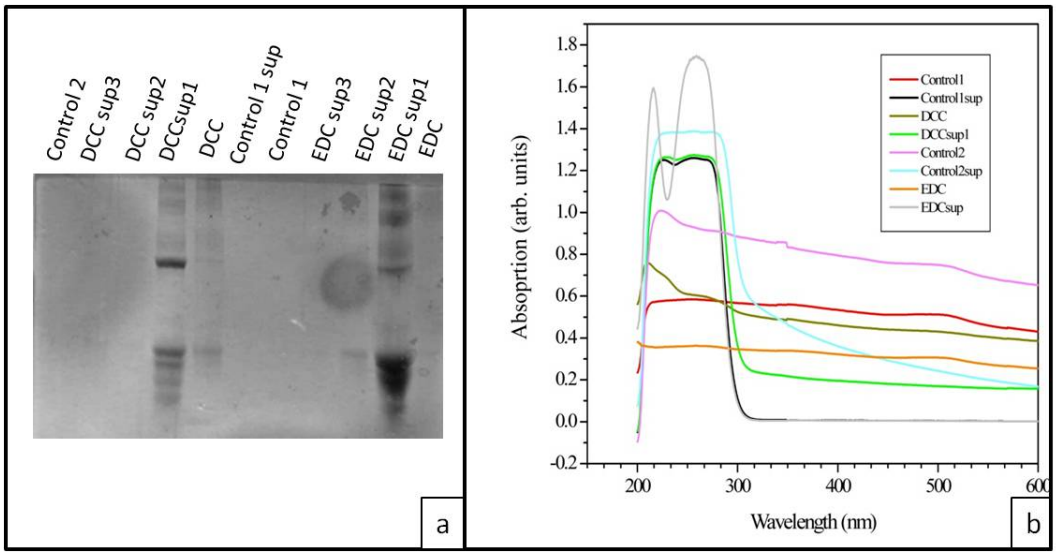

Figure 3.6: **Comparison between EDC and DCC as coupling reactants:** MnO@Poly1 NPs were coupled with Ova by the use of EDC (see sample EDC) or DCC (see sample DCC). Upon completing the reaction, unbound protein was washed off by centrifugation (DCC/ EDC sup1-3). Control samples were also performed by incubating MnO@Poly1 NPs with EDC/DCC, respectively and NHS and MES but without Ovalbumin (control1/2). a: 10 % SDS-PAGE stained with CBB. b: UV-Vis measurements of MnO@Poly1+Ova using EDC or DCC as coupling reagent. Washing supernatants were applied as well.

3.3.2 Biofunctionalization of MnO@PEG-Poly NPs

Within this thesis, Poly1 was replaced by the same backbone polymer that was further coupled with PEG (see 2). The advantage of using this polymer (PEG-Poly) was that MnO NPs functionalized with PEG-Poly were more stable in aqueous solutions. Unlike MnO@Poly1 NPs, MnO@PEG-Poly NPs could not be centrifuged; excess polymer or bioactive groups could not be separated as easy as for MnO@Poly1 NPs. However, since NBD dye still was attached and the character of the polymer was not changed drastically, the same issues as were seen for Poly1 occured for MnO@PEG-Poly NPs in regard to applying methods as the Bradford assay. Therefore, this polymer was not tested extensively for its binding properties. The only test applied was binding of CpG. This single stranded (ss) DNA is characterized by being rich in cystein groups and can activate TLR3 which then will lead to an activation of the human host immune system. CpG was coupled to MnO@PEG-Poly NPs as was already described for Ova or Poly(I:C), using EDC. Samples were then directly applied to UV-Vis without any further purification step. Two samples in total were prepared, a negative or control sample by mixing MnO@PEG-Poly NPs with water instead of CpG and a positive control (MnOPEGPolyCpG). PI could not be used for this sample since this is a dye that intercalates into double strands, not single strands. The UV-Vis results are shown in figure 3.7. Both curves were normalized to the NBD maxima at 486.5 nm for better characterizion of the absorbance between 200 and 300 nm. A slightly higher absorption in this region for the positive sample (MnO@PEG-Poly+CpG) was observed (see gray curve) which was attributed to bound CpG.

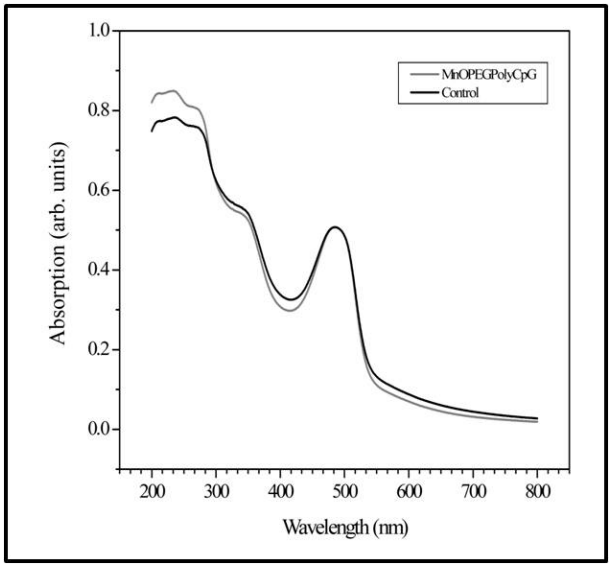

Figure 3.7: **UV-Vis data of MnO@PEG-Poly+CpG:** MnO@PEG-Poly NPs were functionalized with CpG (MnOPEGPolyCpG, gray line) by EDC coupling. Further, a control sample was used to confirm the successful binding (black line, control). Both curves were normalized to the NBD peak of PEG-Poly.

3.3.3 Biofunctionalization of MnO@DA-PEG NPs

PEG-Poly was further simplified using DA-PEG. For this purpose PEG_{800} was coupled with dopamine (DA), thereby merging the anchoring group and the group responsible for water solubility. Free amino groups on one side of the PEG chain ensured that further modification was possible. This polymer did not feature a fluorescence dye, however, DCC coupling of dyes such as atto 465 or NBD were possible. The general idea of combining fluorescence properties and bioactive properties on the surface of NPs that further could be used for MRI contrast enhancement was therefore kept.

Pretests of DA-PEG using the Bradford solution: MnO@DA-PEG NPs were synthesized as already mentioned for MnO@PEG-Poly NPs and are also described in 2. Pretests with only the polymer (DA-PEG) were made to test, whether the polymer itself is suitable for the Bradford assay whioch can be used to detect proteins such as Ova. Therefore, a sample was incubated with Bradord solution. An aliquot of ova was additionally added but was not coupled. All samples including control samples were analyzed via UV-Vis as are given in figure 3.8.Due to missing NBD, DA-PEG does not absorb between 450 and 800 nm (DAPEG, see green line in figure 3.8). The Bradford solution showed a maxima at 660 nm which was also present for DA-PEG incubated with Bradford (BrOvaPEG, black line). When Ova was co-incubated with Bradford solution (OvaBr, wine red), this maxima was shifted to 595 nm, a fact that was independent of whether DA-PEG was present or not (see OvaPEGBr, blue line in figure 3.8). In conclusion, DA-PEG did not interfere with the Bradford solution as was shown for PEG-Poly or Poly1, leading to promising results for the applicability of this test. However, before any further tests could be made, unbound DA-PEG polymer needed to be washed of the surface of MnO@DA-PEG in order to ensure that Ova binds to the MnO@DA-PEG NPs and not to free polymer.

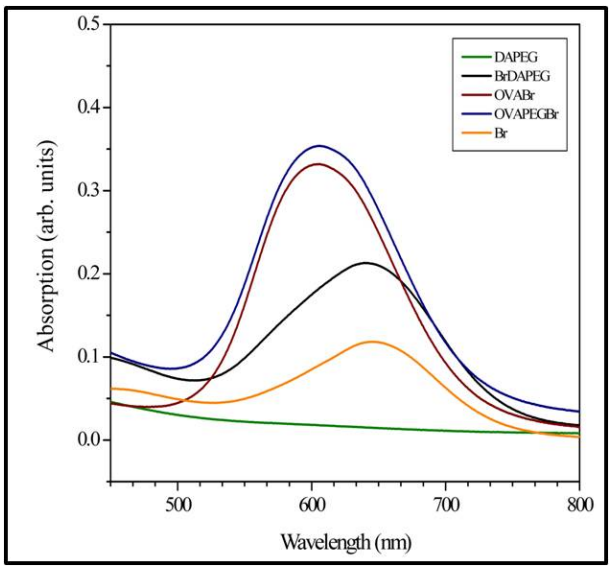

Figure 3.8: **UV-Vis measurements of DA-PEG polymer incubated with Bradford solution:** Green: DA-PEG polymer, black: DA-PEG polymer incubated with Bradford solution, wine red: Ovalbumin solution with Bradford, blue: Ovalbumin with DA-PEG and Bradford solution and the Bradford solution by itself in orange. All samples were incubated with Bradford solution for 15 min prior to measurements.

Amicon Ultra filter devices for separation of bound and unbound polymer: MnO@DA-PEG as well as MnO@PEG-Poly were stable in water for months when kept at 4 °C. This had one major disadvantage which is that unbound polymer and even more so bioactive groups, could not be washed off by centrifugation. Precipitation with hexane resulted in precipitation of unbound polymer as well as MnO@DA-PEG and MnO@PEG-Poly NPs, respectively. Dialysis of MnO@DA-PEG NPs could not be applied either, since Mn^{2+} tended to leach (unpublished results of Dr. T. Schladt). A different approach was therefore tested. Amicon ultra filter devices are centrifugable devises with a membrane that features a specific cut-off size (e.g. 50 kDa). Molecules that are larger cannot trespass this membrane and are retained within the storage vessel and can be collected after the final run. These devices follow the principle of a dialyis, howeverm, since they can be centrifuged, all tests can be accalerated to a couple of minutes. A sample of MnO@DA-PEG NPs were applied to such a device with a 50 kDa membrane. After centrifugation, the flow through was collected and the lost liquid in the storage was refilled. These washing steps were repeated up to 8 times. The original sample, the first flow through and the retained sample were characterized using AAS. All results were plotted and are shown as black columns in figure 3.9 a.
MnO@DA-PEG NPs have a brown color due to the MnO core. When using a 50 kDa mem-

brane, the flow through sections also featured this color, whereas the final retained sample was colorless. This already gave a hint that the membrane might have been too big for the applied NPs, a fact that was confimed by UV-Vis measurements (decrease in overall absorption and especially in the region of DA-absorption at 280 nm, data not shown) as well as AAS (see figure 3.9, a black column). The first flow through was 5 times more concentrated than the retained sample. In total, approximately 4 % could be retained in comparison to the original sample.

Ovalbumin has an approximate size of 42.8 kDa, a size that is at the border of the 50 kDa membrane. When coupled to MnO@DA-PEG NPs, the size of the NPs should be enlarged to allow retention within the storage vessel. Coupling was done with the help of EDC and NHS as described above. These samples were again applied to a filter device with a cut-off size of 50 kDa. The original sample, as well as the first flow through and the retained sample, were characterized with AAS, and were in addition to all other washing steps loaded on a SDS-PAGE. As figure 3.9 a (light gray columns) shows, the majority of Mn^{2+} was found in the flow through, albeit the concentration of the retained sample was doubled when compared to untreated NPs. Still it was only 8 % compared to the original sample. Interestingly, SDS-PAGE revealed that the monomer of Ova was washed off with the first washing step (lower band in SDS-PAGE, see figure 3.9 b). The higher running dimers of Ova were found from the first eluent throughout the flow through sample 5. Dimerization is rather common for this protein, however, since the dimer has double the size than the monomer (85.6 kDa), it should have been retained by the Amicon ultra filter device.

As a final approach, the cut-off size was decreased from 50 kDa to 30 kDa and 10 kDa, respectively. Again, the original sample, the first flow through and the retained sample were characterized with AAS (see figure 3.9, dark gray column for 10 kDa and gray for 30 kDa). For samples applied to the 30 kDa membrane, the concentration decreased stepwise from the original sample via flow through one to the retained sample. Nearly 15 mg/ml however were retained by the membrane which equaled 32 % and was more than 6 times higher than for samples applied to a 50 kDa membrane. For a 10 kDa membrane, this value of 19.7 mg/ml was even higher. Unclear was, why the flow through fraction had a higher concentration than the original one. It probably was due to a mistake during the AAS measurement. For both membranes however, NPes were found within the membrane and could not be washed out even with more drastic methods such as 10 % SDS.

All results taken into account, the use of Amicon ultra filter devices clearly had limited success. Only filters with a small cut-off sites were successful to retain significant amounts of MnO@DA-PEG NPs. Whether a separation between MnO@DA-PEG NP and unbound poly-

mer is possible, needs to be proven by additional tests such as using a much higher polymer content in comparison to MnO NPs. If the use of these filter devices will be helpful for future experiments with biogroups remains questionable.

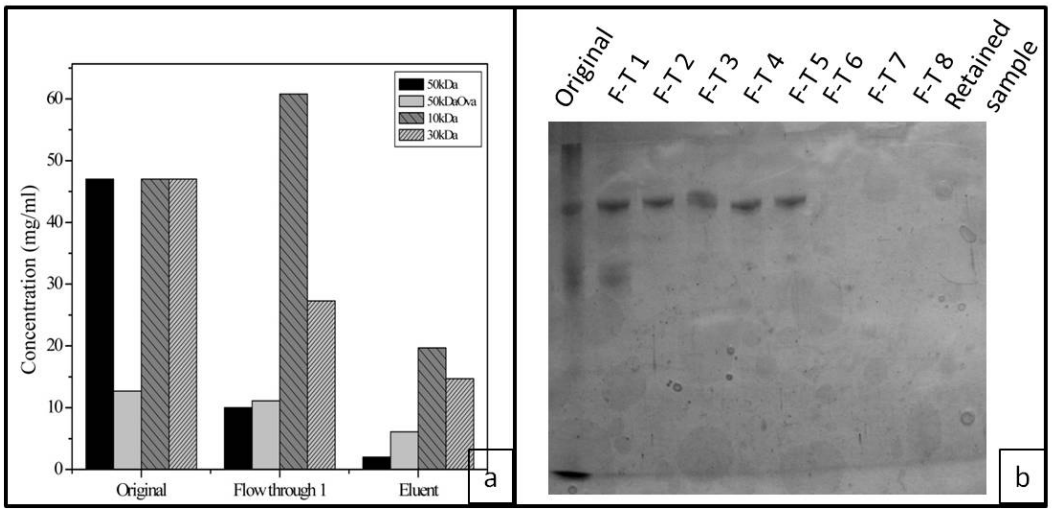

Figure 3.9: **Usage of Amicon filter devices for MnO@DA-PEG NPs:** Results after applying MnO@DA-PEG on Amicon ultra filter devices. a: AAS measurements for the original samples, the flow through and the retained samples. Tested were Amicon ultra filter devices with a cut-off size of 50 kDa (black), MnO@DA-PEG nNPs with bound Ova (50 kDaOva, light gray), membranes with a cut-off size of 10 kDa (dark gray) and finally 30 kDa membranes (gray). b: 10 % SDS-PAGE of MnO@DA-PEG NPs coupled with Ova and after applying to a 50 kDa Amicon ultra filter device. The gel was stained with CBB.

3.3.4 Applicability of SiO_2@MnO and SiO_2@Fe_3O_4 NPs

Finally metal oxide nanoparticles that were surrounded with a thin silica shell were used and were applied to a 50 kDa membrane as well as a 300 kDa membrane. Generally all procedures were done the same way as for MnO@DA-PEG NPs. SiO_2@MnO NPs in water were applied to a 300 kDa Amicon filter device wherease SiO_2@Fe_3O_4 NPs were used for 50 kDa membranes. Both membranes were centrifuged. The flow through was collected and the missing liquid in the filter was replaced. After 2 to 3 runs the retained sample was collected and the filter was washed with water. The original sample and selected flow through samples as well as the retained sample were characterized using UV-Vis and AAS. SiO_2@MnO and SiO_2@Fe_3O_4 NPs had a slightly brown color due to the core. For both membranes a colorless flow through was found. In case of the 300 kDa filter device, a small amount of SiO_2@MnO NPs embedded themselves within the membrane structure and could not be removed afterwards. The results for AAS and UV-Vis are shown in figure 3.10.
When a filter device with a cut-off size of 50 kDa was used, the concentration of iron within the retained samples as was measured by AAS nearly reached the value of the original sample (see figure 3.10 b, dark gray columns). Only a small amount was found in the first flow through. This was further confirmed by UV-Vis. The silica shell used to cover Fe_3O_4 NPs was not functionalized with a fluorescence dye, therefore specific peaks within UV-Vis data were not expected. Due to the NP color, an increase of the general absorption with decreasing wavelength was observed (see figure 3.10 a, orange and blue line). The retained sample showed generally the same absoprtion pattern as the original one. All flow through sections absorbed rather weak. These patterns could mainly be attributed to the chemicals that were used during the synthesis such as igepal.
SiO_2@MnO NPs were tested using a membrane with a higher cut-off size. The concentration of the original sample was much lower than that of SiO_2@Fe_3O_4 NPs. When all collected samples were characterized by AAS, it was shown that the retained sample showed the highest concentration compared to the flow through samples (see figure 3.10 b, light gray columns). When compared to the original sample however, this value could not be reached. As already mentioned, SiO_2@MnO NPs were also found inside the membrane and could not be washed off. Again, when UV-Vis was applied, a distinct peak was not expected due to missing attached dye. Generally the same trend described for the 50 kDa membrane was observed (see figure **??** c). However, one peak was seen for the original sample around 300 nm (orange line). The retained sample showed a shifted peak (blue line, shifted to 250 nm). This could be attributed to the fact, that chemicals used during the synthesis were washed off using the filter devices and did not interfere with the spectra anymore. The flow through sections showed

weak absorptions between 220 nm and 300 nm (black and red lines).
The use of Amicon filter devices should improve the purification of silica covered NPs drastically. So far, binding and separation of bioactive groups to these NPs was not successful but these NPs showed the most promising results for being used for bio-functionalization, especially since leaking of Mn was comparably low.

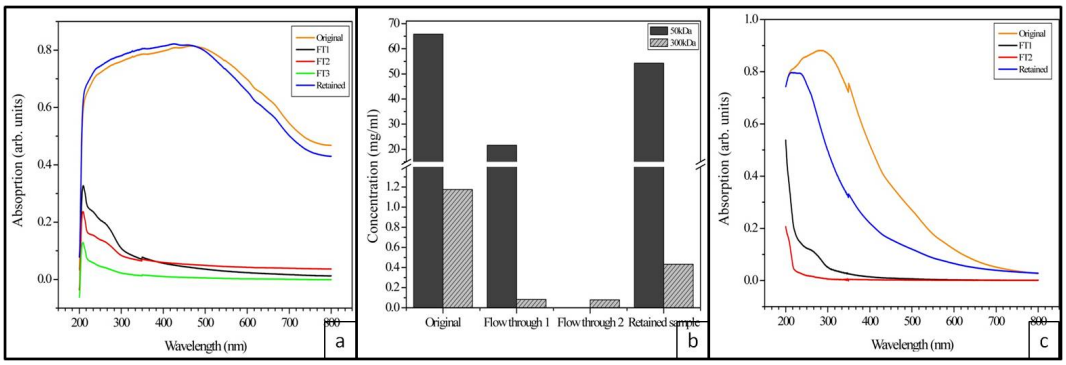

Figure 3.10: **UV-Vis and AAS results for silica functionalized magnetic NPs:** a: UV-Vis taken from the original sample, flow through and retained samples of SiO_2@Fe_3O_4 NPs after applying to amicon ultra filter devices. Centrifugable filter devices with a cut-off size of 50 kDa and 300 kDa were used. b: AAS results showing the Fe and Mn concentration of silica covered oxide nanoparticles thereof. The concentration is given in mg/ml. Black colums show results for SiO_2@Fe_3O_4 NPs tests with a 50 kDa membrane, gray curves show the results for SiO_2@MnO NPs and the use of a membrane with a 300 kDa cut-off site. Samples of this experiment were also characterized with UV-Vis (c).

3.4 Disussion and Outlook

The surface functionalization of MnO@Poly1 NPs was greatly improved by adding NHS to the coupling solution and by further dropping the pH from originally pH 7 to pH 4.5 using MES buffer. Although the presence of Poly(I:C) and Ova could be proven using different techniques such as Western and Northern blot, UV-Vis, agarose gel-electrophoresis and SDS-PAGE, the main question of how much was bound on the surface, could not be satisfactorily be adressed. During this thesis, the focus was shifted towards MnO@DA-PEG and MnO@PEG-Poly NPs which were monodispers and showed a long term stability. However, the main advantage of MnO@Poly1 NPs, meaning that excess polymer and excess proteins, DNA or RNA could be centrifuged off, could not be transferred to these NPs. Any trials using Amicon filters, dialysis bags or ultra-centrifugation (unpublished results by Steve Pr/"ufer), failed. As light scaterring experiments already showed (see 2), the amount of polymer was too high, possibly leading to micelles of DA-PEG or PEG-Poly. Gravimetric measurements confirmed this observation (data not shown). The first step should therefore be, to decrease the polymer amount upon MnO functionalization. As a second step, it is necessary to determine, how many addressable amino groups can be found on the surface of MnO@Poly1, but also MnO@DA-PEG and MnO@PEG-Poly NPs. It is possible to fluorescent dyes in combination with click-chemistry which will bind to the surface amines. The absorption level can then be used to determine the amount of amine groups. [65]. Once this factor is known, the coupling reaction can be modified accordingly. Further, the detection of the bioactive group needs to be improved. Pease et. al have used electrospray-differential mobility analysis (ES-DMA) to determine the coating thickness. [66] Using this system, they were able to estimate how much DNA was bound to their gold nanoparticles. Other have estimated the DNA content by using PAGE and ethidiumbromide staining. [67] Measuring zeta-Potential in combination with dynamic light scattering might be another possibility. [68]. Real time PCR is in addition a very interesting technique. This system is based in the use pf polymerase chain reaction (PCR), coupled with the introduction of fluorophores to the terminal site of the target DNA.[69] However, since Poly(I:C) does not show any encoding specicities, primers, used in the PCR reaction might not bind to the N- and C- terminus of the DNA double strand, leading to inhomogenities in the DNA amplification. Therefore, it is questionable if such a system might work. CpG on the other hand features all necessary sequence inhomologies. However, since this single strand is rather short, again, primer design might lead to difficutlies and false results. It has to be noted that so far, no standart technique has been described in the literature to allow the exact estimation of bound bioactve group. Without question, fluorophores, which

can be bound to DNA, RNA as well as protein, will help in this context.
SiO_2@MnO NPs are, to some extent, centrifugable. Therefore excess biogroups should be washed off. In addition, ultra-sentrifugation should allow the the separation between bound an unbound biogroup. Further, Amicon ultra filter devises can be used with much bigger cut-off sites than for MnO@DA-PEG. Smaller molecules should be easily washed off.
Modifications of RNA is a common technique to enhance the stability in blood or serum which is otherwise rather low for naked RNA (Kim, Review 2009). The focus of many publications thereby is the to bind the negatively charged RNA to polycationic polymers, lipids or cell penetrating peptides (CPPs) by electrostatic interactions. This bond seems to be strong enough so that a covalent bond is not necessary. Taking this detail into account, EDC coupling possibly is not necessary at all. Since the aminogroups of the peptide should additionally be positivly charged, PEG-Poly or DA-PEG do not need to be modified further. Theoretically, this concept should be transferable for CpG just as well. Contamination by EDC, NHS or MES is thereby not necessary anymore. So far, one issue of EDC coupling and simultaneous use of PEG-Poly or DA-PEG was that further washing steps did not follow to circumvent any cross contamination. All chemicals where thereby sterile filtered, possibly decreasing the chemical concentration, or, as for MES buffer, chemicals were autoclaved. Since EDC further hydrolyses in water, the efficiancy will be decreased. All these precautions will become abundant, once covalent binding will be abstained from.

CHAPTER 4

In vitro studies with different metal oxide nanoparticles

4.1 Introduction

Nanoparticles (NPs) are very promising candidates for drug delivery, tissue engineering or can be used for *in vivo* imaging. [6, 15, 16]. The application of NPs will without doubt increase in the years to come. Until mid 2006 alone, 130 nanotech based drugs and delivery systems have enterred pre-clinical or clinical trials, if not being in commercial development already. The same is true for 125 imaging and diagnostic devices. [70] However, the initial enthusiasm was muted by different studies, which accounted for unexpected side effects. [71] The influence of NPs are thereby not only focussed on systems deliberatly applied *in vivo*. In some cases, the contact happened without knowing about it. One of the most applied NPs are TiO_2. Due to their white color, they are present in cosmetics, sunscreens and in dental implants but also show promissing results for tissue engineering. [72] First considered as chemically inert, newer studies now revealed that they might promote pulmonary diseases and could enable the development of cancer. [72, 73] Another promising candidates are iron oxide NPs (MNPs, either Fe_3O_4 or γ-Fe_2O_3). First considerred as non-toxic due to the ability to be taken up by the host iron pool, evidences get stronger that MNPs influence macrophage driven diseases such as artheriosclerosis, rheumatic arthritis or neuroinflammation. [6] The fact that these NPs can also be found in the brain confirm that the blood brain barrier (BBB) can easily be bypasses, probably using the 4-5 nm sized gap-junctions. [74, 9] Since MNPs can undergo oxcidation via the Fenton reagent way, reactive oxygen species (ROS) can be produced in larger scale. [6]

MNPs are extensively studied, MnO NPs however are a rather young field and has not gained such great attendance.

Manganes is an essential trace element and is part of various metallo-enzymes such as the superoxide dismutase (SOD), puryvate carboxylase or the glutamine synthetase in the central nervous system which allows the reduce of the transmitter glutamic acid. [75] Mn is especially concentrated in tissues which feature a relatively high number of mitochondria such as the liver, muscles or the brain. Different *in vivo* studies have revealed that MnO_2 NPs have the ability to distribute within the host system (in the current cases rats) after NPs were applied by inhalation. These NPs were not exclusively found in the alveolar of the lung. Further, accumulations within the brain were observed. These studies clearly indicated that the natural borders can be easily overcome by MnO_2 NPs. [76, 75] However, these studies concentrated on MnO_2 NPs which were not checked for monodispersity or where surface modified in any given way. The MnO NPs used in this thesis however, were purposivly designed for enhanced body distribution and low toxicity.

However, its has become obvious that caution is necessary when NPs are used and that *in vitro* studies are necessary prior to extensive *in vivo* studies. This chapter is therefore dedicated to cell viability assay, focussing on MnO NPs functinalized with different polymers. In addition different composite materials such as Au@MnO were tested.

4.2 Experimental Section

Generally, the equipment and solvents mentioned in chapter 2.2 were used. In this chapter, the experimental procedures are mentioned, which were not desribed previously.

Materials: $FeCl_3$, was purchased from ABCR, Fe_3O_4 and CuO from Riedel-deHaen. The proliferation assay CyQUANT® NF Cell Proliferation Assay was purchased from Invitrogen. **Cell culture and toxicity assay:** The human renal cell carcinoma line (Caki 1) was kindly provided by the group of Prof. Dr. P Langguth, Institut für Pharmazie and Biochemie, Johannes Gutenberg-Universität, Mainz. Cells were grown in McCoys 5A media supplemented with 10 % fetal bovine serum (FBS), 1 % Penicillin-Streptomycin (PEST, 10000 U/ml Penicillin and 10 mg/ml Streptomycin) 2 mM L-glutamine, 1x Mycokill and 1x MEM non essential amino acids. Cell cultures were routinely grown in 75 cm^2 sterile cell culture flask and were contained at 37 °C, 95% relative humidity and 5% CO_2 until reaching the confluence of $2{,}1 \cdot 10^6$ cells/ml. The media was removed and adherent cells were washed twice with 1x phosphate buffer saline (PBS). Cells were collected by adding 1 ml EDTA-trypsin solution and the plate was incubated at 37 °C for 5 min. Trypsin was inhibited by adding 4 ml cell culture media. The combined sample was centrifuged at 1000 xg and the cell pellet was resuspended in 5 ml cell media supplemented as described above. The cell number in this sample was estimated by diluting 20 μl cell solution with 10 μl water and 10 μl trypan blue and applying this sample to a cell counting chamber (Fuchs-Rosenthal, Marienfeld) with a depth of 0.2 mm. The measurement was doublicated and the average cell number was used. The chamber factor of the cell counting chamber was 5000. Multiplying the average cell number with this value yields the cell number/ml, further mutliplication with the cell suspension volume (5 ml) leads to the overall cell number in the sample. Cells were then diluted and applied to a 75 cm^2 steril cell culture flask (final concentration 60,000 cells/ml) or were diluted acccordingly for the toxicity assay. The cytotoxicity assay was performed according to the supplier. Cells were grown in 96 well plates under standard conditions in 100 μL McCoys 5A. The density was 15,000 cells/well. In 6 wells only media was added to allow background subtraction. After 24 h of cell growth, different concentrations of MnO based nanoparticles functionalized with polymer or DA-PEG in McCoys 5A were added (10 μl sample + 90 μl cell culture media). NPs were sterile filtered using a mixed ester 0,22 μm filter prior to use. The incubation time was set to 24 h. After this period of time, the wells were washed twice with 50 μl PBS before CCK8 was diluted in cell culture media according to the supplier. Previous tests ensured that phenolred did not interfere with the measurments. Finally, the increase of the absorption at 450 nm was

measured using an ELISA plate reader. Results were normalized to a control sample.

Images of NP uptake by Caki1 cells: Cell images were done with the help of Anna Pietuch and Jan Rother in the group of Prof. Dr. A. Janshoff at the Universität Göttingen (Institut für Physikalische Chemie). Cells were cultivated on Isis plates using standard procedures described above. In a typical experiment, cells were grown until confluence was reached. MnO@PEG-Poly and MnO@Poly1 were added in a concentration of 400 μg/ml MnO@Poly1. Note that this concentration is not in regard to Mn as measured by AAS. The sample was centrifuged, dried and weighted before resuspending again in water. The concentration given here therefore is in accordance to MnO@Poly1. Excess nanoparticles were washed off using PBS. Lysosomes were stained using Lysotracker DND-22 blue. Cells were then observed using a fluorescence microscope.

Transmission electron micrographes: MnO nanoparticles were either dispersed in DMF or where surface functionalized using Poly1, PEG-Poly or DA-PEG. MnO@Poly1 was characterized while being in DMF, the other two samples were first transferred to water. Additionally, the pellet formed during the transfer of MnO@PEG-Poly and MnO@PEG-Poly kept in water at 4 °C was tested. For all cases, 2-3 drops of the corresponding sample was given to a TEM-grid and was dried at room temperature for 2 h (organic solvents) and up to 24 (water as solvent). All samples were measured on a Philips EM 420 TEM.

Cell culture and cytotoxicity-assay for HeLa. Cervical cancer cells (HeLa cells) were kindly provided by PD Dr. W. Brenner (Institut für Urologie, Klinik und Polyklinik, Universitätskliniken, Mainz). The HeLa cells were cultivated in accordance to Caki1 cells using RPMI 1640 media (Sigma-Aldrich, Germany) supplemented with 10 % FBS, 1 % PEST, 2 mM L-gluthamine and mycokill. Cells were incubated at 37 ° C, 5 % CO_2 and 95% relative humidity: CCK8 was used in accordance to previous described methods and the cells were incubated with this chemical for 3 h before the absorbance shift at 450 nm was tested. Wells without cells were used to allow background substraction. All results were normalized to wells that did contain cells, but where media was added instead of NPs.

Double in population: 1 ml of a 20,000 Caki1 cells/ml solution was placed into 24 well plates and incubated at 37 ° C, 5 % CO_2 and 95 % relative humanity. Every day for a total of 16 days the cell number was estimated by adding 100 μl trypsin for 5 min. The plate was placed back into to the incubator for this duration. 900 μl cell media was added to stop the trypsin digest and the cells were counted using a counting chamber. All results were tripled and the final cell number within the well was calculated according to the literature [77]. This step was repeated every day at roughly the same time. All results were plotted against the time.

Proliferation assay for Caki1 and HeLa: The proliferation for Caki1 cells and HeLa cells

was done by using the CyQuant proliferation assay kit provided by Invitrogen. For this test 96 well plates were populated with 15,000 Caki1 cells/well and 12,500 HeLa cells/well, respectively. Cells were incubated for 24 h before NPs were added. The corresponding sample and concentration is described in the experimental section. Cells were additionally incubated for 24 h and then washed with 50 μl PBS before CyQuant proliferation was added according to the supplier. In short 1x HBSS (provided) was diluted with the component A and B in a ratio 1:500 (for each component). 50μl of this solution was added to the 96 well plate and was incubated for 1 h at 37 ° C. The emission of the dye was measured at 538 nm (exitation 485 nm) using a ?. All results were tripled and normalized to cells incubated with media.

Isolation of mononuclear peripheral human blood cells (PBMC's): Human peripheral blood mononuclear cells (PBMC's) were isolated from healthy volunteers. Human lymphocytes were obtained by density gradient centrifugation using Ficoll (PAA Germany) as described by the manufacturer. Briefly, 22 ml of EDTA (2.7 %) containing blood solution was layered on top of 12 ml Ficoll and the two layers were centrifuged at 400 xg for 30 min at room temperature. PBMC's (monocytes, lymphocytes and basophiles) were collected at the interface and washed twice with RPMI 1640 cell culture media supplemented with 5 % FBS (PAA, Germany) and 2 % Penicillin-Streptamycin (PEST; Gibco, Germany) by centrifugation at 250 xg for 15 min. The final cell number was estimated using a Neubauer counting cell. Cells were cultivated in RPMI 1640 medium (PEST and 5 % FBS) at 37 ° C, 5 % CO_2 and 95 % relative humidity. Dilution of cell solution with Trypan blue (1:1) (Cat. No. T0887, Sigma-Aldrich, Germany) allowed the distinction of vital and dead cells. If not stated otherwise, the cell density used in all experiments was set to 5.38 mio cells/ml.

Cell viability assay (MTT based): A cell proliferation assay was performed using *in vitro* cell counting kit 8 (CCK8, Sigma-Aldrich, Germany). The peripheral blood cells were diluted to 5.38 mio cells/ml and were cultivated in 96-wells plate. The cells were incubated for 1 h and 24 h at 37 °C, 5 % CO_2 and 95 % relative humidity with given concentrations of DA-PEG functionalized MnO NPs (2.5, 6.5 and 10 μg final concentration) as well as $MnCl_2$ (6.5 μg final concentration). As control, the cells were incubated under the same conditions but without additives. After incubation, CCK8 (10 μL of 1:10 dilution) was added to each well and the plates were incubated for 3 h at 37 ° C, 5 % CO_2 and 95 % relative humidity and the absorption of the reduced formazan product measured at 450 nm using a 96-well plate reader (Titertek Multiscan PLUS, MKII, Rheinbach, Germany). All results were tripled and statistically evaluated.

Induction of ROS production in PBMC's: 10 mio cells/ml were incubated in a 24 well plate and were then supplemented with MnO@DA-PEG-NBD (5.5 μg/ml) for 1 h at 37 °C,

5 % CO_2 and 95 % relative humidity. Additionally H_2O_2 (27 μM) was added to this sample to start the ROS production. Afterwards, the cells were incubated with MitoSOX^{TM} Red mitochondrial superoxide indicator (M36008, Molecular Probes, Invitrogen, Karlsruhe, Germany) (4 mM) prepared according to the manufacturer's instruction (10 min, 37 ^{o} C).PBMC's were observed under a CLSM Nikon eclipse TE 2000-U. As control, cells incubated with MitoSOX^{TM} Red and H_2O_2 (27 μM) as well as both separated components were analyzed in parallel.

4.3 Results

4.3.1 Growth characteristics of Caki1 cells

Double in population of Caki1 cells: The renal human kidney cancer cell line (Caki 1) is an immortal, adherent cell line. As a first test, the double of population for this cell line was tested. Therefore, 20,000 cells/ well were grown in 24 well plates. For a period of 16 days, the cell number for each well was counted and the cell number was plotted against the incubation time. It was observed that roughly the first seven days the population did not increase much in number (data not shown). This changed drastically after one week to follow an exponentiel growth for about five days. After this time, growth decreased and eventually leveled off. In this time the population did not grow anymore due to limited space of these adherent cells within the wells. The population doubled after 11 days, which is in accordance to the literature [77].

Pretest for toxicity assays using CCK8 on Caki1 cells: When magnetic NPs, drugs etc. shall find their application *in vivo*, it is of utter importance that their toxicity is as low as possible. Therefore, *in vitro* assays are perfomed beforehand. Most experiments in this thesis were done with the renal human cancer cell lines (Caki1) but also with a human cervical cancer cell line (HeLa) and healthy peripheral mononuclear human blood cells (PBMC's), as will be described later in this chapter. Before cell cytotoxictiy tests could be performed, the optimal cell number for these tests needed to be estimated. For this purpose 96 well plates were populated with different number of cells (100 to 400 cells per ml) and were kept at 37 °C for 24 h and to a maximum of five days. After 24, 48, 72 and 96 h one plate was singlet out and the cells were washed with PBS prior to adding of cell counting kit 8 (CCK8) according to the supplier. Every 30 min for a total of 4 h the absorption at 450 nm was measured. All results were plottet against the incubation time and are shown in figure 4.1.
In all cases the absorption increased with the incubation time. This increase was also in accordance to the original cell number plated into the 96 well plates. The higher the cell number, the higher the absorption at 450 nm. The increase was linear in all cases, a stagnation was only seen after 96 h. This was also the only sample were the absorption was higher for the sample with 300 cells/ well than for 4000 cells/ well. After 4 days of incubation, samples whith such a high cell concentration possibly reached the limits of the wells, so that the nutritiens became low and cells deceased. Since the absorption after 24 h incubation did not lead to a platform formation, cells did not reach semiconfluent growth. Therefore as a second test, cells were grown again in 96 well plates for 24 h. Then, the wells were observed under an

invers microscope. The cell number was significantly higher in comparison to the previous test. Semiconfluent growth is considered condition when dealt with toxicity assays. The general setup of the plates is shown in table 4.1. After 24 h the sample B10 and B11 (15,000 and 20,000 cells/ well, respectively) reached semiconfluence growth, meaning that roughly half of each plate was populated with Caki1 cells. After 48 h incubation at 37 °C, well B9 reached this state, after 72 °C, wells B9-11 showed signs of starvation; B6-7 reached semiconfluence growth at this point. For all following experiments, if not stated otherwise, the cell number for a 24 h incubation with NPs was set to 15,000 cells/well and the incubation time for CCK8 was set to 3 h to be able to measure within the linear increase of CCK8 as was established with the previous cell experiments (see figure 4.1).

Table 4.1: Setup for population of 96 well plates with Caki 1 for semiconfluence growth.

Cells x100/ well	media	10	20	30	40	50	60	100	150	200
Well	B2	B3	B4	B5	B6	B7	B8	B9	B10	B11

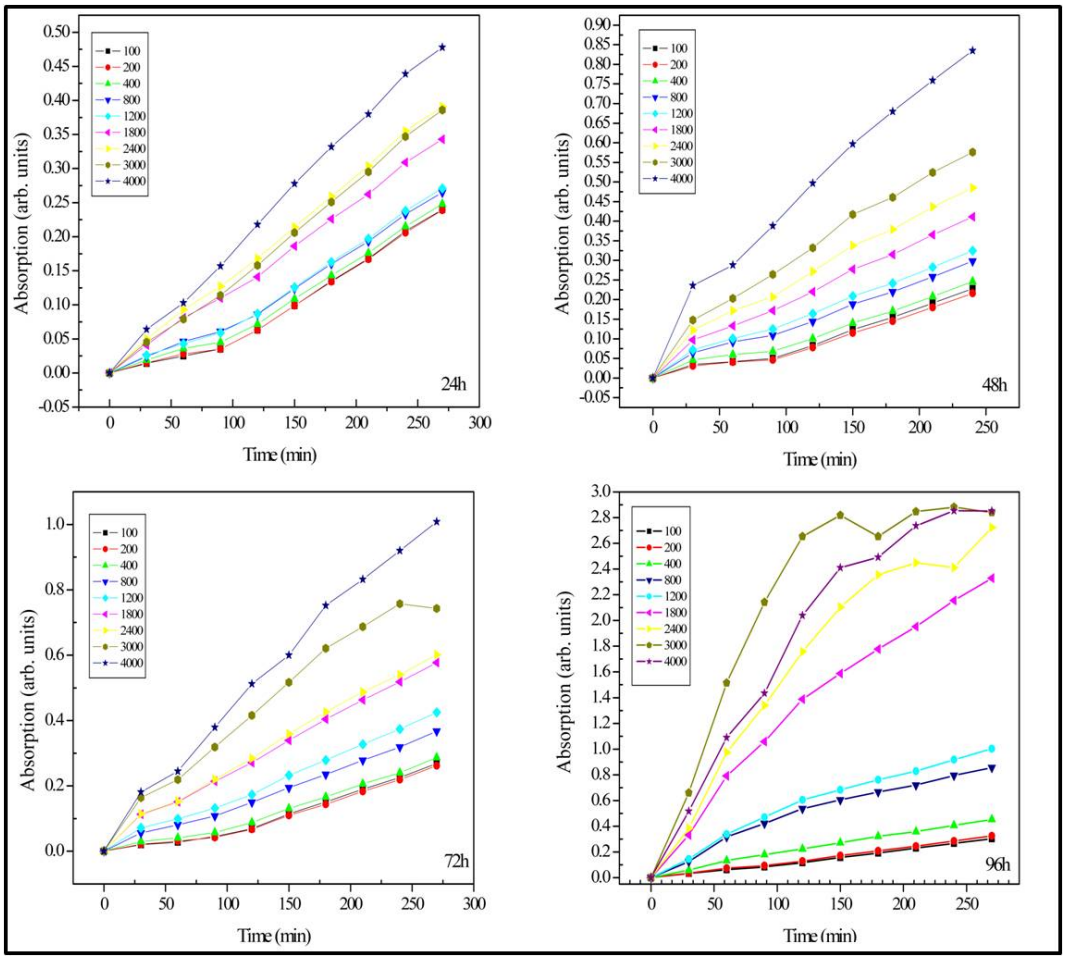

Figure 4.1: **Vitality pretest for Caki1 using CCK8:** Four 96 well plates were populated with different numbers of cells/ml and were incubated for 24, 48, 72 and 96 h. CCK8 was applied according to the supplier and the absorption at 450 nm was measured every 30 min for a total of four hours. All results were not modified any further but were directly plottet against the incubation time. Black: 100 cells/ml, red: 200 cells/ml, green: 400 cells/ml, dark blue: 800 cells/ml, light blue: 1,200 cells/ml, pink: 1,800 cells/ml, yellow: 2,400 cells/ml, brown: 3,000 cells/ml, purple: 4,000 cells/ml

4.3.2 Influence of the surface modification of MnO NPs

Manganese itself is a micro element and as such important for a healthy diet. However, when taken up in too high amounts, this element can also lead to toxic side effects. The influence of the surface moidification of MnO NPs were tested using Caki1. The vitality of these cells after being incubated with MnO@PEG-Poly, MnO@DA-PEG, MnO@Poly1 and SiO_2@MnO NPs, respectively, for 24 h was measured using the CCK8. Surface functionalized MnO NPs were diluted with cell media in a ratio NP:media 1:10 before application. Cells were thereby routinely grown in 96 well plates and were incubated for 24 h before NP application. CCK8 features a dye (WST8) which can be reduced by living cells leading to an increase in the absoprtion at 450 nm. Compared to control samples (only media added), the final vitality is obtained as percent in comparison to the control. The higher this value, the less toxic the applied sample. MnO@DA-PEG, MnO@PEG-Poly and SiO_2@MnO NPs were sterile filtered prior to use, MnO@Poly1 NPs could not be sterile filtered and were therefore applied directly. All results were tripled, the difference in each value allowed estimation of the error of this method. All results are given in figure 4.2.Two different concentrations of MnO NPs were tested, 10 μg/ml (dark gray) and 5 μg/ml (light gray). Concentrations are referred to the Mn concentration as was measured with AAS. Generally, it was observed that all values were above 60 $\%$. MnO NPs functionalized with different polymers or silica could therefore be considered as non-toxic. For each sample apart from $MnCl_2$, the difference between the single concentrations was evanascent small. The highest toxicity was observed for MnO@Poly1 NPs and Si_2O@MnO with a decrease of approximatly 20 $\%$.

Uptake of MnO@Poly1 and MnO@PEG-Poly NP in Caki1 cells: MnO@Poly1 and MnO@PEG-Poly NPs were applied to Caki1 cells with the help of Jan Rother and Anna Pietuch (AK Janshoff, Institut für physikalische Chemie, Universität Göttingen) and were then characterized using fluorescence microscopy. Due to the applied NBD dye, MnO NPs could be detected by the green fluorescent color. MnO@DA-PEG NPs were not applied, although DA-PEG-NBD could successfully be synthesized and MnO@DA-PEG-NBD NPs featured the NBD absorption at 550 nm (data not shown). The results for MnO@Poly1 NPs and MnO@PEG-Poly NPs are given in figure 4.2 b and c. Caki1 cells incubated with MnO@Poly1 NPs were pictured without an additional filter (see figure b.2) and with a filter that detects green fluorescence of NBD (see b.3). The overlay image of both showed that MnO@Poly1 NPs and Caki1 cells could be co-localized. This image however could not reveal whether NPs were taken up by the cell or were simply attached to the surface.
When MnO@PEG-Poly NPs were applied to Caki1 cells, the green fluorescence of the NBD

dye could again be detected. In addition, the lysosomes of the cells were stained with a blue fluorescence dye that binds to those cell particles that play an important role for the uptake of foreign particles into the cell. The green fluorescence of MnO@PEG-Poly NPs could be co-localized with the cellular lysosomes making it feasible to state that MnO@PEG-Poly NPs were taken up by Caki 1 cells via the endozytotic pathway.

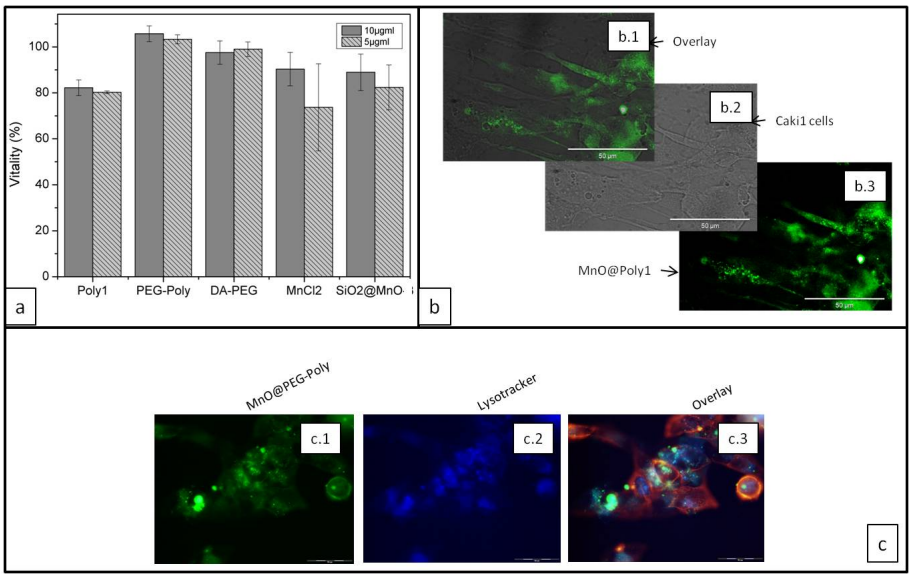

Figure 4.2: **Vitality assay for MnO NPs with different surface protection:** Caki1 cells were cultivated routinely in McCoys 5A media in 96 well plates. After 24 h, MnO NPs functionalized with either one of the used polymers or silica were applied after dilution with cell media in a ratio 1:10. Cells were incubated for 24 h and were washed using PBS. Upon incubation with CCK8 for 3 h, the absorption shift at 450 nm was measured and compared to a control sample. All results were tripled. b: Caki1 cells were incubated with MnO@Poly1. NPs thereby appear green due to the attached NBD-dye. Cells were also pictured without a fluroescence filter. b.1 shows the overlay picture. c: Caki 1 cells incubated with MnO@PEG-Poly NPs. Due to the attached NBD-dye, NPs showed a green fluorescence. c.2: Lysosomes of the corresponding cells were stained with Lyso-tracker which appeared blue. c.3 gives the overlay image.

4.3.3 Toxicity assays based on MnO@DA-PEG NPs

Toxicity of MnO@DA-PEG nanoparticles and the influence of their age: Poly-(ethylene glycole) (PEG) is FDA approved and finds regular use in numerous drugs to avoid fast clearance by the host immune system. MnO NPs that were functionalized with this polymer, displayed excellent water solubility and were stable when kept at 4 °C for months. Different charges of these MnO@DA-PEG NPs were tested *in vitro* using Caki1 cells. The diamter of the MnO core of these NPs thereby only differed slightly. The concentration was estimated using AAS and is given in accordance to Mn present in each sample. All used MnO@DA-PEG NPs are further described in table 4.2. Especially interesting was measuring whether these NPs displayed a different behavior towards Caki1 cells after being stored at 4 °C for a given time. All samples were set to a final concentration of 10 μg/ml. Generally, when working with cells, one has to keep in mind that cells can suffer osmotic shock once the cell media is diluted beyond a certain critical point. Dilution with water up to 10 % is considerred to be acceptable. Since the synthesis of magentic NPs is limited, the overall concentration of NPs present in one well could not be exceeded to 10 μg/ml. Therefore, the cell number itself was changed within a well. Cells were routinely grown in 96 well plates for 24 before different MnO@DA-PEG NPs were added by mixing 90 μl cell media with 10 μl NP solution. After in-

Table 4.2: MnO@DA-PEG NP composition that was used in different toxicity assays

Label of sample	Size of MnO core	Age in days
KS254-1	8 nm	12
KS254-2	8 nm	21
KS254-3	8 nm	44
KS254-4	8 nm	76
KS254-5	8 nm	91
KS254-6	8 nm	110
KS277-M	8.5 nm	28
KS304-1	8 nm	12
KS304-2	8 nm	27
KS304-3	8 nm	47

cubating Caki1 cells with the corresponding MnO@DA-PEG NPs for 24 h, wells were washed with PBS, CCK8 was applied and cells were again incubated for 3 h before the absorption of

the reduced dye of CCK8 was measured. The results were normalized to a control sample and were plottet in figure 4.3. Generally the results indicated that MnO@DA-PEG NPs were non-toxic for Caki1 cells, independently on the number of cells they were applied to, since all vitality results are above 60 %. This value is generally believed to be the critical value for cytotoxicity and non-cytotoxicity. With the exception of 254-1, 96 well plates, which were populated with less than 15,000 cells/well, were not as vital as the samples with the higher number of cells. This became rather obvious for the sample 177-M. The vitality increased from 70 % to 100 % when the cell number was doubled. Such a drastic observation was not made for sample 254. However, again with the exception of sample 254-1, another trend was obvious. Samples 254-2 to 254-5 were all taken from the same mother solution, which was steril filtered before use. The difference between these samples was the time between synthesis and toxicity assay. The longer these period was, the less toxic the NPs become (254-2: vitality of 68 % to 254-5: vitality 98 %). This behavior was stepwise and again independent of the cell number. However, the process was not as drastic for samples applied to 15,000 cells/well. The same was true for the sample 304 which was freshly prepared for these tests. The freshest sample was 12 days old and displayed a vitality of 90 %, wherease the oldest sample was nearly three times as old and displayed nearly no toxic effects (304-3). All samples however, displayed a higher vitality than sample 254 applied at roughly the same time frames (e.g. 254-2, 21 days versus 304-2, 27 days or 254-3, 44 days and 304-3, 47 days). This might be attributed to the fact that the samples 254 were applied to less cells thereby increasing the concentration of MnO@DA-PEG per cell. Interestingly between the 12 days old sample 254-1 and the 12 days old sample 304-1, there seemed to be no differenc in vitality.

Influence of cell media dilution on cell viability: Due to synthetic restrictions, MnO NPs could not be created in concentrations higher than 100 μg/ml. To avoid stressing the cells, this solution was then diluted 1:10, thereby reducing the concentration even more. To test whether the 1:10 dilution step with cell media was required, samples were created with a higher amount of NPs by mixing 100 μl solution with no cell media, 75 μl NP solution with 25 μl cell media and 30, respectively 17 μl with 70 and 83 μl cell media. As a control, water was mixed with cell media in roughly the same steps. Cells were incubated for 24 h and the toxic effects were tested with CCK8. Figure 4.4 a displays the results.
In general it can be stated that the toxicity increased with decreasing media amount of the applied sample. The highest decrease in vitality was reached when the complete media was replaced by water or NP solution (100 μl/well). When more and more of the applied sample was replaced with media, the viability of Caki1 cells increased again to be completely restored

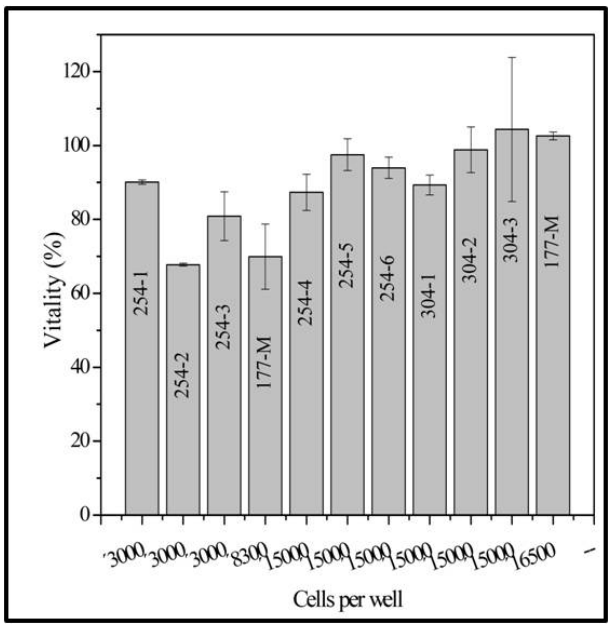

Figure 4.3: **Toxicity assay for MnO@DA-PEG NPs:** Caki 1 cells were incubated with MnO@DA-PEG NPs. All NPs featured a MnO core that slightly differes in core size (see table 4.2). The amount of the cells within the well differed between 300 and 15,000 cells/ well. CCK8 was used for the toxicity assay. All results were normalized to a control sample.

when the cell media was diluted 1:10 with water. MnO@DA-PEG NPs did not reach the vitalities as was observed before (see above). These results however, clearly state that a change in ratio below 1:10 is not possible since the decrease in nutrients for the Caki1 cells influences the result.

Reactive oxygen species formation: Some of the toxic behaviors that were observed due to this study might occur from reactive oxygen formation within the host cell. A rather sophisticated system to test for this formation is the use of Mitosox Red. This dye can cooperate into the cell and targets the cell mitochondria where most of ROS is usually formed. Upon oxidation, the dye excibits a red fluorescence that can be either detected using a fluorescence microscope or a plate reader which can detect fluorescence. When Caki1 cells were incubated with this dye, ROS acitvation was induced with H_2O_2. A difference between these cell samples and untreated cells was not observed (data not shown). Probably this was due to the fact that cancer cells have a very active metabolism leading to a increased ROS production.

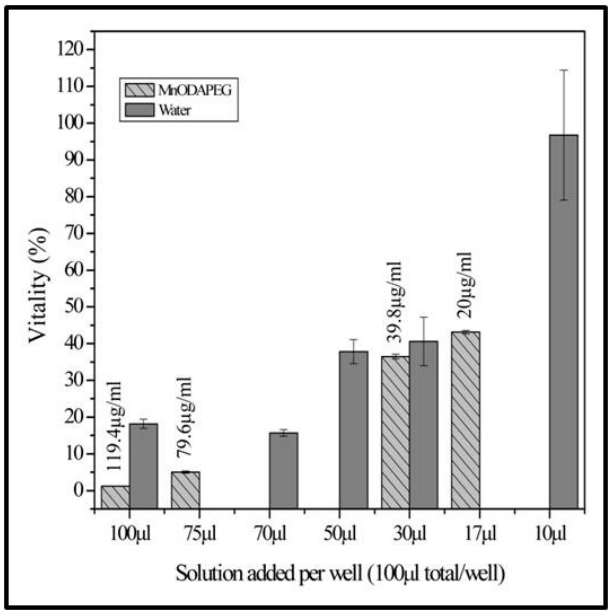

Figure 4.4: **Influence of dilution and surface functionalization on cell toxicity:** Caki1 cells were cultivated in 96 well plates. The toxicity was estimated using cell counting kit 8 (CCK8) according to the supplier. a: Caki1 cells were incubated with water (100 μl, 75 μl, 50 μl, 25 μl and 10 μl). All samples were topped up with cell culture media to 100 μl. The same was done for a steril filtered samples of MnO@DA-PEG NPs.

4.3.4 Toxicity of MnO and Fe_3O_4 based composite NPs:

Not only MnO NPs were tested in regard to cell compatibility but also composite NPs that featured either MnO or Fe_3O_4. Samples were kindly provided by Heiko Bauer (SiO_2@MnO) and Bahar Nakhjavan (FCu19-2, FCII-I, B52, B53) and were functionalized with DA-PEG if not stated otherwise. The latter ones were not sterile filtered. All samples are further described in table 4.3. Additionally $MnCl_2$, $FeCl_3$, Fe_3O_4, $CuCl_2$ and CuO were solubilized in water using an ultrasonic bath and were applied to allow analogy studies between NPs and bulk material.

Table 4.3: MnO and Fe_3O_4 based NPs were tested on Caki1 cells.

Label	**Composition**	**shape**
FePt	MnO-FePt	cubic (Paper von Oskar checken)
$FeCl_3$	aqu. solution of $FeCl_3$	
Fe_3O_4	aqu. solution of Fe_3O_4	
FCu19-2	$Cu_xFe_{3-x}O_4$	spherical
ptF-1	Pt-Fe_3O_4	dumbell-like
FCII-I	Co-Fe_3O_4	rhomboid
B52	Cu-Fe_3O_4	cloverleaf
B53	Cu-Fe_3O_4	cubic
$CuCl_2$	aqu. solution of $CuCl_2$	
CuO	aq. solution of CuO	
278	Au@MnO	dimers (6 nm Au, 25 nm MnO)
280	Au@MnO	dimers (9 nm Au, 20 nm MnO)
281	Au@MnO	nanoflowers (13 nm Au, 25 nm MnO)
$MnCl_2$	aqu. solution of $MnCl_2$	
SiO_2@MnO	MnO core + SiO_2 shell	spherical

Fe-based NPs: The first NPs that will be discussed here are iron based NPs. All particles were applied by diluting 10 μlNP solution with 90 μl cell culture media. After 24 h, the toxic behavior was mesaured by decreased absorption at 450 nm compared to a control sample. The results are given in figure 4.5 a. MnO-FePt NPs were functionalized with DA-PEG and were sterile filtered prior to use. The final concentration in the 96 well was 5-10 μg/ml. Addition-

ally $FeCl_3$ was added in a final concentration of 10 μg/ml. This sample was prepared in water without steril filtration. Platinum based chemotherapeutical drugs are in regular clinical use to fight cancer. Therefore, it was somewhat surprising that the toxic effect was with 18 $\%$ for 5 μg/ml and 30 $\%$ for 10 μg/ml rather low compared to almost 50 $\%$ decrease in vitality for $FeCl_3$. When the cell number was reduced to 3000 cells/well however, the vitality for MnO-FePt NPs (8.6 μg/ml) was decreased to 10 $\%$ (data not shown) so obviously the toxic effect of these NPs was dependent to the cell concentration. Additional iron oxide NPs were tested that were further functionalized with Copper or Cobalt. These NPs could not be synthesized in greater amount which is why the concentration had to be kept low. Due to this, samples were not steril filtered prior use to not lower the concentration any further. Pt-Fe_3O_4 NPs (pTF-1) thereby showed the same toxic behavior as MnO-FePt NPs with a 100 fold higher concentration. Rhomboid shaped Co-Fe_3O_4 NPss (FCII-I) displayed the second most toxic behavior of all Fe_3O_4 NPs, although these NPs were rather diluted. Spherical $Cu_xFe_{(3-x)}O_4$ NPs (FCu19-2) were even more toxic, however their concentration was more than double of the Co-Fe_3O_4 NPs. Interestingly Fe_3O_4 itself was not toxic to the cells (viability nearly 100 $\%$) but when a solution of $FeCl_3$ was added in a five fold higher concentration, the toxicity changed drastically. Copper itself also lead to a response by Caki1 cells. In this case the oxide was not as toxic as $CuCl_2$ (viability 70 $\%$ compared to 20 $\%$). However, a direct comparison was not possible since the concentration of both differed. A difference between cloverleaf shaped Cu-Fe_3O_4 NPs (B52) and cubic Cu-Fe_3O_4 NPs (B53) could not be observed.

Au@MnO based NPs: Au@MnO NPs were further tested. The synthetic route for these NPs can be altered in such a way that either nanoflowers or nanodimers are formed. Nevertheless, all samples featured an Au core surrounded by MnO NPs. To enable water solubility, all samples were functionalized with DA-PEG and were diluted with cell media in a ratio 1:10 to form a final concentration of 10 μg/ml. After incubating the cells with NPs for 24 h the vitality was tested using CCK8. The difference between each sample is described in table 4.3. Due to the synthetic route, generation of equally sized Au cores was rather difficult. Therefore, to allow for comparison, the dimer sample 278 and the nanoflower sample 281 were compared since both samples have MnO NPs with approximately the same size (25 nm). Interestingly, when the Au core as well as the shape of the NPs was changed from dimer to nanoflower like shape, the reaction of Caki1 cells were roughly the same. The vitality decreased by 5 $\%$. However, when the shape was kept as a dimer, the MnO pedals were de- and the Au core increased, the vitality deacreased by 20 $\%$ (see 280). All three samples were further tested over a period of 4 weeks. For this purpose not only Caki1 cells but also HeLa cells were

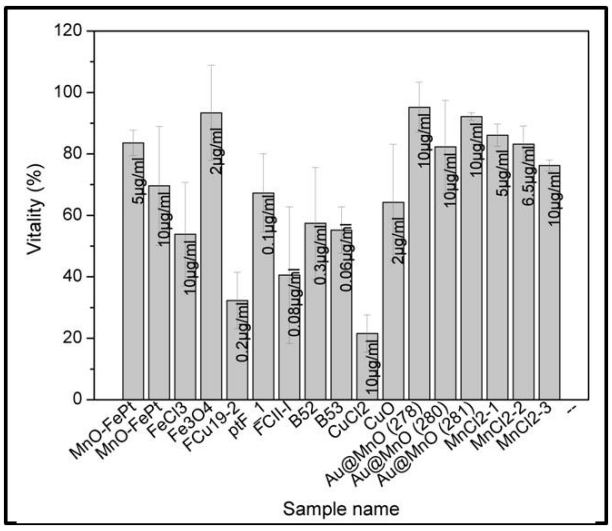

Figure 4.5: **Toxicity assay for metal oxide NPs of different compositions:** Caki1 cells were incubated with different metal NPs for 24 h. In some cases the synthesis of these NPs did not allow for the use of high concentration. The final concetrations are given as label in the plot. After washing CCK8 was applied according to the supplier. All results are normalized to the control.

tested. The latter once were tested twice wherease Caki1 cells were tested three times in total. A trend in the vitality results, as was observed for MnO@DA-PEG NPs, was not observed (data not shown), however, both cell lines reacted the same way. In both cases the vitality was muted for all samples when tested for the second time. These values then increased again for Caki1 when tested a third time. As a result, they reached the same values as the first test for the sample 278; remained static for 280 and increased by 30 % above the control sample for Au@MnODA-PEG NP sample 281. Since both cell lines showed decreased vitality for the second test, there seemed to have been problems with the incubation chamber, media etc. rather than the NP age beeing involved.

4.3.5 Behavior of different cell lines towards toxicity and proliferation

Toxicity assay for Caki1 and HeLa cells: MnO@DA-PEG NPs and Au@MnO NPs were tested. All samples were surface functionalized with DA-PEG and are described in table 4.3 and 4.3, respectively. Generally, both cell lines were treated as already described above. 96 well plated were populated with 15,000 cells/well Caki1 cells and 12,500 HeLa cells/well. A test prior the assay confirmed that HeLa cells do grow faster than Caki1, meaning that 12,500 cells/well were already sufficiant to allow semiconfluent growth after 24 h. Cells were incubated with NPs in a dilution of 1:10 with cell media. The final concentration was 10 μg/ml. After an additional incubation time of 24 h, CCK8 was applied and the absorption was measured at 450 nm. All results were tripled and compared to a control sample. For the proliferation assay, CyQuant was used according to the supplier by mixing component A and component B in a ratio of 1:500 in HBSS buffer. 50 μl of this solution was added to the wells after washing twice with PBS. The samples were incubated for 1 h at 37 °C and were evalutated by measuring the emission at 538 nm (extinction was set to 538 nm). All results were tripled and normalized to a control sample.

Toxic behavior of MnO NPs: The first results discussed here will adress the vitality differences between the cell lines towards NP application. The results are plotted in figure 4.6 C. This plot shows that Au@MnO NPs did not show significant loss of vitality for Caki1 cells. Only when dimer sample 280 was applied, the vitality was slightly decreased. The same was true for MnO@DA-PEG NPs, albeit both samples showed a decrease of roughly 5 $\%$. HeLa cells generally displayed the same behavior towards Au@MnO NPs. When the size differences between the Au core and the MnO dimers got lower, the vitality of the cells decreased. However, this effect was much more pronounced for HeLa cells than for Caki1 cells. On the contrary, for the two samples with identical MnO sizes (25 nm, sample 278 and 281), the vitality increased to be even higher than the control sample. MnO@DA-PEG NP sample 254 displayed the same behavior than the Au@MnO dimer NP sample 280, wherease $MnCl_2$ and the sample 304 displayed toxic behavior.

Proliferation versus vitality: The vitality assay used in this thesis is based on the fact that living cells have numerous enzymes that can oxidize and reduce chemicals that are added from the outside. CCK8 is a dye that gets reduced by electron carriers. CyQuant works on another basis. In this case, a fluorescence dye is applied that binds to the DNA of living cells.

A membrane carrier that is also provided enables that this component is directly transferred to the nucleus of the cell. The higher the resulting emission of the respective dye, the more DNA is present. Figure 4.6 A shows the results for Caki1 cells. All values of proliferation were higher than those for vitality. In addition, apart from $MnCl_2$ and MnO@DA-PEG sample 254, the proliferation values were higher than the control. Discrepancies ranged between 40 % (sample 278) and roughly 20 % (samples 280 and 281). Proliferation does not state whether a compound is toxic or not. It only states, whether the proliferation of a sample is hindered or not. The number of apoptic or necrotic cells cannot be determined with this method. A direct comparison between the toxicity assay and the proliferation assay is therefore not possible. However, a combination of both will lead to a better understanding of the influence of nanoparticles on the cell.
When HeLa cells were tested, a correspondance between toxicity and proliferation, as was observed for Caki1 cells, did not occure. Au@MnO NPs lead to an increased proliferation when dimers were present (sample 280) but was lower than the control for the other two samples. In this case the proliferation was lower than the vitality. Proliferation was higher than vitality for both MnO@DAP-PEG NP samples. For the fresher sample the proliferation did distinctly increase to 130 % what is even more than double the value of the vitality assay. The same was true for $MnCl_2$. Finally the proliferation values of Caki1 cells and HeLa cells are plotted in figure 4.6 D. Both cell lines corresponded well in proliferation means for the NP sample Au@MnO 280 as well as MnO@DA-PEG NP sample 254. In all cases the proliferation was 100 % or slightly elevated copmared to the control sample. A muted elevated proliferation was observed for the samples $MnCl_2$ and dH_2O for Caki cells. An increase by 30 % was observed for the NP sample MnO@DA-PEG 304 wherease the proliferation for Au@MnO NP sample 278 was 40 % above the control sample for Caki1 cells. Generally it has to be stated that the proliferation did not decrease significantly below the control sample for either one of the cell lines. The change in vitality therefore probably does not occur on the proliferation level.

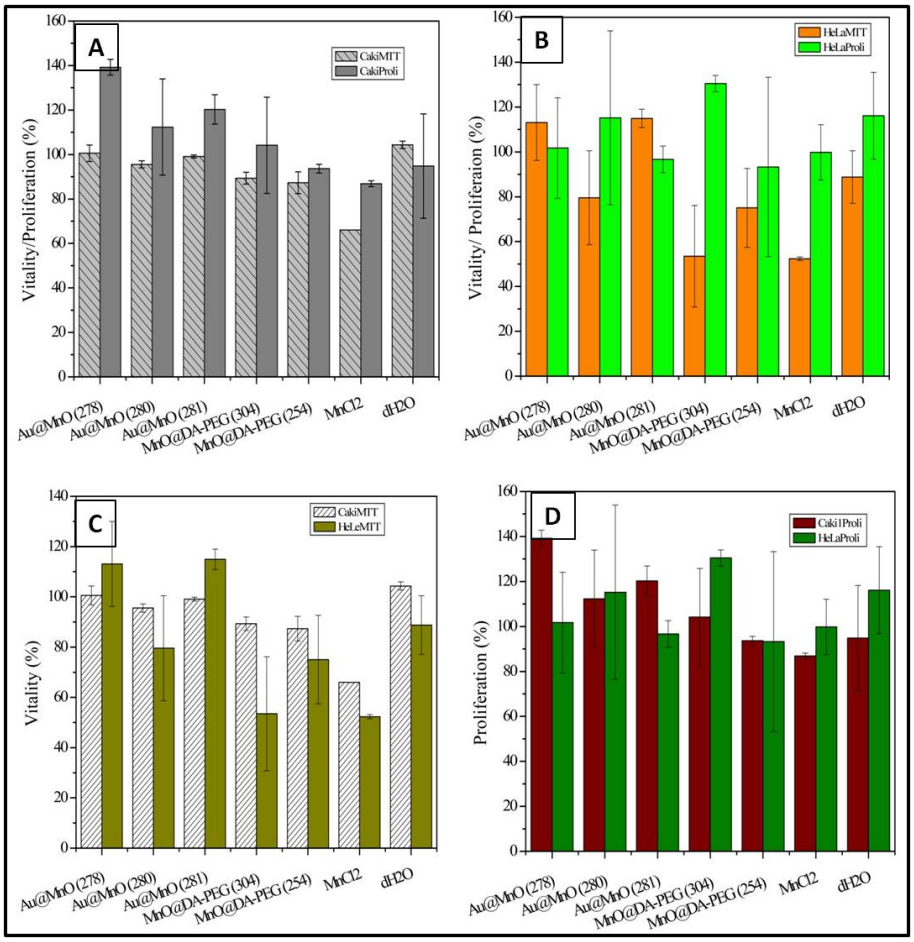

Figure 4.6: **Toxicity and proliferatin assay for Caki 1 and HeLa cells:** Caki1 cells and HeLa cells were routinely grown in 96 well plates. For Caki1 15,000 cells/well and for HeLa 12,500 cells/well were used. Both population showed semiconfluent growth after incubating for 24 h. Different NPs were diluted with cell media until a final concentration of 10 μg/ml was established. For toxicity test, cells were washed and then incubated with CCK8 according to the supplier (MTT). The proliferation was tested using CyQuant NF proliferation assay in accordance to the supplier. All results were normalized to samples containing media. A: Proliferation (light gray) and toxicity (dark gray) assay for Caki1 cells. B: Proliferation (light green) and toxicity assay (orange) for HeLa cells. C: Toxicity assay for Caki1 (white) and HeLa cells (dark yellow). D: Proliferation assay for HeLa (dark green) and Caki1 cells (red). For all cases the same NP samples were used.

4.3.6 Mononuclear peripheral human blood cells (PBMCs)

Testing metal oxide NPs on human cancer cells can already give an indication of whether these samples are suitable as a drug carrier or work as contrast agents. If the vitality is not significantly increased, the tumor will not grow on NP application. If this value is not decreased to a low level, the tumor will not lead to necrotic tissue that then might find access to the blood vessels, spreading surviving cancer cells though the body. However, all these tests cannot state how healthy cells will react to the applied NPs. Therefore, mononuclear human peripheral cells (PBMC's) were isolated and were incubated with different samples of NPs. Unlike cancer cells, the cell culture of these cell types is rather difficult. Cells still feature the growth arrest and cannot be kept as immortal cell line. Therefore, all cell samples were isolated freshly and were then directly incubated with NPs. The viability was then again estimated using CCK8 and control samples.

Viability assay: The focus of these experiments was laid on MnO NPs functionalized with DA-PEG. These experiments were done with the help of PD Dr. J. Brieger, HNO, Universitätsklinik Mainz. The PBMC's were taken from healthy volunteers and were isolated using a Ficoll gradient system. This is based on a synthetic polysaccharid of succrose and epichlorhydrin. The rather big erythrocytes and eosinophils are concentrated at the bottom of the tube after centrifugation. Lymphozytes, basinophiles and monocytes can be found at the interlayer and can then be collected. For this purpose blood was mixed with EDTA to avoid clogging. This sample was diluted with PBS and was then slowly added to Ficoll covering this polysaccharid. Subsequently, separation was achieved by centrifugation. Figure 4.7 shows a sample before and after the centrifugation step. When freshly added, the sample still has its characteristic red color which originates from erythrocytes. After centrifugation, these cells accumulated at the bottom, wherease the yellow blod plasma can be found on top of Ficoll. The targeted colorless cells (PBMC's) were concentrated at the interface layer between the plasma and Ficoll. In all preparations that followed, some erythorcytes remained in the interlayer staining the final sample slightly red.

Cells were counted using a Neubauer cell counting plate. The cell sample contained monocytes, lymphocytes and basophiles. The cell size of each cell type varied, thereby making it hard to distinguish between each cell type under the microscope making counting dificult. A routinely used method for cell counting is the Casey 1TT counter. In this totally computer controlled systems, cells run on a column and get separated according to their size. In this system, dead cells run faster than those alive, allowing theoretically an easy distinction. PBMC's

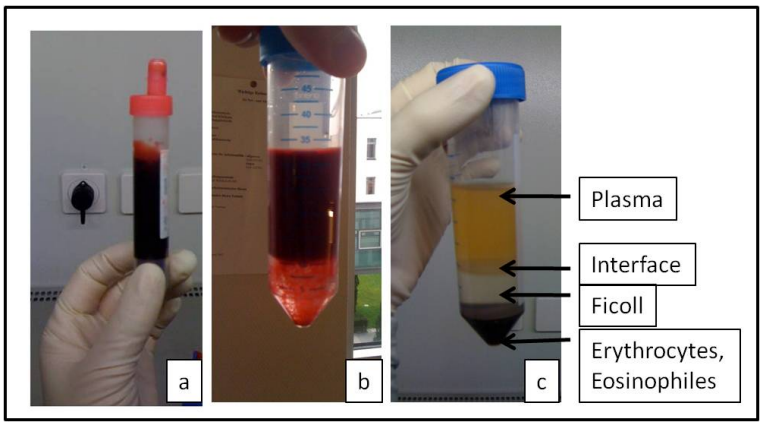

Figure 4.7: **Isolation of PBMC's:** PBMC's were isolated using a Ficoll gradient system. a) blood was taken from healthy volunteers and was mixed with EDTA to avoid clogging. b) After dilution, the sample as applied to Ficoll in a 50 ml centrifugal tube and was then centrifuged to allow separation of blood plasma, erythrocytes and eosinophiles (c). PBMC's were collected at the interface.

were either directly applied to this system (Lymphos-1 and -2, respectively), or were incubated with Casy-blue, a chemical that deliberately kills all cells within the sample. All results were recorded and are given in figure 4.8.

The cell debris of dead cells had a rather small diameter and therefore eluated quickly from

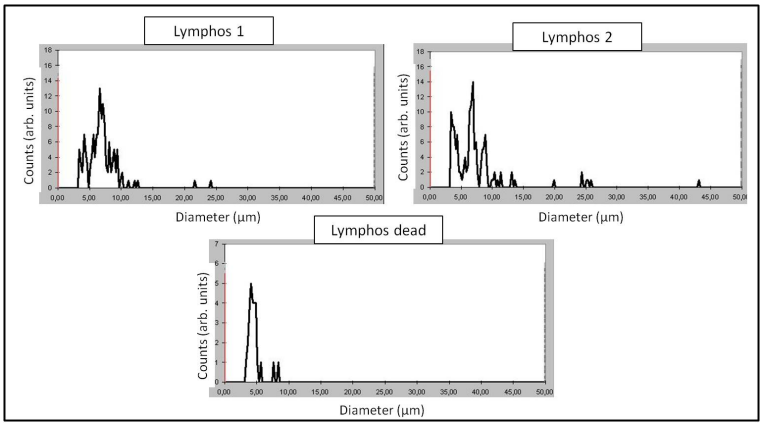

Figure 4.8: **Separation of different cell types using Casy 1TT:** Freshly prepared samples of PBMC's were loaded on the Casy 1TT cell counting apparatus. One sample was thereby measured twice (Lymphos-1 and -2). Cells were further killed with Casey blue and were loaded on the system to allow comparison to living cells.

the column (Lympho dead). Some counts were collected later but were rather small. However, when freshly prepared PBMC's were loaded, numerous counts were also collected at around

2.5 μm which can either be attributed to cell debris or the monocytes. The next major peaks were collected between 5-10 μm. This sample was measured twice (Lymphos-1 and -2). Both patterns however were not identical, making it immpossible to distinguish between single cell types. This method therefore was not suitable for cell separation and cell counting. For this reason, cells were incubated with trypan blue, a chemical which allowed to distinguish healthy cells from dead ones. The cell number for cell viability assays was set to 5.38 mio cells/ ml which equals 0.538 mio/ well. PBMC's were rather unstable and could not be kept for a longer time. Therefore, cells were incubated with MnO@DA-PEG NPs by adding 10 μl of the NP solution to 100 μl cell suspension in 96 well plates. The final concentration of these NPs was set to 2.5, 6.5 and 10 μg/ml. The incubation time was set to 1 h and 24 h, respecitvely. CCK8 was added according to the supplier and the absorption was measured at 450 nm. PBMC's are not adherent, therefore any washing steps were abstained from. Separating NPs from cells by centrifugation led to imprecise results which was why this method was not used. Control samples of media with NPs ensured that these samples did not have any influence on CCK8. The resulting absorptions were normalized to media containing samples and are shown in 4.9. The vitality for cells that were incubated with NPs for 24 h was higher than for those with a shorter incubation time. This behavior could be observed for all samples were manganese was present. When water was added as a control sample, the vitality stayed at nearly 100 $\%$ and was independent of the incubation time. A second general trend showed that the vitality of all samples was below 60 $\%$ leading to the conclusion that the NPs showed toxic behavior towards PBMC's. The vitality decreased with increasing Mn concentration after incubation for one hour. When additionally H_2O_2 was added, the vitality was comparable to that of MnOIII (10 μg/ml). $MnCl_2$ did not show such a drastic effect for cells incubated for one hour. When the incubation time was increased to 24 h, the results were all roughly at the same value. The highest vitality was reached for cells incubated with MnOII (6.5 μg/ml).

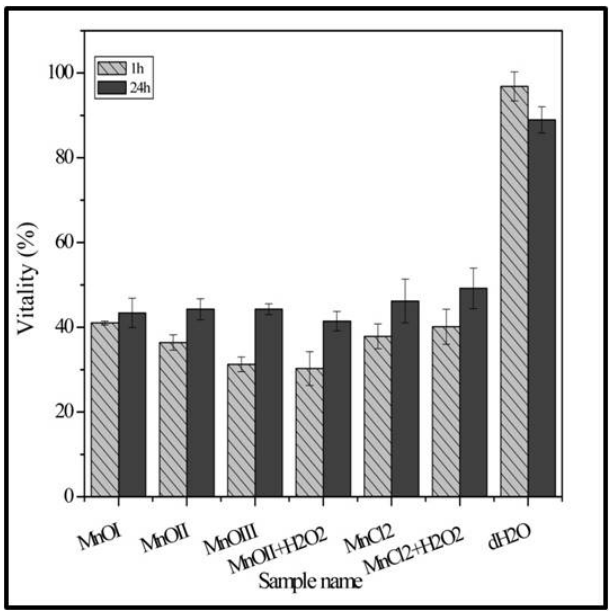

Figure 4.9: **Vitality assay for PBMC's** Peripheral mononuclear human blood cells incubated with MnO@DA-PEG NPs of different concentrations (MnOI: 2.5 μg/ml, MnOII: 6.5 μg/ml, MnOIII: 10 μg/ml) and as comparison $MnCl_2$ in solution (10 μg/ml). Additionally H_2O_2 was added to allow ROS production. The incubation time was 1 h to 24 h and the cell number per well was 0.538 mio and the vitality was estimated using CCK8 compared to a control sample.

Reactive oxygen species generation: Cells can undergo apoptosis after they are exposed to reactive oxygen species (ROS). These can be formed e.g. after irradiation but also natuarlly as a side product within the mitochondria or other metabolic incidents. ROS formation can also be induced by chemicals such as H_2O_2. The ROS formation can be measured by using specific dyes such as Mitosox Red. 24 well plates were populated with PBMC's and were incubated with MnO@DA-PEG-NBD NPs (5.5 μg/ml) for one hour before Mitosox Red was applied according to the supplier. ROS production was activated by adding H_2O_2. The cells were observed with an invers microscope. As can be seen in figure 4.10 staining was most successful when ROS production was induced by adding H_2O_2. This effect was weakend when MnO@DA-PEG-NBD NPs were added (MnOII).Interestingly successful staining was significantly lowered when both, NPs and H_2O_2 were added to PBMC's. When compared to images which showed all cells, it became clear however that the concentration of MitoSox Red was not high enough to induce staining in all cells (data not shown).

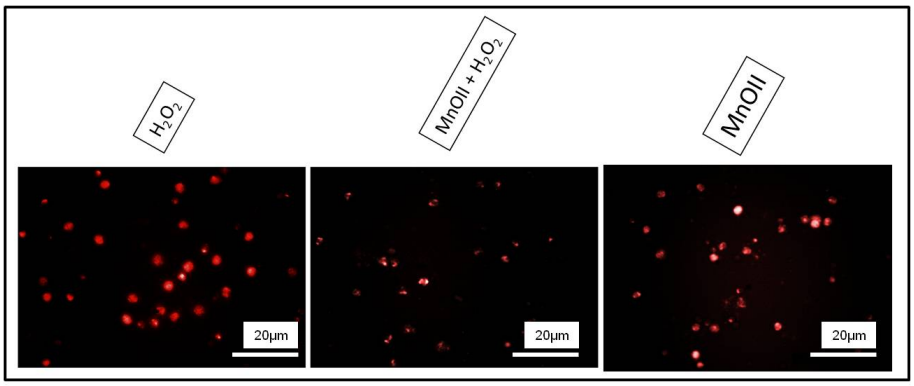

Figure 4.10: **Microscopic images of PBMC's co-incubated with Mitosox Red:** 24 well plates were populated with 10 mio PBM cells/ml and were incubated with MnO@DA-PEG-NBD NPs (5.5 μg/ml). One sample was incubated with H_2O_2 or both, respectively. Cells were stained with Mitosox Red and were observed under a CLSM.

4.4 Discussion and Outlook

It is of general believe that toxic side effects are influenced by the size and the shape of nanomaterials as well as the surface modification thereof. [70] The studies which are described in this chapter focussed on the influence of mainly sperical NPs on Caki1 cells and HeLa cells. Thereby, the viability and proliferation was tested for both cell types and different NPs. In addition, the influence of the preparation time and the storage time was tested in regard to MnO NPs. The influence of the size and shape of these NPs were tested as well as the influence of the chemical nature. Although the choice of the used cells were also dependent on the accesibility, it is reasonable to use kidney cells for toxicity studies, since it could be shown that numerous NPs preferentially accumulate in the kidney or are excreted via the renal pathway. [78]

This studie showed that any toxic behavior was independent to the choice of surface functionalization using different polymers or silica. MnO@Poly1 NPs showed a decrease in the viability of about 20 %, which needs to be dedicated to the observed agglomerates. Possibly due to those polymers, the membrane structur of the cells was altered, thereby leading to the observed toxicity. The dicrease observed for SiO_2@MnO NPs cannot be attributed to their size. Interestingly, upon increasing the concentration to 30 μg/ml within one well, the viability was restored completely to 100 % (data not shown). This result clearly demonstrated that additional tests are necesarry. The low overall toxicity however, might be attributed to PEG which was present on all NP samples applied. This polymer is known for its non-fouling properties, has FDA approval and several drugs have been modified with this compound to allow enhanced body distribution.

Although DA is considerred to be an ideal anchouring group, critical remarks can be found. Firstly, catechols can be oxidized rather easily under aerobic conditions, leading to dark and insoluble polymers. Further, DA can react in a redox dependent way with the surface atoms of the metal oxide NPs which they are supposed to protect. [15] Studies focussed on Fe_3O_4 NPs so far, implicating that these clusters can decompose in the presence of DA by forming a Fe-semiquinone intermediate. [79] MnO@DA-PEG NPs did not show such a behavior (unpublished results Filipe Natalio). However, it cannot be excluded that DA has an influence on the oxidation state of MnO NPs and could be the reason for the observed Mn leaching (see chapter 2).

If DA-PEG accelerates the Mn leaching, it could also explain the decrease of the toxicity for long term cell culture tests. It was observed that there is a connection between the age of the MnO@DA-PEG NP sample and cell viability. The older the sample, the less toxic are those

for Caki1 cells. If the amount of Mn leaching is greatly enhanced for the older MnO@DA-PEG samples, the amount of free Mn ions should be higher in this samples. Since ions cannot enter cells that easily and since MnO@DA-PEG NPs are taken up activily, the size and possibly the number of MnO@DA-PEG NPs is smaller for older samples. Therefore, less cells are effecteda and the viability increases. Such a behavior was observed for Ag NPs and escherichia coli. The group of Prof. Dr. H. Lappin-Scott thereby came to the same conclusion, supporting the observations taken here (unpublished results). Mn ions are diluted with the applied cell media. The incubation time thereby is with 24 h possibly short enough, so that the nutrients within the media are adequate and a short increase in the Mn content does not influence the growth of Caki1 cells.
Generally, the effect of MnO NPs *in vitro* are not studied as extensively as for iron oxide NPs. However, the general observations correspond well with tests done by Choi et al., [80] where MnO NPs and Fe_3O_4 NPs were functionalized with DA-PEG and were incubated with different cell types, one being lung cancer cells A549. In this study, Fe_3O_4 NPs displayed a cell depended cytotoxicity, which in all cases was smaller than for MnO NPs. The toxic effect was much smaller when cells were incubated for 4 days rather than just two days. The authors dedicated this to the fact that NPs are taken up by the corresponding cells and that therefore new born cells do not interfere with these NPs. The longer the incubation time therefore, the higher the viability. This further confirms the theory that when MnO@DA-PEG NPs leach, the number of NPs decrease thereby effecting less cells.

Cupper oxide NPs functionalized with DA-PEG were tested on Caki cells after an incubation time of 24 h. In all three cases, a viability of $< 60\,\%$ was observed (see figure 4.5) albeit the concentration for each NP sample was rather low. Due to synthetic limitations, for each test, the highest possible concentration was applied. Comparative studies for the different shapes therefore is not reasonable. However, different studies confirmed that Cu-oxide NPs show rather toxic behavior towards cells *in vitro* but also *in vivo*. [70, 71] The first contribution thereby described the influence of CuO as well as $CuZnFe_2O4$ NPs. [70, 81] These studies confirmed that iron oxide NPs are relatively safe in regard to ROS production, DNA damage experiments and cell cytotoxicty. The authors therefore accounted the toxicity to the cupper part within $CuZnFe_2O_4$ NPs. Interestingly, both studies came to different results when comparing Cu containing solutions with CuO NPs. Farko and Furgeson reported on $CuSO_4$ solutions which displayed an increased toxicity towards zebrafish *in vivo*, [70] wherease Li et al. described $CuCl_2$ solutions tested on human lung cancer cells *in vitro*. [81] The different compounts as well as the different organisms thereby make it hard to compare both studies.

In this chapter, CuO as well $CuCl_2$ solutions were tested. Since CuO shows low solubility in water and since different concentrations were used, a definitive conclusion can not be made. In addition, it should be kept in mind that neither one of the samples were sterile filtered to avoid additional dilution. Possible contamination thereby can not be excluded and might have also played a role in the results observed.
The observed toxitiy of MnO-FePt NPs had to be addressed to Pt. Pt is known to intercalate into the dsDNA and since the toxic effect became apparent when the number of cells were lowered, it became apparent that the number of NPs /cell does play a more important role than the concentration itself. The same possibly holds true for Pt-Fe_3O_4.

Generally, data published for Au NPs is not consistent but different results that proof the toxic behavior but also non toxic behavior for these NPs can be found. [82, 83] Further, there is evidence that the toxicity observed is size dependent when Au NPs were tested in the size range between 3 to 100 nm. [84] In the current chapter, a decrease of viability for HeLa and Caki1 cells below 60 $\%$ could not be observed, indicating the low toxic behavior of these NPs. However, Au@MnO NPs with a Au NP size of 9 nm and MnO dimers fo 20 nm showed a decrease of the viability compared to Au@MnO dimers with a Au size of 6 nm and 25 nm sized MnO NPs as well as Au@MnO nanoflowers with a Au core size of 13 nm and MnO pedals of 25 nm. The Au size alone therefore can not be made responsible. MnO NPs in this size range were not tested in cell culture. Therefore it cannot be excluded that the decrease in size from 25 to 20 nm was responsible for the decrease in cell viability. However, there could also be the explanation of shielding effects of the Au core. With decrease in MnO NP size and increase in the Au core, the core itself was not shielded as effectively as was the case for the second dimer sample (278) or the nanoflower sample (281). Since Au itself does not bind DA-PEG effectively but prefers thiol tagged ligands (Schladt 2010), it can be surmised that the Au core still was unfunctionalized and therefore accessible. It could be shown that Au NPs are taken up by the cell via endozythosis but also that Au NPs can be found freely in the cell cytoplasma. [85] Upon agglomerating close to the mitochondria, especially when Au NPs were surface functionalized with charged surface groups, pre-apoptotic signals were released from this organelle. The better accesibilty of Au nanoparticles might have resulted in the decrease of viability as was observed.

A definit trend for the influence of NPs on the proliferation of Caki1 and HeLa cells could not be observed other than that in most cases the proliferation level was higher than that of the CCK8 test. These results indicate that toxicity did not appear on the cellular level. However,

the results need to be reviewed carefully since the MTT based CCK8 test can also be seen as a proliferation assay and vice versa. The amount of overall DNA increases with the cell number as does the enzymtic concentration which help reduce the triazolium salt found in the CCK8 assay. Therefore, the proliferation assay could be seen as a more sensitive MTT assay. Additional studies such as the cell membrane integrety using the LDH assay or the change of the morphology of cells upon NP incubation should be performed to understand the cellular reactions which take place within these cells.

The general influence of NPs to cells of the immune system needs to be tested more extensively prior to *in vivo* application, since it was shown that NPs can induce hemolysis, thrombogenicity and can activate the complement system resulting in allergic reactions or anaphylaxis.[86] However, standardized tests are not established so far. PBMC's are not tested extensively in the literature. Additionally, reports are not consistens. TiO_2 NPs for example, are supposed to be toxic in concentrations between 20-100 μg/ml and showed DNA damage and enhanced levels of p53 in a dose and time dependend manner. [32] However, when NPs with roughly the same size but from a different company (Sigma-Aldrich) were tested, a DNA damage could not be shown. [87] When PBMC's were incubated with MnO@DA-PEG NPs, a dose dependence was not observed and interestingly, when these cells were incubated for 24 h instead of 1 h, the viability increased. An explanation for this might be that lymphocytes or macrophages capture these NPs by endozytosis, get activated and the cell numbers propagate. Thereby, the concentration of MnO@DA-PEG NPs in the cell media decreases and the newly formed cells do not take up any more NPs. The viability decreases. Thereby, an incubation time of 1 h might not have been long enough for such an immediate effect. The results however clearly shows that more tests are necessary to allow a definit explanation for these observations. In addition, supporting tests such as LDH measurments or enhanced protein expression of e.g. p53 or Caspase 3 are necessary.
Generally it has to be stated that, albeit numerous studies of NP synthesis have been made, the influence of NPs administered in purpose for biomedical achievments or inhaled accidentially due to urban distribution is a process that only starts to be addressed. The influence of different NPs thereby are dependent on the nature, the size but also the cell culture that is tested and will presumably be the focus on numerous other studies in the near future. [78, 88, 85, 89] Since many studies focus on specific NPs and since a single paramteter which is responsible for nanotoxicity could not be singles out so far, comparison studies are hard to find. [78] Therefore, the results observed in this chapter are only valid for the applied frame conditions. However, the general observation seems to hold true that cationic NPs are more toxic to cells

than negatively charged, or even better, non charged NPs. [90] A possible reason is that these NPs can bind to negatively charged groups on the cell surface and can then penetrate through the cell membrane. When agglomerating at the mitochondria or even after passing through the first membrane of this bi-layerd organelle, the sensitive ionic balance can be altered, thereby interfering with the mechanisms of this powerhouse. Additionally, there are indications that the length of the PEG chain also results in interference with the cell membrane, thereby influencing the toxic effects. [91] The synthesis of DA-PEG polymers with different chain lenghts and different functional groups such as carboxylic groups and neutrally charged methyl groups was possible, however so far, MnO NPs functionalized with these polymers could not be transferred into the aqueous phase. Comparative studies with these NPs will be very interesting.
Further, the altering the NPs size itself should give interesting results of whether the size influences the toxicity towards Caki1 cells. Additionally, an upscale in the synthesis procedure should allow the use if higher concentrations of NPs thereby allowing the measurment of LD_{50} times for Caki1 cells. So far, MnO NPs need to be considerred as non toxic under the investigated conditions, thereby being in good aggreement with other data. [80, 24] Only when higher concentrations were used than 10 μg/ml, as described in this chapter, were toxic side effects visible. [92, 23]
Currently, the cell culture of healthy human kidney endothelial cells is established. Once these cells can be cultivated routinely, incubations with MnO NPs should reveal, if a NP induced damage can be observed for healthy cells as was reported earlier. [78]

CHAPTER 5

Applicability of MnO nanoparticles for photodynamic therapy and imaging

5.1 Introduction

In 1900, Oscar Raab made the stunning observation that the protozoon *Paramecium caudatum* die upon light exposure and the presence of an acridine dye. Von Tappenheimer realized 7 years later that the presence of oxygen is also required. [93] The reason why, could however not be solved in this model. The importance of this observation however, had to wait until the mid 1960s, when Richard Lipson used the fluorescence capacity of haematoporphyrin (HpD) to detect cancer cells and additionally treat a patient with breast cancer by light exposure after HpD administration. [33] The first phase III clinical trials with this component, which nowadays is known as Photofrin, took until 1978. Today, this cancer treatment is referred to as photodynamic therapy (PDT) and is generally accepted method to fight cancer.

For a successful treatment, three components are necessary, being a photosensitizer (PS, HpD in the above mentioned example), oxygen and a light. Generally, PDT treatment follows four steps. First, the PS is administered, then the target tissue is irradiated (usually using light with the wavelength of the maximal absorption of the PS), then reactive oxygen species are formed and finally the cells within the target tissue die. [3]. So how does this therapy works exactly at the molecular level? PS can be found in their enegergetically ground state (P_0). Upon excita-

tion, an excited state (P_1) is formed with two relaxation possibilities. The unwanted reaction thereby is the relaxation into the ground state, resulting in the fluorescence or the emission of light. The bigger part of the PSs however, are characterized by being poor fluorescent molecules so that a spin inversion to the triplett state (T_1) is preferred. In a type I reaction, an electron transfers to the surrounding molecules resulting in free radicals. These can in turn react with oxygen. Superoxides, hydrogen peroxides and hydroxyl radicals are produced. In a type II reaction, a direct energy transfer to oxygen is possible, leading to singlet oxygen ($^1O_2$), which is considered the predominat species resonsible for cell death in PDT. $^1O_2$ can react almost unhindered with proteins, lipids and nucleic acids. This, as oxygen stress described process, will ultimately lead to cell death. This whole process takes between 24 to 48 h and is much faster than chemotherapy or radiation treatment. Since this method can additionally be applied on outgoing patients, hospitalization, as in the case of surgery, is redundant. Most photosensitizers are derivatives of protoporphyrin or chemical pre-forms thereof. Since all compounds can be found in the human body, clearance and toxicity to healthy tissue is minimalized. The only side effect observed is a prolonged light sensitivity of the patientŽs skin, making it necessary to stay inside for roughly a month to not risk a serious sunburn. PDT can be administered locally, not harming the neighbouring tissue. Furthermore, it was shown that upon irradiation, multiple signal transduction pathways thereby directly activate apoptosis. Large numbers of cytokines and inflammatory mediatiors are released and agglomerate within the treated tissue. The host immune system is therefore directly involved. Since the metabolic pathways that are altered in many tumors, are not involved, PDT can in addition be aplied to all types of cancer. [33]

However, this method also has its limitations. First generation PS have their absorbance maxima below 800 nm. This limits the penetration depth of the applied light source. Therefore, second generation PS are under current investigation, with an absorbance maxima in the longer wavelength region of the light spectra. A second drawback is the chemical nature of the PS themselves. Usually, they are hydrophobic in nature and show agglomeration in aqueous solutions with a decreased efficiency in PDT. Using nanoparticles (NPs) to improve the solubility in water, showed promising results. Predominatly, the approach of encapsulation of the PS is under investigation. [3, 94, 95, 96] These approaches concentrate on delivering the PS to the target site. Examples where the PS is bound to the surface of NPs are less prominent. [97]

MnO NPs can also be used as transport vehicles, thereby using the enhancement in MRI contrast to follow the path of applied NPs *in vivo*. In addition, protoporphyrin IX (PP) , the most

applied PS in clinical studies,was covalently bound to poly-(etyhlene glycol) (PEG). This molecule was further equipped with the NP anchoring dopamine derivative hydrocinnamic acid (DA), linking the metallic NP with the PS. PEG does further improve the solutbility of MnO NPs and PP. In this chapter, the synthesis of thereby designed MnO@DA-PEG-PP NPs will be adressed, together with long-term stability in body fluids, toxic behavior towards Caki1 cells and the applicability of these NPs in PDT.

5.2 Experimental Section

Please note that the synthesis of DA-PEG and MnO@DA-PEG were already described in the previous 2. **Chemicals:** FITC-labeled Annexin-V (Annexin-V-FLUOS kit, Roche Diagnostics GmbH, Penzberg, Germany), propoporphyrin IX (PP > 95 %, Sigma Aldrich), 4',6-diamidin-2-phenylindol dilactate (DAPI, Sigma Aldrich).

Equipment: A light microscope, together with an AH3-RFC reflected light fluorescence attachment was used for fluorescent imaging with combination to the software AnalySIS (Olympus, USA). **DA-PEG-PP.** As a first step, an NHS ester of PP was synthesized by dissolving 0.1 mmol in 10 mL of dry DMF under inert conditions. The reaction flask was wrapped with aluminum foil. HOBt (0.24 mmol) was added and the solution was kept stirring for 5 minutes. After this time, DCC (0.3 mmol in 1 mL dry DMF) was added and stirring was continued for 30 min. Finally, NHS (0.3 mmol in 1 mL dry DMF) was added. For reaction completion, stirring under inert conditions and in the dark was continued over night. During this time, the urea side product was formed, which was removed by centrifugation. The final product was kept as DMF stock solution in the dark at -40 °C.

Coupling of NHS-PP and DA-PEG-NH_2 was performed by mixing both components in a molar ratio of 1:2 (typically 0.05 mmol PP and 0.1 mmol DA-PEG) in 5 mL chloroform under inert conditions and by covering the reaction flask with aluminum foil. After 24 h, DA-PEG-PP was precipitated using hexane. After centrifugation, the pellet was washed twice by redissolving in chloroform and precipitation in hexane. The final product was kept as stock solution in chloroform at -40 °C in the dark.

Cell culture and cytotoxicity-assay. The general setup described in 4 was followed. 96 well plates were populated with 10^5 cells per well, were kept at 37 °C, 95% relative humidity and 5% CO_2 for 24 h before MnO@DA-PEG and MnO@DA-PEG-PP were added in a dilution of 1:10. The final concentrations within the wells were 2.5 - 10 μg/mL. Cells were again incubated for 24 to 48 h. The cell vitality was measured using the cell counting kit 8 (CCK) as described in 4. All results were tripled and normalized to a control sample. Prior to use, all NP samples were sterile filtered in accordance to 2.

Applicability of PDT to MnO@DA-PEG-PP treated Caki1 cells: For this assay, 6 well plates were populated with Caki1 cells and were kept at 37 °C, 5% CO_2 and 95% relative humidity until reaching confluent growth. MnO@DA-PEG and MnO@DA-PEG-PP were added in a final concentration of 100 μg/ml. Cells were again incubated for 48 h and were exposed to light of a wavelength of 630 nm using a He-Ne laser. The intensity was adjusted to 40 mW cm^{-2} for a period of 30 min, corresponding to an incidental dose of 72 J cm^{-2}. The

excitation wavelength was chosen in regard to the absoprtion in the long-wavelength region of PP. Cells were then washed twice with PBS. RPMI 1640 cell culture medium supplemented with 10% FBS, mycokill, L-glutamine and PEST was added. Phosphatidylserine (PS) presentation on the surface of cells is known as a sign for apoptosis, which can then be detected by FITC-labelled Annexin V. Necrosis was tested, using propidoum iodine (PI). The fluorescence analysis was performed with a light microscope, together with an AH3-RFC reflected light fluorescence attachment. The images were co-localized using the software AnalySIS. To confirm that MnO@DA-PEG-PP can be localized within Caki1, cell cores were stained using DAPI.

Magnetic Resonance Imaging. A clinical 3.0 T MR scanner was used, following the general description given in 2. In a second T_2 measurement T_E was varied from 15 ms up to 480 ms.

5.3 Results and Discussion

Long-term stability and applicabilty of Mno@DA-PEG nanoparticles as promising MRI contrasting agents with low *in vitro* toxicity were already described in 2 and 3. The focus of this chapter will be the use of those nanoparticles for photodynamic therapy. Therefore, DA-PEG was slightly modified by coupling protoporphyrin IX (PP).
MnO@DA-PEG-PP were synthesized as desribed in 2. Thereby, as synthesized MnO nanoparticles featured a hydrophobic oleate layer which was replaced by ligand exchange using either DA-PEG or DA-PEG-PP using chloroform as solvent. Transfer to the aqueous phase was done by hexane precipitation, immediately redissolving NPs in water. The final water soluble fraction was concentrated and sterile filtered and the concentration of this sample was then measured using AAS. All concentrations mentioned in this chapter refer to the Mn concentration within the used sample.

MRI activity: As already discussed elsewere, MnO@DA-PEG nanoparticles have the ability to shorten T1 weighted relaxation time, thereby increasing the brightness of the corresponding image. To ensure that this is also the case for MnO@DA-PEG-PP, nanoparticles were diluted to yield concentrations between 5 and 40 mM and where applied to a clinical 3.0 Tesla MRI. When images were T_1 wheighted, it could be clearly seen that with increasing concentration an increase in the brightness of the image could be observed (see figure 5.1 a). MRI thereby cannot only provide the image itself, the shortening of the T_1 relaxation time can also be measured. The corresponding results are given in plot 5.1 b. It can clearly be observed that the relaxation time decreases with increasing concentrations of Mn which makes these nanoparticles ideal candidates for MRI contrasting agents. Between 5 and 20 nm this shortening was nearly proportional to the concentration. Between 20 and 40 nm this behavior could not be observed anymore. A possible reason for this might be a saturation effect. Contrasting agents have a preferention to be effective for either T_1 or T_2 wheighted contrast. However, they also effect the contrast which they do not primarily enhance. For the current case, MnO nanoparticles show a decrease in the T_1 relaxation time. However, T_2 is also effected. Since T_2 wheighted contrast agents show a negative contrast, the T_1 signal is weakend. When a specific concentration is reached, the positive T_1 contrast cannot be enhanced further. For MnO@DA-PEG-PP, this concentration obviously was reached when 40 mM were applied.

Stability of MnO@DA-PP in body fluids: A second important issue for *in vivo* applicability was the effect of human body fluids in regard to the agglomeration effect of MnO@DA-

PEG-PP NPs. Therefore a sample together with MnO@DA-PEG NPs were diluted with blood serum or water as a control sample. Samples were kept at different temperatures (4 °C, room temperature or 37 °C) for up to one week. Blood serum samples without nanoparticles were also prepared. Figure 5.1 c shows examplary samples of blood serum incubated with MnO NPs (+s) as well as control samples of nanoparticles diluted with water which all were kept at 37 °C for one week. Samples kept at two different temperatures are not shown but generally displayed the same results. The long term stability of the applied samples could clearly be observed by the absence of any nanoparticle related agglomeration. All samples kept their brown color which originated from MnO nanoparticles. A difference between MnO@DA-PEG or MnO@DA-PEG-PP could not be observed. However, in all samples a white precipitation formed during this week, which could also be observed for samples kept at lower temperatures as well as samples of blood serum without NPs. Upon loading on a SDS-PAGE, it was shown that all agglomeration contained numerous proteins which precipitated faster at elevated temperatures (see figure 5.1 d), shown are precipitated samples at room temperature). Again, only selected samples were shown, all other samples however gave the same result. Since this behavior was observed for all samples, MnO NPs did not influence the protein degradation. In addition, no agglomeration occurred for MnO NPs kept in water instead of serum. This observation supports the SDS-PAGE results that precipitation occured exclusively due to protein degradation.

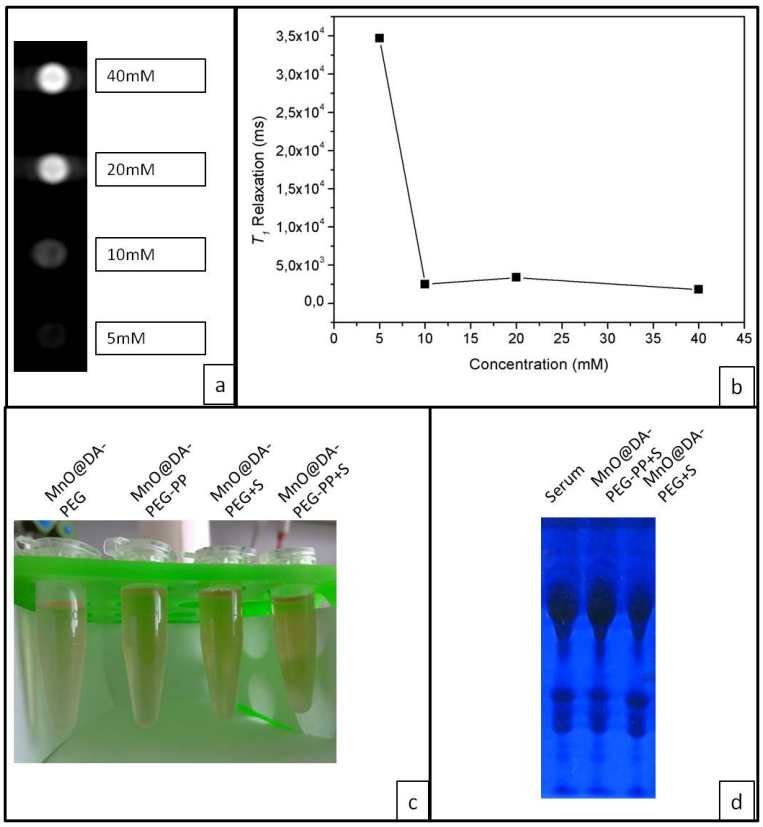

Figure 5.1: **MRI measurements and stability in body fluids:** a: T_1 wheighted MRI images of differently concentrated MnO@DA-PEG-PP NPs in water. b: T_1 relaxation times (ms) of samples measured in a. c: MnO@DA-PEG and MnO@DA-PEG-PP were incubated with water or blood serum (+s) at 37 °C for one week. d: 10 % SDS-PAGE stained with CCB after loading precipitations of blood serum samples which did occure.

***In vitro* uptake and vitality assays:** Due to bound PP, MnO@DA-PEG-PP NPs showed a red fluorescence, a fact that was used to detect NPs within cells. To further ensure that NPs were taken up rather than just concentrating on the cell surface, the cell cores were stained using DAPI, a blue fluorescent dye. Using a fluorescence microscope, both dyes could be addressed separately (for MnO@DA-PEG-PP see figure 5.2 a.2) and could then be co-localized (see figure 5.2 a.1). These images in addition to former *in vitro* experiments for MnO@PEG-Poly (see 2), make it feasible to state that nanoparticles were taken up by Caki1 cells after an incubation time of 48 h. Since MnO@PEG-Poly were further taken up by endocytosis (again see 2), it can be assumed that MnO@DA-PEG-PP were engulfed by Caki1 using the same pathways.

Besides the possible uptake of NPs in cells, the toxicity of the mentioned particles should be

as low as possible to not harm cells that are not target of this method. Therefore Caki1 cells were routinely grown in 96 well plates for 24 h before MnO@DA-PEG and MnO@DA-PEG-PP NPs, prediluted with cell culture media, were added. Cells were then incubated for 24 and 48 h, respectively. Excess NPs were washed off and cells were incubated with CCK8. Upon incubation for 3 h, the absorption of the reduced formazan of CCK8 was measured at 450 nm. All results were tripled and were normalized to control samples. The results are given in figure 5.2 b. Note that the concentration given in this plot referes to the Mn concentration of the samples previous to 1:10 dilution with cell culture media. The final concentration therefore was 10, 7.5 and 5 μg/ml. MnO@DA-PEG-PP NPs are referred to as PP, MnO@DA-PEG NPs are abbreviated with PEG.
Generally it was observed that MnO@DA-PEG and MnO@DA-PEG-PP did not interfere significantly with Caki1 cells in terms of vitality, additionally being independent of the concentration of the sample (black and light gray columns in figure 5.2 b). In all cases, the vitality did not increase significantly (roughly 5 %), clearly stating that under the conditions tested here, MnO@DA-PEG and MnO@DA-PEG-PP were non toxic.

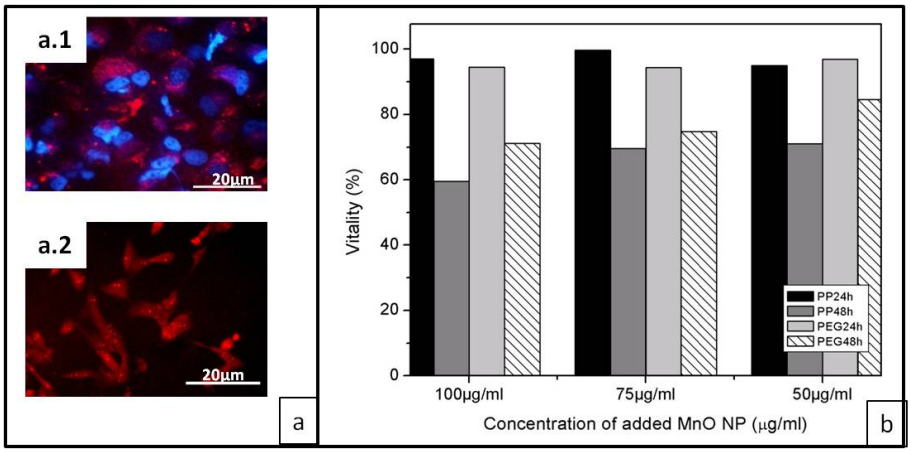

Figure 5.2: ***In vitro* uptake and toxicity of MnO@DA-PEG-PP NP:** a: Caki1 cells incubated with MnO@DA-PEG-PP. NPs showed red fluorescence due to bound PP (a.2), cell cores appeared blue due to staining with DAPI. a.1 shows an overlay image. b: Vitality assay of Caki1 cells incubated with MnO@DA-PEG and MnO@DA-PEG-PP for 24 and 48 h. Vitality was measured using CCK8 after incubation for 3 h. All results were tripled and normalized to a control sample.

Applicability of MnO@DA-PEG-PP for PDT: Caki1 cells were routinely grown in six well plates which were equipped with cover slips. After confluent growth was reached, cells were washed and cell culture media without phenolred was added. MnO@DA-PEG-PP were di-

luted with media to give a final concentration of 100 μg/ml. Upon incubation for 48 h, cells were exposed to irradiation using a He-Ne laser (635 nm) for 30 min. Cells were then observed under a fluorescence microscope. In addition, control samples without bound PP were tested as well as Caki1 cells which were incubated with MnO@DA-PEG-PP but without irradiation steps. All results are given in figure 5.3.

The upper lane (A-D) shows results of Caki1 cells incubated with MnO@DA-PEG. Since these nanoparticles did not carry a fluorescence dye, all pictures appear blank under the fluroescence microscope. When Caki1 were incubated with MnO@DA-PEG-PP, the red fluorescence could be adressed and nanoparticles were visible in the proximity of Caki1 cells (see figure 5.3 E). Images E and I show Caki1 cells incubated with MnO@DA-PEG-PP before (E) and after (I) irradiation. It can be observed that the shape of the Caki1 cells changed dramatically upon irradiation. This already was an indication that cells did undergo apoptosis. This was further affirmed by staining with FITC labelled Annexin V. Upon the early stage of apoptosis, cells transfer phosphatidylserine to the surface of the cell membrane. Annexin V can bind to this lipid. When additionally a dye such as FITC is coupled, phosphatidylserin on the cell surface can be indirectly illuminated. Untreated cells thereby showed no fluorescence signal for FITC (figure 5.3 F). However, after irradiation, Caki1 cells showed a green fluorescent signal (J). Interestingly when the overlay image is observed, these green stained cells were in close proximity to those that showed a red fluorescence. MnO@DA-PEG-PP nanoparticles from apoptotic cells might have already left these cells, whereas cells with positive MnO@DA-PEG-PP staining might not have enterred the apoptotic state yet.

To ensure that Caki1 underwent programmed cell death rather than necorisis, a second assay was performed. In this case, propodium iodine was used. This dye can intercalate into double stranded DNA. Since this compound cannot enter living cells and since dsDNA gets degraded during apoptosis but not necrosis, a signal can only be observed, when cells burst in an uncontrolled way. Figure 5.3 G and J show the corresponding results. A signal however was not obserrved neither for the non-irradiated nor the irradiated sample, confirming that cells died due to apoptosis rather than necrosis.

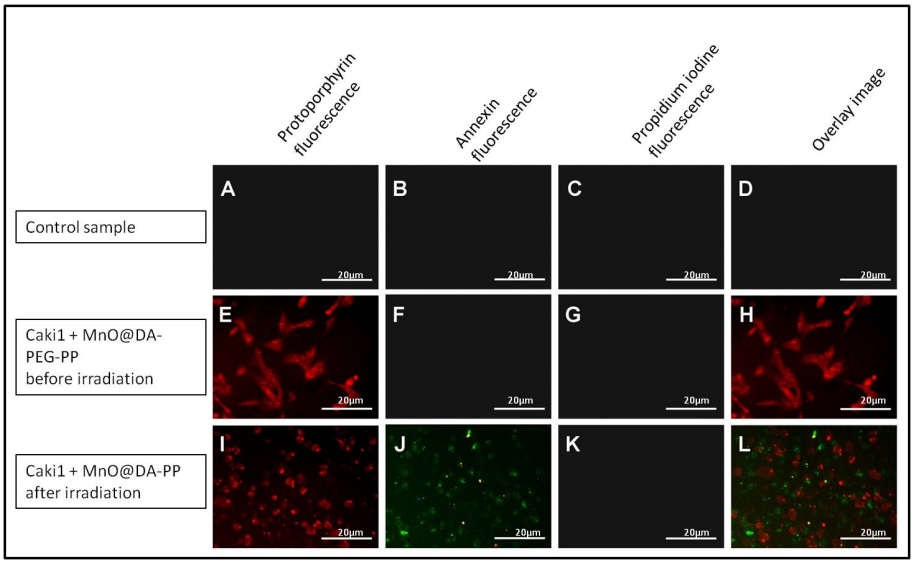

Figure 5.3: **In vitro uptake and PDT treatment using MnO@DA-PEG-PP:** Caki1 cells were incubated with MnO@DA-PEG (A-D) as well as MnO@DA-PEG-PP NPs(E,I). Due to PP NP can be detected by red fluorescence. Cells were observed prior to (E-H) and after irradiation (I-L). Apoptosis was measured using FITC labeled Annexin V, necrosis was tested using propidium iodine. The final colum shows overlay images.

5.4 Conclusion and Outlook

MnO@DA-PEG-PP NPs displayed no toxic behavior towards Caki1 cells although these NPs were taken up by the cells. The red fluorescence of PP could be addressed in the presence of cell core staining by DAPI. In addition, these NPs did not show signs of agglomeration when incubated with human blood serum, even when temperatures as high as 37 °C were applied. Upon irradiation, Caki1 cells underwent apoptosis when MnO@DA-PEG-PP NPs were present.

What still needs to be clarified is, how effective these NPs are in regard to killing tumor cells. This could be done by irradiation of a cell sample with MnO@DA-PEG-PP and subsequently applying CCK8 to this sample and a non-treated sample. The difference between both should clarify the PDT efficiency.

Secondly, the fact that MnO@DA-PEG-PP NPs really produce $^1O_2$ and again, how efficient this system thereby is, needs to be shown. Disodium 9,10-anthracenedipropionic acid (ADPA) has thereby shown to be very effective to measure the prescence and the amount of synthesized $^1O_2$. This compound shows an increase of the absorption at 400 nm in dependence of the amount of $^1O_2$ within the sample. [97]

Furthermore, the toxicity of MnO@DA-PEG-PP NPs towards healthy cells should be tested and finally *in vivo* experiments are necessary to proof if these NPs are more effective as PDT samples than others.

CHAPTER 6

Microbiological studies on protein expression as feasible candidates for drug delivery

6.1 Abstract

In cooperation with Assistant Professor Dr. Don Ronning, the study focused on the microbiological expression of the single chain antibody fragment (scFv) against p53. Therefore a specific system was developed to create a peptide that has additional features that shall help in the purification process of binding to nanoparticles. During the three month stay in Toledo, Ohio, protein expression experiments as well as crystallization set ups were done focussing on the *escherichia coli* (*E. coli*) proteins TnsE and TnsB as well as the *mycobacterium tuberculosis* protein Lsr2.

6.2 Introduction

Crystallyzing proteins is a fascinating area of research and the final protein crystals can allow for better understanding of protein-potein, protein-DNA, protein-drug interactions and many more. Protein crystals are rather unstable, unnumbered conditions might need to be tested before the first crystals are formed. However, the limiting factor in the whole process is the protein itself. Fortunatly, standard methods were developed and improved nowadays, so that the target protein can be synthesized in larger amounts. In addition, the protein can specifi-

cally be altered to allow further characterization.
Escherichia coli (*E. coli*) has turned out to be rather helpful for protein synthesis, even if the target proteins are not *E. coli* related. This can be achieved by introducing the protein encoding DNA into the bacteria. So as a first step, the corresponding DNA needs to be isolated and amplified. Amplification of DNA is done by polymerase chain reaction (PCR). The target DNA, plasmid DNA or chromosomal DNA that contain the target sequence, are incubated with primers, buffer, NTPs and a polymerase. The latter one usually is a heat stable polymerase such as the taq polymerase originating from the bacterium *thermus aquaticus*. But before this protein can start, the double stranded DNA needs to be denatured. This happens by heating the reaction mixture to 90 °C. A small area of double stranded DNA needs to be created in order to give a starting point for the polymerase. For this purpose small complementary DNA strands are included into the mixture, so called primers. They are designed in such a way that they form the 3 and the 5‘end of the final DNA product. To allow the annealing of these primers,the temperature is lowerd to 45 °C to 65 °C, depending on the primers used. The next step is the elongation step. The temperature is again increased to the optimum temperature of the polymerase used. The DNA is elongated from the primers on, thereby creating a new, but now shorter DNA double strand. All steps are then repeated up to 40 times, resulting in high amounts of the target DNA. After purification, this DNA can be stored at -20 °C until used. Typically all these steps are done automatically by a so called DNA cycler which is commercially available by numerous companies.
Bacteria do not only feature chromosomal DNA but also small circular DNA that is referred to as plasmid DNA. These plasmids are able to transfer from one bacteria to another, taking their genomic information with them. A process called horizontal gene transfer. In the lab, this plasmid uptake can be forced upon bacteria by a rather simple method. The cell wall of the target bacteria can be discriminated using $CaCl_2$. This ionic salt decreases the ionic forces between the negativly charged cell membrane and the negativly charged DNA that shall be taken up by the bacteria cell. For this process, the cells are heated up to 45 °C to allow the formation of small pores in the cell membrane. The target DNA can be introduced into the plasmid by a combination of restriction enzymes which break the dsDNA at distinct cut sites and ligases which ligate the target DNA (Insert) with the plasmid. Plasmid and competent cells (bacteria cells treated as desribed above) are mixed and transferred to agar plates supplemented with an antibiotic. The used plasmids are commercially availabe and usually feature a gene casette that encodes for antibiotic resistance. Only those bacteria will grow that took up this plasmid. Sometimes the desired protein can be toxic to the host cell, or might influence the growth. This can be attributed by another feature of the plasmid. Genes are inserted in such a way

that their transcription is controlled by the lac operon. *E. coli* can metabolise lactose with the help of three proteins which are encoded by the genes lacZ, lacY and lacA all found in the lac operon sequence. The first one encodes for β-galactosidase which cleaves the sugar bond to yeald galactose and glucose. β-galactoside permease, encoded by lacY, is a membrane bound transport protein, allowing the cellular uptake of lactose. lacA encodes a β-galactoside transacetylase. This enzyme transfers an acetyl group from acetyl-CoA to β-galactosides. These enzymes are only expressed in the presence of lactose.
The plasmid positive cell culture is grown until a specific density (usually OD 0.8) is reached. The target protein expression is started by adding the lactose analog isopropyl-β-D-thio-galactoside (IPTG). This molecule binds to the repressor of the lac-operon, thereby activating the protein expression of the proteins that are under the control of this operon. Commercially available plasmids are designed in such a way that all genes encoded into the plasmid are under control of this operon. Once expressed, the target protein can be purified rather easy, if it is a soluable protein. Membrane proteins are not discussed here. In general proteins are altered in such a way that they also feature a fusion tag such as polyHis or thiorodoxin. These tags can bind to metal affinity columns, which significantly improve the purification procedure. In addition, a cut site for a restriction enzyme such as prescission protease is synthesized between the tag and the core protein, by which the cleavage of tag and protein is enabled.
Once the protein is isolated and purified, the crystallization process can start. Generally there are three different methods that can be applied. One method is the hanging drop or vapor diffusion method. A buffer is placed into a reservoir and one drop on the lid of the well. The protein sample is added to this drop. Slowly drying can initiate the crystallization process. Another possibility is to mix a drop of the protein sample and a drop of the coresponding buffer and place it into a 96 well plate. Mineral oil helps to prevent a too fast evaporation process. The third method is basically similar to the hanging drop method. The protein sample - buffer mixure is not placed on the lid but is rather located on a step, beeing elevated in regard to the buffer. All trays need to be kept at ambient temperatures until crystals are grown.
The motivation for this stay was to express and isolate the proteins Lsr2, TnsE and TnsB. For each of these proteins a separate introduction will be given. The results for these experiments will be presented in accordance to each project. Finally a single chain fragment (scFvp53) that encodes for the single strand of an antibody against p53 was created. It was constructed in such a way that it features a polyHis tag and a prescission cut site. This protein was chosen to bind to magnetic nanoparticles. The polyHis tag then shall help for better separation between bound and unbound protein.

6.3 Experimental Section

Materials: Prescission protease (human rhinovirus - HRV3C; altered to N-terminal His-GST-dual-tagged version; ≈47 kDa on SDS-PAGE, recognizes the sequence LEVLFGP); SDS-PAGE (Invitrogen NuPAGE 4-12 % bis-tris gel) run on a Novex minicell apparatus (Invitrogen, xcell sure lock); metal affinity column (HisTrap^{TM} packed with Ni sepharose ^{TM}; GE Healthcare); cationic exchange column
(HiTrap^{TM} SP FF(sulfopropyl moieties), GE Healthcare); Fast Protein Liquid Chromatography (FPLC) system (Akta^{TM}FPLC^{TM}, Amersham Biosciences), dialysis membrane (Fisher Scientific 2000 kDa); size exclusion column (Superdex^{TM} 200 column); Amicon ultra filter device (Amicon Ultra centrifugal Filter devices,
10MWCO and 30MWCO); UV-Vis spectrophotometer (Genesys^{TM} spectrophotometer from Thermo Electron Cooperation); primer (IDT Iowa, USA), polymerase PFx50 (Invitrogen, USA), pET 32 (Novagen, USA), restriction digest proteins (New England Biolabs)
Organisms: *E. coli cells* XL10 (Stratagene, Santa Clara, USA), Top 10 cells (Invitrogen, USA) JM101, M15 (Qiagen, Germany)
SDS-PAGE and staining with coomassie brilliant blue (CBB): Sodiumdodeculsulfate - polyacrylamide gelelectropheresis (SDS-PAGE) is a very common technique to separate proteins according to their size. A solution of acrylamide and bisacrylamide in Tris buffer polymerases after tetramethylethylenediamine (TEMED) and ammonium peroxide (APS) are added. Due to cross-linking a solid network of polyacrylamide is formed with specific pore sizes which can be controlled by either the concentration of acrylamide-bisacrylamide or the concentration of cross-linkers (APS and TEMED). The resulting gels can either be made directly in the lab or can be purchased. All SDS-gels used for detection of protein expression were, if not stated otherwise, purchased by Invitrogen as NuPAGE 4-12 % bis-tris gel. The composition for the self made gels are described in table 6.1. NuPAGE MES SDS running buffer (1 x) was used to immerse the commercial gels, for all others SDS running buffer was used (0.1 % SDS, 25 mM tris, 192 mM glycin, 0.5 mM EDTA). Protein samples were incubated with 3-4 x sparmix (24 % glycerol; 0,4 mM bromophenolblue; 4 % SDS and 1.4 M β-ME) in a ratio sparmix-sample 1:3 or with NuPAGE LSD sample buffer 4 x in the same ratio. Samples were heated up to 70 °C for 5 min before loading onto the gel. The running time was set to 50 min at 120 V.
Gels were stained using coomassie brilliant blue R 250 (CBB) solution (0,25 % CBB; 40 % ethanol and 7 % acetic acid). Staining was kept at 5 min (after treatment of 30 sec in the microwave). Destaining was 3 h to overnight using a 5 % acetic acid solution. Gels were also

Table 6.1: Composition of a 10 % resolving SDS-PAGE with a 6 % stacking gel for protein separation

	Resolving Gel	**Stacking Gel**
H_2O	14.8 ml	5.8 ml
Tris/ HCl 1.5 M pH 8.8	2.5 ml	2.5 ml (pH 6.6)
Acrylamide/ bisacrylamide 40 %	2.5 ml	1.5 ml
Glycerol 100 %	0.2 ml	0.2 ml
SDS 10 %	0.1 ml	0.1 ml
TEMED	0.01 ml	0.01 ml
Ammonium peroxide (APS) 10 %	0.1 ml	0.1 ml

heated in the microwave for 30 sec to allow faster destaining.
In the case of Lsr2, the SDS-PAGE was stained using silverXpress silver staining kit according to the supplier (Invitrogen).
As a molecular size marker the New England biolabs protein marker broad range (NE M), protein marker M12 (Invitrogen) or Roti standard marker (Roth, Germany) were used. Pictures were taken using a Canon camera.
Concentrating proteins: The two main ways to concentrate proteins are either by using ammoniumsulfate ($(NH_4)_2SO_4$) or specific filter devices such as Amicon ultra. The first method is also known als salting out. The neutral salt is added in its solid form to the protein sample up to a concentration of 4 M. With time the ammonium sulfate dissolves, thereby binding more and more bulk water. Less water is available for the protein in the solution; hydrophobic patches are exposed on the protein surface. Additionally protein-protein interactions increase; as a result the protein precipitates and can then be collected using a centrifuge with a fixed angle rotor. The resulting pellet can be resuspended in buffer. Dialysis might be necessary afterwards. All steps were carried out on ice, the centrifuge was cooled to 4 °C. Amicon ultra filter devices are centrifugable tubes that feature a membrane with a definit cut-off size (eg. 30 kDa). The sample is applied and centrifuged until the desired volume is reached. These devices are constructed in such a way that they cannot run dry. The advantage hereby is that the protein does not precipitate. However, this method does take longer than the salting out process.
Polymerase Chain Reaction (PCR): PCR was exclusively used for scFvp53. 1 μl of either plasmid DNA or insert DNA (30 μl) was mixed in ice with 1 μl BamH1 scFvp53 primer and

1 μl NdeI scFvp53 primer as well as 1 μl polymerase PFx50; 1 μl dNTP; 1 μl formamide; 5 μl PFx50 buffer 10 x as well as 39 °l dH_2O. The reaction mixture was then applied to a thermocycler personal (Eppendorf). The running cylce was as follows: hot start (95 °C for 5 min), denaturation (95 °C for 30 sec), annealing (56 °C for 45 sec) and elongation (68 °C for 1 min). The last three steps were repeated for 34 times. A final elongation step was set to 68 °C for 10 min. After completion, samples were incubated with 10 glycerol and were loaded on a 1 % (w/v) agarosegel. The gel running time was 1 h at 80 V, the running buffer was TBE buffer 10 x (0.9 M tris base, 0.9 M boric acid and 32 mM EDTA) that was diluted to 1 x with water. The resulting bands with the appropriate size were cut out of the gel and the DNA was isolated using the QIAGEN gel extraction kit according to the supplier and are referred to as insert DNA.

Restriction digest of plasmid and insert DNA: 30 μl of the plasmid pET32 were incubated with 3 μl NE buffer 3; 1 μl NdeI; 0.5 μl BamHI and 0.5 μl CIP (calf intestinal alkaline phosphatase). 30 μl of the Insert DNA were incubated with 3.25 μl NE buffer 3; 1 μl NdeI and 0.75 °l BamHI. Both reaction mixtures were mixed gently and were placed on a heat block at 37 °C for 1.5 h. All samples were then mixed with glycerol and loaded on a 1 % (w/v) agarosegel at 80 V for 1 h. The corresponding lanes were cut out and the DNA was isolated using the QIAGEN gel extraction kit according to the supplier.

Ligation of plasmid DNA with insert DNA: Different ligation procedures were followed, however, only the two that succeded are described in detail. All ligations with T_4 ligase are described in the results and discussion section of scFvp53. 1 μl of T4 DNA dilution buffer 5 x were incubated with 2 μl insert DNA; 2 μl pET32 and 5 μl T4 DNA liagtion buffer (Ligation 1). The reaction mixture was mixed. 0.5 μl T4 ligase (New England Biolabs) was further added. After 5 min incubation at room temperature, 1 °l of this mixture was added to competent XL10 on ice. After 30 min incubation on ice, the cells were heat shocked at 42 °C and then were placed back on ice for 2 min. 250 μl LB media were added and the mixture was incubated at 37 °C for 1 h. The cell solution was spread on agar plates. Carbenicillin (works equally as ampicillin) was added to the liquid agar solution before the solution solidified. This allowed for a positive selection of succesful ligation. Colonies did grow after 48 h of incubation at 37 °C. For a second succesfull ligation, the pET32 amount was increased to 3.75 μl while the insert DNA amount now was 0.75 μl (Ligation 4). The mixture was incubated at room temperature for 20 min before application to competent XL10 cells. Every other step was kept the as described above. This ligation lead to a single colony after 24 h and additonal colonies after 48 h. All colonies were picked; transferred to 5 ml carbenicillin-LB media each and were cultivated at 37 °C until the media was turbid. The cells were collected by cen-

trifugation. The plasmid was isolated using the QIAGEN spin miniprep kit according to the supplier. The isolated plasmid was digested using BamHI and NdeI as described previously. Additionally, the isolated plasmid DNA was sequenced with the help of Genterprise (Mainz, Germany). Both test revealed that the insert was successfully incooperated into pET32. The results are given in the appendix

Protein expression of Lsr2, TnsE, TnsB and scFvp53: The final constructs were used as prepared or as provided by the group of Dr. D. Ronning. as prepared gylcerol stocks. Those were thawed and transferred to LB media. The amount of media did depend on the purpose of the culture. For Lsr2; TnsE and TnsB 4 L cultures were used, since these constructs were succesfully tested for water soluble proteins. For scFvp53 the media amount ranged between 5 ml to 250 ml. In all cases, antibiotics were added in dependence of the plasmid that has been used (Lsr2: 0.1 mM chloramphenicol and 0.26 mM carbenicillin; TnsB: 0.1 mM chloramphenicol and kanamycin, respectively; TnsE: 0.1 mM ampicillin or carbenicillin and 0.1 mM ampicillin or carbenicillin for scFvp53, M15 cells additionally have a kanamycin restistance, 0.1 mM were added). Cultures were kept at 37 °C until they reached an OD of 0.6. The protein expression was started by adding 1 mM IPTG. The incubation time and temperature varied in regard to the protein expressed. For Lsr2 the temperature was 16 °C and the duration varied between 12 and 42 h. TnsE was induced with IPTG at 20 °C for 20 h; TnsB at 16 °C for 23 h. scFvp53 was incubated at 12 °C (over night), 16 °C (over night), 18 °C (samples taken after one and three hours) and 37 °C (samples taken after 1 and three hours for JM101 and M15, samples were collected completely after 4 hours for XL10 cells). The bacterial cells were collected by centrifugation and were then resuspended in the corresponding buffer (Lsr2: 20 mM sodium phosphate pH 7.5; 1 M NaCl; 25 mM Imidazol; 5 mM β-mercaptoethanol (β-ME) and 10 % glycerol); (TnsE and TnsB: 20 mM Tris pH 7.5; 0.5 M NaCl; 25 mM Imidazol; 5 mM β-mercaptoethanol (β-ME) and 10 % glycerol); (scFvp53: directly in 3-4 x sparmix or Lsr2 resuspension buffer). To each resuspended sample DNase (Roche, 10 mg/ ml, final concentration 2.5 - 5 μg/ ml) and lysozyme (100 mg/ ml stock solution, Fisher Scientific, final concentration 25 - 50 μg/ ml) were added and the sample was incubated on ice for 20 min. Finally the cells were sonicated for a period of 10 min (pulse for 30 sec then pulse off for 2 min; the initial outputlever was 0.5 but was increased to up to 4). Soluble cell parts and proteins were separated from the crude cell substrate by centrifugation. The pellets were washed twice with the corresponding buffer (see above) and all supernatants were combined.

Protein isolation using a metal affinity column: All proteins that were expressed in this thesis did carry an His-tag that allowed the separation using a metal affinity column. The column was preloaded using a $NiCl_2$ solution. Before the cell supernatant was applied, it was

filtered using pall life science acrodisc PF syringe filters (0.8/ 0.2 μm). As loading buffer, the coresponding buffer for resuspension was used (see above). The fully automated FPLC system Akta^{TM}FPLC^{TM} was used during this process. To elute the protein a protein specific elution buffer was used. The composition corresponded with the elution buffer, however, the amount of imidazol was raised to 250 mM. Representative samples of different fractions that were collected during the run were loaded on a SDS-PAGE. All samples that contained the desired protein were pooled and kept on ice before further usage.

Cleavage of the polyHis-tag: To allow for correct folding of the protein and since the tag might change the crystallization behavior, the tag was cleaved using precission protease. A coresponding cut site was introduced for each protein on the DNA level. The slightly altered precission protease from human rhinovirus was developed and expressed in the lab and also carried a polyHis-tag itself thereby allowing the purification of the desired protein from the precission protease. All samples that were pooles after the first metal affintiy column were incubated with a sample of precission protease (usually 1 ml). The sample was then dialysed over night at 4 °C against the resuspension buffer as described above. The sample was then loaded on a metal affinity column using the same method and the same samples as is described above. Representing fraction samples were again loaded on a SDS-PAGE. All fractions that contained the desired protein were pooled and kept at 4 °C until further usage.

Cationic exchange column (Lsr2): Lsr2 is a DNA binding protein. Therefore a cationic exchange column was applied to separate the protein from DNA and RNA. Before this column was applied, the combined fractions of the polyHis-tag free protein was dialysed over night against cationic exchange buffer A (CEB-A: 20 mM sodium phosphate pH 7.5; 50 mM NaCl; 1 mM EDTA and 5 mM β-mercaptoethanol). The sample was then loaded on a HiTrap^{TM} SP FF column that was operated by the Akta^{TM}FPLC^{TM} system from Amersham Biosciences. For elution, the NaCl concentration was increased to 1 M. Representing fraction samples were loaded on a SDS-PAGE.

Size exclusion column: Some proteins can bind unspecifically to the metal affinity column. Therefore the final purification step was done using a size exclusion column. All samples were concentrated to 5 ml and were then loaded on a sephadex 200 column. Imidazol that was still present before application was first dialysed off over night at 4 °C. This column does not need a gradient and therefore only one buffer was used for each protein (TnsB and TnsE: 20 mM sodium phosphate pH 7.5; 0.3 M NaCl; 1 mM EDTA; 5 mM DTT and 10 % glycerol); (Lsr2: 10 mM tris pH 7.5; 150 mM sodium malonate; 2 mM EDTA and 0.5 mM TCEP). Successfull purification was tested using SDS-PAGE. Samples were kept at 4 °C until further usage.

Incubation of TnsE with β-clamp and trypsin digestion: TnsE is a β-clamp binding pro-

tein. However, the exact formation of this dimer and the crystal structure is unkown so far. The β-clamp might also form such a tight complex with TnsE that cannot be broken even by trypsin digestion. The β-clamp sample was provided by Dr. D. Ronning. Measuring the absorption of the TnsE sample at 280 nm and comparing this value to the literature (http://expasy.org) allowed the estimation of the concentration of TnsE in the sample. Both proteins were mixed in a molar ratio of 1:1 and were diluted with buffer Fanta 4 (20 mM tris pH 7.5; 0.5 mM TCEP; 150 mM NaCl and 1 mM EDTA) to result in a final volume of 2 ml. This sample was then loaded on a size exclusion column as described above. Fractions were loaded on a SDS-PAGE. Samples with TnsE were pooled and kept at -80 °C after concentrating using $(NH_4)_2SO_4$ and after measuring the concentration. Samples that contained TnsE and β-clamp were treated the same way. For the trypsin digest a stock sample of 0.1 μl was used that was diluted with the corresponding protein sample 1:100 or 1:10 fold. The reaction was stopped by mixing 5 μl of the reaction sample with 10 μl phenylmethylsulfonfluorid (PMSF, 1 $\%$ stock solution). PMSF is known to inhibit serin-proteases. For papain, the stock solution was 10 mg/ml. The concentration in the protein sample was lowered from 7.2 mg/ml to 0.4 mg/ml. In a typical reaction 36 μl of the protein sample prepared as described above was mixed with papain (0.25 μl) and was kept at room temperarture. Samples were taken before, directly after, 2 min after and 5 min after papain was added. The reaction was stopped by taking 8 μl of the protein mix, add it to 10 μl of PMSF (1 $\%$) and 6 μl gel loading dye, imidiatly transferring the sample to liquid nitrogen before heating to 70 °C for 5 min. All samples were characterized using SDS-PAGE.
Crystallization setup: Different setups were used during this thesis, one being the hanging drop method. The second possibility is to place each 1 μl of the buffer and the protein solution in a small well containing mineral oil. Both trays were kept in a wine cooler at constant 24 °C. The latter one has the advantage that a huge number of buffers can be readily purchased and thereby screened. The screening system HR2-134 (Hampton research) was used. The conditions for the best results can be found in the results section. Additionionally to the purchased buffers, different conditions were tested as well. These conditions can also be found in the results section. For observating the crystallization formation, Nikon SMZ1500 microscope was used with the 1.0 x, a 0.75 x to 11.25 x zoom. Documentation was done with a Nikon coolpix 995 camera.

6.4 Lsr2

6.4.1 Introduction

Mycobacteria are a group of bacteria with approximatly 100 subspecies. They own their name to the fact that their cell wall composes waxy compounds (lat.: Myco=fungus and waxy). The most prominent subspecies are *M. smegmatis*, *M. bovis* and *M. tuberculosis*, which was discovered more than 120 years ago. The last two cause tuberculosis predominatly in cattle or humans, respectively. *M. smegmatis* is considerred nonpathogenic, but it features 86 % sequence homology towards *M. tuberculosis*. Therefore numerous knockout tests, overexpressions etc. are first tested for this strain. Tuberculosis is a very serious infection. Estimated 2 billion people worldwide are infected, sometimes without even knowing it, and 1.5 to 2 million people die each year. The reason for why this bacillus leads to so much trouble is the fact that it can stay in a dorment phase within the host body until the breakout occurs. It is mostly triggered by immuno-deficiency as can be found e.g. as a result of HIV infection. TB is a pulmonary as well as systemic desease which can spread via droplet inhalation. *M. tuberculosis* is then ingested by alveoar macrophages as is the case for any other bacterial intrusion. The bacteria are taken up by so called phagosomes which then fuse with lysosomes. Lysosomes are organelles within the human cell that have a lower pH (roughly 4.5) than the surrounding media and feature enzymes such as hydrolyses which have their working optimum at this pH. The combination of both is effetctive in destroying cell debris, waste materials as well as viruses and bacteria. *M. tuberculosis* however has found a way to inhibit the formation of phagolysosomes, thereby keeping the pH at 7 and the digestive enzymes at bay. When the macrohpage contaning the tubercle bacilli die, *M. tuberculosis* can spread through the lymphatic or the blood vessels to distant tissues. The result is a systemic response of the host immune system. The surviving bacilli are trapped within granulomas, never to leave the host again. A latent TB infection was established. To create an active TB, the bacilli now need to overcome the immune system. This can take days as well as years and is primed especially when the immune system is weakened by other deseases such as HIV.
Albeit *M. tuberculosis* has been identified over a century ago and can now be routinely cultivated in the lab, an effective cure has not yet be established. Targeting essential proteins might lead to a breakthrough in TB treatment. An essential nutrient for *M. tuberculosis* is iron, a metal that is not easily accessable to the bacilli. Special proteins are therefore necessary to keep the iron concentration high enough. In 1999 the group of B. W. Gibson characterized a low molecular protein which shows an increase of expression during high iron concentrations. [98] This protein turned out to have a high sequence homology to Lsr2, a dominat T-cell anti-

gen found in *mycobacterium leprae* in 1991. [99] The role of *M. tuberculosis* Lsr2 however seems to be a completly different one and remains a secret up to now. Since all attempts to create a *lsr2* knockout for *M. tuberculosis* were in vain, the current understanding of the roles of Lsr2 were taken from experiments with *M. smegmatis*. Numerous studys revealed that Lsr2 takes part in a rather long list of cellular activities. It regulates the expression of the *M. tuberculosis iniBac* operon which is an antibiotic regulated gene, [100] protects mycobacteria against reactive oxygen species and influences the colony morphology and biofilm formation in *M. smegmatis*. [101] *lsr2* knockout strains of *M. smegmatis* show a flat, shiny mucoid appearence and have the ability to spread over soft agar surfaces faster than the wild-type. [102] It is generally understood that Lsr2 is a histone like protein that has the ability to bind to AT rich DNA. As a natural homodimer, it can bridge adjacent DNA strands. In gram negative bacteria such proteins are well known. *E. coli* features a protein that is called histone-like nucleoid-associated proteins (H-NS) and although the sequence similarity between H-NS and Lsr2 is rather low ($< 20\,\%$), they each can replace one another in knock-out experiments with *E.coli* and *M. smegmatis*. [103] Lsr2 prefers binding to horizontally aquired AT-rich DNA that can be easily detected in the otherwise GC rich genome of *M. tuberculosis* (G-C content 65-67 $\%$). [103] By actively blocking the DNA site by forming protein oligomers, RNA polymerase is trapped or occlusioned from the promoter region of the DNA that is bridged by Lsr2. As already mentioned, knock-out *M. tuberculosis* strains failed to be created so far, emphasizing the essential role of Lsr2. Until now, NMR studies were perfomed to result in an understanding of the structure of Lsr2, crystallization studies however were either not undertaken or not successful. [104] The aim of this study was to find the correct conditions to form crystalls of *E. coli* expressed Lsr2 in the absence and the presence of AT-rich DNA.

6.4.2 Results and Discussion

The Lsr2 construct was kindly provided by Dr. Julie Boucau. The protein was designed in such a way that thioredoxin (Trx) was fused with Lsr2 resulting in a Trx-Lsr2 construct with a total size of 26.5 kDa. A polyHis-tag was included and both, the thioredoxin + polyHis-tag and Lsr2, were separated with a prescission protease cut site. A permanent XL10 cell culture with glycerol was kept at -80 °C. A sample was thawed and transferred to 4 L of LB media supplemented with chloramphenicol and carbenicillin. Cells were kept in a shaking incubatior until the media was turbid. Adding of IPTG activates the transcription of the plasmid carrying the DNA code for Lsr2, therby acitvating the protein expression. To ensure that the protein expression does not harm the host cells, the incubation temperature was lowered from 37 °C to 16 °C. After collecting the cells, sonication and incubation with lysozyme and DNAse lead to two fractions after centrifugation. The soluable supernatant with Lrs2 and other water soluable *E.coli* proteins and the crude cell substrate with hydrophobic proteins, cell walls and cell organelles. As a first purification step, the supernatant fraction was loaded on a metal affinity column. Priour usage, the column was washed with a solution of $NiCl_2$ and therfore appeared green. The loading was done manually, wherease the fraction collection and the increase of the imidazol gradient was automatically done by a FPLC system. During the process the measurment of the conductivity and UV-Vis measurments at 280 nm gave indications in which fraction proteins can be found. Therefore aliquots of these samples were loaded on a gradient SDS-PAGE. Fractions that were collected during the increase of the gradient were preferred since Trx-Lsr2 was equipped with a polyHis-tag that allows binding to the metal affinity column. After collecting the Trx-Lsr2 fractions, the imidazol concentration was lowered by dialysis. Since the polyHis-tag of the protein only serves the purpose of purification it was then chopped off together with the Trx fusion protein using prescission protease. The protease was added to the Trx-Lsr2 solution in the dialysis bag and incubated over night. This sample was again loaded on a metal affinity column. The protein was now expected in the flow through fractions at a low imidazol concentration. All fractions were characterized by SDS-PAGE. Figure 6.1 shows the SDS-PAGE before (a) and after incubation with precission protease (b). As already mentioned, hydrophibic components were separated from hydrophobic ones and cell debris by using sonication and centrifugation. One sample of the pellet and one of the supernatant fraction was also loaded on the gel and are represented by Lsr2 P (for pellet) and Lsr2 S in the metal affinity column I SDS-PAGE. It can be stated that a rather big amount of Trx-Lsr2 can be found in the pellet fraction since this sample runs at about 26 kDa. A possible explanation is that the sonication step was not performed long enough, thereby some cell walls still stayed intact. Lsr2 is a DNA binding protein. When cells are

sonicated, proteins can get in close contact to degradated DNA. To circumvent this, DNAse is added. However, the concentration might not have been enough, leading to Trx-Lsr2 - DNA constructs that might have a different solubility behavior as the crude protein. To increase the soluble fraction, longer sonication and higher amount of DNAse might be helpful.

When the hydrophilic cell part was loaded on the metal affinity column, the flow through was

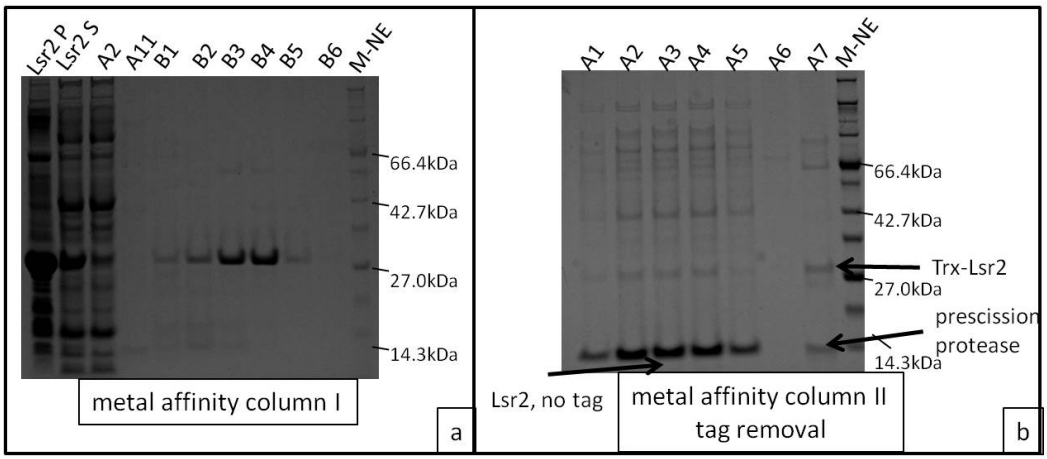

Figure 6.1: **SDS-PAGE of Lsr2 with and without Trx and polyHis-tag:** Gradient SDS-PAGE stained with coomassie brilliant blue. Different fractions of the metal affinity columns were diluted with 3- 4 x sparmix prior loading. Lsr2 can be identified according to its size in comparison to the marker used. a: Prpurufication of trx-Lsr2 construct, b: purification of Lsr2 after prescission protease digestion.

collected. A representative sample for this flow through is A2. This sample also contained a protein that has the same running behavior on the SDS-PAGE than Trx-Lsr2. It is possible that this is not Trx-Lsr2 but rather an *E. coli* protein. If it is Trx-Lsr2, it did not bind to the column. This might have two reasons. One is that the protein was not folded correctly so that the His-tag is not accesable but rather buried in a pocket of the protein. Another possibility is that the column itself was over loaded, additional protein could not be bound. Since sufficient amounts of Trx-Lsr2 could be isolated, this issue was not further addressed.

A11 represents a sample that was collected between the flow through and the start of the imidazol gradient. Since this lane appears empty it is feasable to state that all proteins that did not bind to the column were completly washed off.

The gradient started with the sample B1; the column run was completed with B6. All fractions from B1 to B5 contained Trx-Lsr2 and were therefore collected, dialysed and incubated with precission protease over night at 4 °C. Trx free protein was then isolated from protein that still contained the tag by a second metal affinity column. The flow through was collected

from A1 to A5. All samples contained Lsr2 that was then decreased in size (12 kDa due to the missing Trx fusion protein). A7 represents the bound sample which was washed off with a higher concentration of imidazol. The SDS-PAGE revealed, that in all cases two lanes and therefore two proteins were present. In the case of A7 the explanation is easy. Lsr2 and the precission protease have roughly the same size. Since the protease does also carry a polyHis-tag, it is very likely that the lower band in the SDS-PAGE represented the precision protease. The larger sample which does not run that far in the PAGE is possibly uncut protein. A band at the same height however also was present in the fractions A1 to A5. The origin of this lane was not quite clear. IHowever, one possibility could be uncut proteins that did not bind to the column. The complete SDS-PAGE showed numerous lanes that could not be referred to either Lsr2 or prescission protease. These lanes however occured in specific gaps at 20 kDa (Lsr2); 30 kDa (Trx-Lsr2); 43 kDa (a possible dimer of Lsr2) and 66 kDa (a possible dimer of Trx-Lsr2). These might have shown dimers of Lsr2 and the uncut precursor or might have been remnant proteins of *E. coli* which were not isolated using the metal affinity column. The first theory thereby is the more likly one. Creation of artefacts has been desribed in [105] and are dedicated to the fact, that the reducatant used can get partially oxidized after the heating process, allowing the protein to form dimers or that the SDS-PAGE show blurred zones. Additionally Lsr2 has an affintiy to form dimers and seems to be active as a dimer [104] and can even form oligomers. [106] The fusion with thioredoxin was supposed to promote production of Lsr2 and to increase its solubility. However, the fusion protein can also be used to increase the proper disulfide formation of the target protein. This might explain the dimerization even when sufficient β-mercaptoethanol was present. Since the affinity columns are only prepurification steps, samples with Lsr2 of the flow through were pooled and dialysed against buffer with freshly added β-ME to prevent dimerisation.

Lsr2 has a predictied pI of 10.08 (https://expasy.org). Therefore a cationic exchange column was used. Due to its basic character, the protein should bind to the column and should be washed off with increasing salt concentration (in this case NaCl). All fractions were loaded on a SDS-PAGE. The flow through fractions are assigned to I1 to I4, the eluated sample was I5. This sample was concentrated (I5 conc) and additionally loaded. All flow through fractions did contain purified Lsr2, the I5 fraction had additionally one lane wich can be asrcibed to Trx-Lsr2. However, when this sample was further concentrated, additional bands appeared. It is possible that either a dimer is formed as desribed above or that well itself was overloaded, so that artefacts appeard. Artefact formation was also described for samples with a high ion concentration. Since this sample was concentrated using Amicon ultra, this seems rather unlikely. Lsr2 was present in all fractions, indicating that the protein did not bind to the column

(see figure 6.2). The column was repeated, however with the same result (data not shown).

This running behavior was also observed for other preparations of Lsr2. The samples I1 to

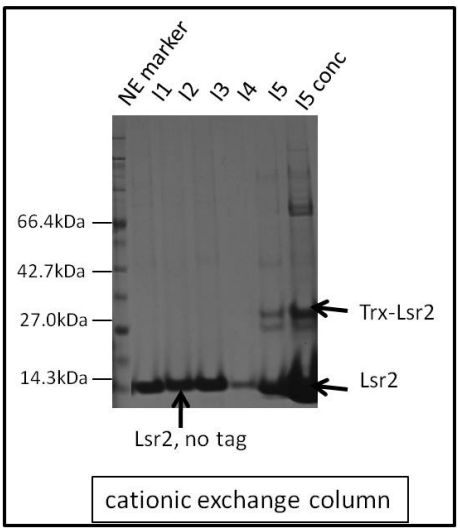

Figure 6.2: **SDS-PAGE of Lsr2 after cationic exchange column** Fractions of the cationic exchange column for Lsr2 were loaded on a gradient SDS-PAGE that was stained with coomassie brilliant blue after running. The new england biolabs multipurpose marker was used to identify Lsr2

I4 of Lsr2 after the cationic exchange column were again pooled and concentrated. The sample I5 was separately concentrated. In both cases amicon ultra filter devices were used. The absorbance at 260 nm and 280 nm were measured. The results are shown in table 6.2. The

Table 6.2: Absorption measurments of Lsr2 samples at 260 nm and 280 nm and the coefficient (260:280)

Absorption	**I1-4**	**I5**
260 nm	1.502	1.503
280 nm	1.23	1.264
A(280)/A(260) ratio	0.82	0.84

A(280)/A(260) ratio gives a hint for the purity of a protein: above 1.8 reveals a nucleic acid free sample. For both fractions the value is too low, meaning that the protein sample is still contaminated with DNA. This problem can be circumvented by precipitating the protein using $(NH_4)_2SO_4$. To test what concentration is necessary, Lsr2 containing fractions from metal

affinity columns and cationic exchange columns were pooled (original sample). This sample was then precipitated stepwise with different concentrations of a 3.8 M $(NH_4)_2SO_4$ solution. After each step the pellet was resuspended, a small sample was kept for loading on a SDS-PAGE and the remaining solution was then again precipitated, this time with a higher amount of $(NH_4)_2SO_4$. The final SDS-PAGE was then stained with silver rather than with coomassie brilliant blue. The silver staining also shows DNA if present. Note that the running behavior of DNA in a SDS-PAGE is different tp proteins or DNA in an agarose gel. The SDS-PAGE after final staining is shown in Fig 6.3.

All samples that were loaded to show the same running behavior. The reason for the nu-

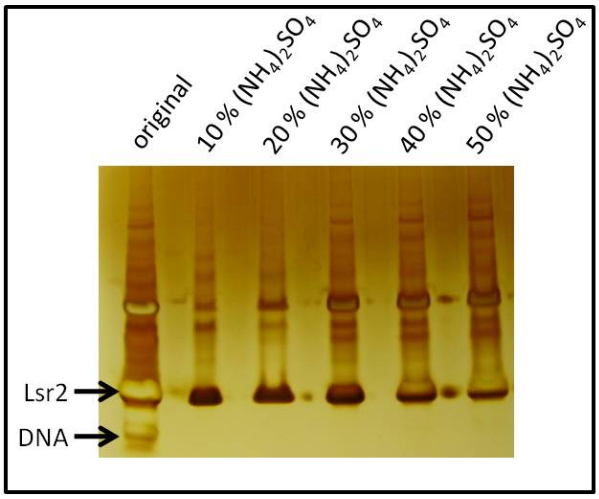

Figure 6.3: **Lsr2 SDS-PAGE using silver staining:** Pooled Lsr2 samples were loaded on a gradient SDS-PAGE. The original sample was stepwise precipitated using $(NH_4)_2SO_4$. The SDS-PAGE was then stained using silver staining.

merous lanes might be due to overloading the SDS-PAGE. The original samples features an additional lane right beneath the LSR2 lane. This lane can be attributed to bound DNA. Lsr2 probably bound this DNA unspecifically during the purification process which is in accordance to the literature. [100][101] In both cases the co-purification of DNA and Lsr2, latter one even tested the activity of DNase I in presence of Lsr2. It could be shown that DNase is significantly limited and all the DNA samples this group incubated with Lsr2 were protected from DNAse by Lsr2. All methods that were used from this time on where simply not harsh enough to separate the DNA and Lsr2. However, a small amount of $(NH_4)_2SO_4$ (10 %) is already sufficient to precipitate the protein only, leaving the DNA in the supernatant fraction. Therefore in future isolations, Lsr2 should be precipitated after the first metal affinity column rather than beeing dialysed.

The final purification step was done using a size exclusion column. This system separates proteins according to their size and not due to interactions with the column. The sample that was loaded was precipitated using $(NH_4)_2SO_4$ before loading to ensure that no DNA is present. Represantative samples were further characterized using SDS-PAGE. The result is shown in figure 6.4.

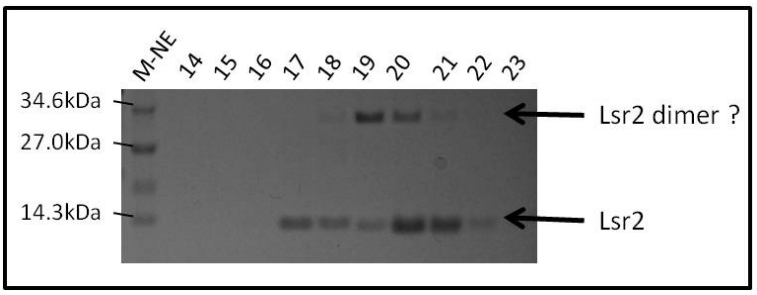

Figure 6.4: **SDS-PAGE of LSR2 after size exclusion column:** Represantative Lsr2 samples after size exclusion column. Samples were incubated with 3-4 x sparmix prior loading. The gradient SDS-PAGE was stained using coomassie brilliant blue. The new england biolabs marker was loaded as well (M-NE)

SDS-PAGE revealed two major bands as a result of the size exclusion column. The lower one represents Lsr2. The one that runs roughly around 30 kDa might be a dimer that was formed during the purification process. The buffer that was used during the column did contain 0.5 mM TCEP as a reducing reagent rather than β-ME since latter one is not stable in water for a longer time. A dimerisation might still be possible. As mentioned above, Lsr2 has an affinity for dimerization. The samples 17, 18, 21 and 22 were collected and concentrated to yeald a final concentration of 125 μM (the absorption at 280 nm was measured and then compared to the data bank https://epasy.org). This sample was then directly mixed with AT-rich DNA which was purchased exactly beforehand. The sample was then dialysed against size exclusion buffer since $(NH_4)_2SO_4$ was still present after precipitation. With this sample crystallization trays were set up using the sitting drop method in mineral oil using the screening system HR2-134 (Hampton research). The most promising conditions revealed crystals that turned out to be salt crystals. The project is currently continued in the group of assistant Prof. Dr. D. Ronning. Currently the thioredoxin tag is replaced with a polyHis-tag, thereby changing the whole construct on the DNA bases.

6.5 TnsE and TnsB

6.5.1 Introduction

Transposons are mobile genetic elements and can therefore change their position within the genom. First discovered 1948 by the botanist Barbara McClintock who resieved the Nobel prize in 1983, numerous examples for these movable DNA segments were found until the current day. It is believed that 35 % to 50 % of the human genome consists of such transposable elements or their relics. [107] Tn7 is such an example. The 14 kb transposon encodes genes that allow for the resistance of bacterial strands against triptometropin, streptomycin and spectinomycin. [108] Encoded as well are the five proteins TnsA-E which enable the transfer of the transposon DNA. The Tn7 transposon turned out to be rather sophisticated, since it can transpose in the chromosomal DNA (TnsABC+D pathway) as well as in plasmid DNA (TnsABC+E pathway) without any harm to the host. Each of the proteins that are encoded by Tn7 has a specific duty and only the combination of four lead to the succesful transposition.

TnsABC These three proteins work together to allow the transposition of Tn7 to the target DNA. TnsA is a restriction endonuclease that induces a double strand break (DSB) in the target DNA. [109] TnsB is a member of the retroviral integrase superfamily and features a triad of acidic residues (DDE). [110] It is a rather interesting molecule, since it regognizes the cis end of Tn7, thereby enabling the correct orientation of Tn7 when transposed. It breaks and rejoines the 3'-hydroxyl group of the donor and the 5'-phosphate group of the target DNA. TnsC is the activator for the transposing machinery. This ATP-hydrolase can bind to double stranded DNA and activates transcription when bound to DNA and TnsE or TnsD. How exactly this mechanism works is under current investigation. TnsABC alone cannot transpose Tn7 to target DNA, unless a mutated from of TnsC is used. [111]

Vertical gene transfer using TnsD: Transposition into the bacterial chromosome occurs at a specific site which is highly conserved in numerous bacterial strands and is called *attTn7*. It is located within the 3'-end of *glmS*, a gene that encodes for glutamine synthetase and crucually necessary for the host bacteria. [107] However, when Tn7 inserts, this gene stays uneffected and the host actually benefits from the transposition of Tn7 since genes for antibiotic resistance are now part of the bacterial chromosome. TnsD has the ability to recoognize the *attTn7* and can attract the rest of the transposition machinery to its site. The binding of TnsB results in a distortion of the host DNA which then attracts TnsC to this site thereby activating the transposition. [110]

Horizontal gene transfer using TnsE: Bacteria do not only feature chrosomal DNA, but

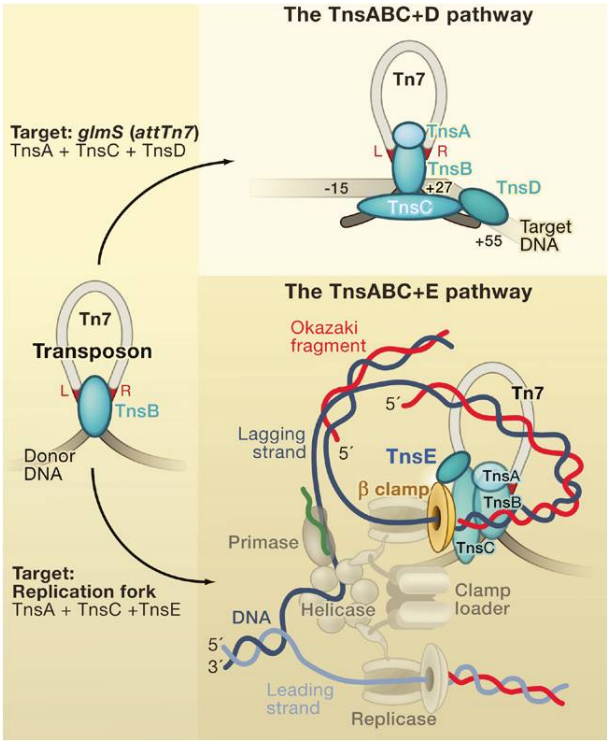

Figure 6.5: **Tn7 transposition pathways:** The two different Tn7 transposition pathways are shown. [112] The DNA sequence that flanks the Tn7 transposon is shown in red. TnsB binds to the donor as well as acceptor-DNA. The TnsABC+D pathway targets the chromosomal DNA at the *attTN7* site. TnsD binds to this site and recruits the transposon machinery proteins TnsABC. The TnsABC+E pathway targets the lagging strand synthesis of conjugal plasmid DNA. TnsE binds to the β-clamp and thereby attracts TnsABC. The transposition probably targets the Okazaki-fragments of the lagging strand synthesis.

also small, circular plasmids. Conjugal plasmids have a special role herein, beeing transferred between two bacterial cells as a singel strand. One strand stays within the donor cell and gets replicated with the help of the host DNA replication system following leading strand replication. The second single strand transfers into the recieving cell. Since this is the complementary strand (5' to 3'orientation), replication in one smooth step is not possible. Lagging strand replication is necessary which is established by creating small DNA fragments (Okazaki-fragments) that are then combined by the DNA ligase. It was shown, that Tn7 does transpose within these conjugal plasmids at many different positions. [107] The reason for this is the binding affinity of TnsE to the β-clamp, a subunit of DNA polymerase III within bacterial cells. This protein is highly active during DNA replication. It can encircle the DNA

and thereby links DNA and proteins. [110] When such a conjugal plasmid with inserted Tn7 now transfers into another bacterial cell, Tn7 joins this transfer, can then start a vertical transposition into the chromosomal DNA and has thereby spread to other bacteria. Additionally TN7 that originates from the chromosomal DNA can insert into conjugal plasmids, helping to spread between bacteria.

The motivation of the following study was to crystallize TnsB as well as co-crystallize TnsE and the β-clamp. A second aspect was to study the conformational change of TnsE when bound to β-clamp.

6.5.2 Results and Discussion

The general steps for purification of TnsE and TnsB are the same than for Lsr2. Therefore one can refer to this section.

Expression of TnsB: A glycerol stock was kindly provided by Prof. Dr. D. Ronning and kept at -80 °C until used. A 100 ml stock was thawed and added to 4 L LB-media supplemented with 0.1 mM kanamycin and chloramohenicol, respectively. The protein expression was induced using 0.25 mM IPTG. The induction temperature was lowered to 16 °C for 23 h. The protein was prepurified using a metal affinity column. The polyHis-tag was then chopped off using prescission protease over night. A size exclusion column lead to pure TnsB protein. The corresponding SDS-PAGEs are shown in figure 6.6. The majority of TnsB bound to the first metal affinity column as can be seen in figure 6.6 metal affinity I in the fractions G8 and G9. These fractions were collected after the imidazol concentration was increased using a gradient. The increase started with the fraction G7, samples before that point represent the flow through fractions that hardly contain a protein with the size of TnsB. The samples containing TnsB were pooled and dialysed over night in the presence of prescission protease. The resulting polyHis-tag free protein was then purified from the prescission protease using a second affinity column. The gradient started with the fraction E5 (see figure 6.6 metall affinity II in a). A small part of TnsB did bind to the column which is probably due to an incomplete polyHis-tag removal. The majority however could be found in the flow through fractions E1 to E4. Those were collected and concentrated using Amicon ultra filter devices (30 MWCO). The final purification step was done using a Sephadex 200 size exclusion column. TnsB did eluat in the fractions 10 to 13 (see figure 6.6 b). These eluated fractions also contained high molecular parts which were possibly dimers of TnsB. The samples 15 to 19 contained TnsB as well as lower molecular proteins which might either be remnants of prescission protease or degradations of TnsB. The fractions 10 to 13 were pooled and concentrated using Amicon ultra filter devices. The absorption of the final sample at 280 nm (A 280 = 1.149) was measured and compared to literature (https://expasy.org).

The final concentration of purfied TnsB was 0.96 mg/ ml. This sample was then used to set up crystallization trays. The protein was dialysed against the following buffer conditions: 20 mM Hepes/ NaOH pH 7.5; 10 mM $MgSO_4$; 150 mM $MgCl_2$; 0.5 mM TCEP and 1 % PMSF. For the crystallization assay different concentrations of sodium acetate were used (0 - 2.75 M). 96 well plates with mineral oil were chosen to crystallize the protein. The same conditions were set up the same way, just the protein was not present. This control should help to distinguish

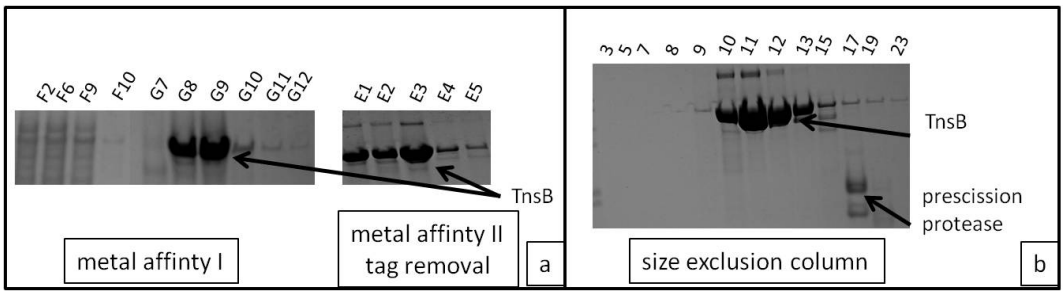

Figure 6.6: **Gradient SDS-PAGE stained with coomassie brilliant blue:** Different fractions of the metal affinity (a) or size exclusion column (b) were diluted with 3- 4 x sparmix prior loading. TnsB can be identified according to its size in comparison to the marker used.

between salt crystals and protein crystals. For all conditions MES, NaOAc and tris were used. The concentration of NaOAc was increased from 0 M to 2.75 M in small steps, however all crystal-like formations that were found were also present in the protein free sample stating that the agglomerations were rather due to salt crystal formation.

A second tray using the hanging drop method was chosen this time using different concentrations of 0.5 M sodium succinate and sodium malonate from 0.025 - 0.2 M in 0.025 M steps. These conditions however also only revealed salt crystals. The buffer that was used for TnsB was slighty changed (20 mM Hepes/ NaOH pH 7.5; 5 mM $MgCl_2$; 0.15 mM TCEP; 0.2 M sodium malonate and 300 mM NaCl). Sodium succinate was added as 0.45 - 0.55 M solution and was raised in 0.02 M steps. The hanging drop method was used and additionally 10 mM $MgSO_4$ was added. The conditions are described in table 6.3. However keeping this setup at 24 °C crystal formation that could be attributed to protein crystallization were not observed. Since neither of the above mentioned setups showed signs of protein crystallisation, malonate present in the protein sample was replaced by 150 mM sodium succinate by dialysis. As a final setup the commercial available crystallisation buffer set HR2-134 using the sitting drop method in mineral oil. Unfortunatly so far no promising results could be achieved.

Table 6.3: Crystallization setup 3 for TnsB using the hanging drop method

Condition 1	**F2**	**E2**	**D2**	**C2**	**B2**	**A2**
NaOAc	2.75 M	2.25 M	1.75 M	1.25 M	0.75 M	0.25 M
Condition 2	**F3**	**E3**	**D3**	**C3**	**B3**	**A3**
NaOAc	2.75 M	2.25 M	1.75 M	1.25 M	0.75 M	0.25 M
$MgSO_4$	10 mM	10 mM	10 mM	10 mM	10 mM	10 mM
Condition 3	**F4**	**E4**	**D4**	**C4**	**B4**	**A4**
$MgSO_4$	80 mM	40 mM	20 mM	10 mM	5 mM	-

Expression of TnsE and binding to β-clamp: As already mentioned, TnsE binds to β-clamp. The precise nature of this binding however is not known so far. The purpose of the expression therefore was, to establish a method to co-crystallize both proteins. When the β-clamp binds to TnsE it is possible that the folding behavior of the latter protein is changed in such a way that parts of the protein which were accessable to e.g. water are now buried deep inside the protein. This might be proven by a different behavior towards protein restriction enzymes such as trypsin or papain and was therefore tested as described below.
First TnsE was expressed as already described below. A permanent culture with the plasmid that encode for TnsE was kindly provided by Prof. Dr. D. Ronning. *E. coli* cells were amplified by growing a 4 L culture at 37 °C supplemented with 0.1 mM ampicillin.
As can be seen in figure 6.7 the original sample (metal affinity I, OS) clearly shows that quite a number of proteins can be found in the soluble fraction of *E. coli*. TnsE cannot easily be dinstinguished in this fraction since the protein was not overexpressed. The sample was pre-purified using a metal affinity column. Eluated fractions revealed two lanes on the SDS-PAGE (E7 to F2). The lane with the higher molecular weight can be attributed to TnsE wherease the protein with the lower molecular weight has an unknown origin. It could either have been an *E.coli* protein which binds unspecifically to the metal affinty column or it was degraded TnsE. The same sample could be found in the flow through as well as in the bound sample of metal affinity II. The non-degraded form of TnsE however still remained in the eluent fraction after increasing the imidazol concentration of the buffer even after the protein was incubated for 12 h with prescission protease. A second incubation with a fresh protease sample did not change this running behavior of this sample. This fact needs to be attributed to the position of the polyHis-tag which was positioned at C-terminus of the protein. It is known that this orientation can sometimes lead to difficulties when the tag shall be removed. Therefore the

fractions J4 and J5 were pooled and concentrated using $(NH_4)_2SO_4$. The protein was collected using centrifugation and was resuspended in size exclusion buffer (see materials and methods for further information). Absorbance measurments at 280 nm were done to estimate the concentration of the sample in accordance with the literature (https://epury.org). A final concentration of 15.2 nmol/ ml, equally to 0.93 mg/ ml was reached. 1 ml of this sample was kept at -80 °C wherease 1 ml was incubated with 165 μl β-clamp (provided by Joe Peters, Cornell University). The buffer which was in accordance to the buffer used for size exclusion column, was used to increase the volume of this sample to 2 ml. To separate free TnsE from β-clamp bound TnsE, a Sephadex size exclusion column was used. Representing samples were loaded on a SDS-PAGE (see figure 6.7 size exclusion for reference). As the PAGE showed, free TnsE did eluate earlier from the column (fractions 37 to 41). TnsE and the β-clamp could be found in the fractions 41 and 42. A mixture of TnsE, β-clamp and possibly the prescission protease was eluated with the fractions 43 to 45. The samples 36 to 41 were collected and referred to as TnsE. The samples 42 to 43 were collected as well and referred to as TnsE+β-clamp. Both samples were concentrated by salting out and were resuspended in 0.4 ml Fanta 4 buffer. These samples were then used for digestion tests using papain and trypsin as well as crystallization setups.

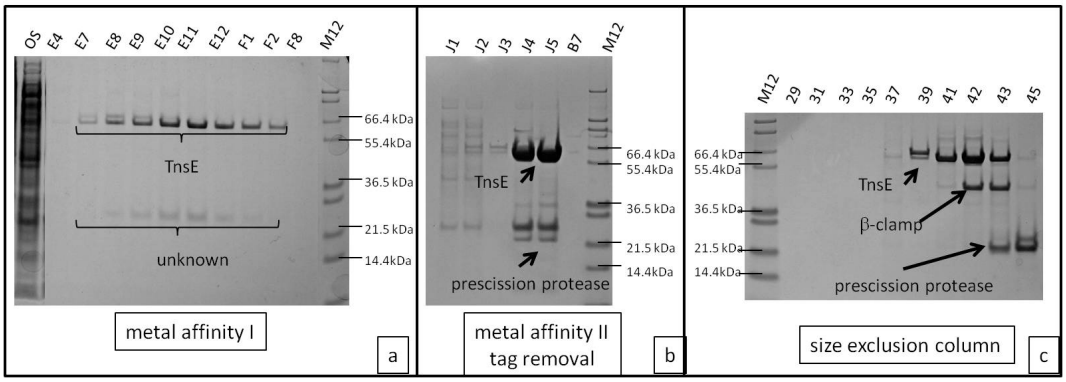

Figure 6.7: **Gradient SDS-PAGE stained with coomassie brilliant blue:** Different fractions of the metal affinity (a and b) or size exclusion column (c) were diluted with 3- 4 x sparmix prior loading. TnsE can be identified according to its size in comparison to the marker used. a: Prepurification od poly-His-tagged TnsE, b: TnsE after incubation with prescission protease and metal affinity column, c: Co-purification of TnsE incubated with β-clamp.

Crystallization setup for TnsE+β-clamp: The protein construct as described above was used to set up crystalization trays in 96 well plates using the mineral oil method. 1 μl of the

protein solution was mixed in one drop of the mineral oil with one drop of each of the buffer solutions provided by Hampton Research (buffer sample HR2-134). The samples were kept at 24 °C and was checked regularly. The best results formed were A1,2,4,7-10,12; B2,6,9,11,12; C1,3,4,8,12;D1,2,4,5-12; E1-7,9,12; F5,12; G3,6,9-12; H3,9,10-12. A list of all conditions of this crystalization setup can be reviewed online (www.hamptonresearch.com). These results were then repeated with just buffer and similar conditions were observed. Therefore it is feasible to state that all crystals formed were salt crystals. An example of such a crystal formed in the presence of TnsE+β-clamp is shown in figure 6.8. The image shows small precipitations on the left downward side and small needle like structures on the top. These formations formed after 24 h and were also found in the sample that did not include either protein. Therefore it is unlikly that protein crystals were formed. With 0.93 mg/ ml the TnsE concentration was possibly to low to result in any protein crystals.

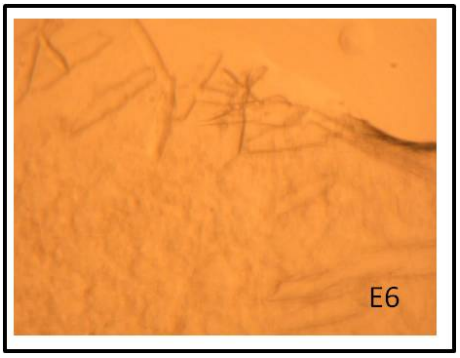

Figure 6.8: **Microscopig images of crystals formed in the presence of TnsE+β-clamp:** Samples were kept in buffer Fanta 4 and buffer E6 (0.05 M calcium chloride dihydrate; 0,1 M bis-tris pH 6.5, 30 % v/v polyethylene glycol monomethyl ether 550, Hampton Research) in 96 well plates and the presence of mineral oil. The trays were kept at 24 °C until crystals formed (24 - 48 h). The magnification was 10 x.

Papain and trypsin digestion of TnsE+β-clamp: When proteins bind their target molecule it is possible that a conformational change occurs. This can lead to a new behavior towards digestion with digestion proteins. Papain is a cystein protease that predominantly cleaves peptide linkage where basic amino acids are present. Trypsin on the other hand cracks protein linkages at the carboxyl side of the amino acids lysine and arginine . This protease is a member of the family of proteases and due to its selectively, digestion is rather restricted. Therefore, the resulting TnsE fragments should be easily identified on a SDS-PAGE. However, when TnsE and β-clamp were incubated with trypsin the majority of the protein did run at the same height as it

did before. Only small amounts were digested even after a total incubation of 40 min at room temperature. Higher concentrations of trypsin did not change this behavior and even when the buffer for this test was changed to lead to a glycerol free buffer, the result stayed the same (data not shown). A final attempt was done by incubating TnsE+β-clamp for 15 min at room temperature, blocking the protease activity by adding PMSF and finally loading the sample on a size exclusion column. Since the protein concentration was fairly low, protein containing samples were precipitated using aceton. The size exclusion step was done three times, a separation however was not possible as shown by SDS-PAGE (see fig. 6.9. All lanes can be either attributed to TnsE, β-clamp or trypsin. Only the final fraction did show some degration ot the protein, however, if this degration is different when β-clamp is not present could not be shown.

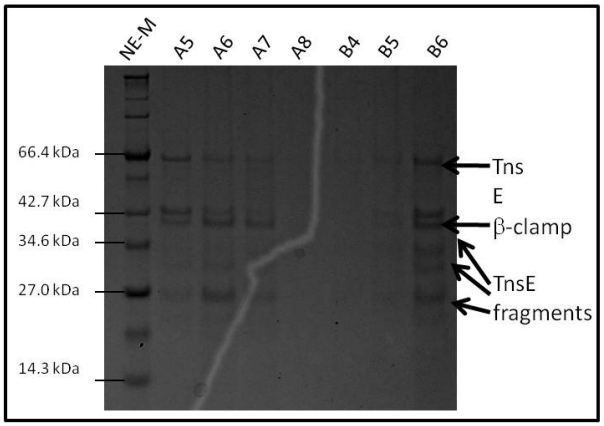

Figure 6.9: **Results of Trypsin digestion for TnsE and β-clamp:** Gradient SDS-PAGE stained with coomassie brilliant blue. TnsE + β-clamp was loaded on a sephadex size exclusion column. Collected fraction were precipitated with aceton and resuspended in water. Lanes were named according to the fraction collected. NE biomarker was added for size reference.

As already mentioned, the ability of trypsin to digest proteins is limited due to its selecitvity. Therefore a more non-selective protease was used; papain. The general technique of trypsin digest was adapted, meaning the a sample of TnsE, TnsE + β-clamp and β-clamp alone were incubated with papain for a certain amount of time (total 5 min). Directly after adding of papain as well as 2 min later, samples were collected. The protease activity was stopped by addition of PMSF. The corresponding protein sample was imediatly frozen in liquid nitrogen. The first tests did not show any promising results (data not shown), but rather some kind of smear in the lower molecular region of the gel. Numerous additional tests were done with the same result. When papain itself was applied to a SDS-PAGE, no distinct line could be seen. Proteases do

show a tendency of self digestion when kept for too long at 4 °C. Therefore the protein sample was obviously too old. When a fresh sample was used, fragments of TnsE were immediately found. A total of five fragments were found in all samples containing TnsE, one running at the same height as β-clamp (see fig.6.10). Three different samples were tested. As a reference TnsE alone (lane 1), TnsE + β-clamp (lane 5) and β-clamp (lane 9) were added to 10 μl PMSF and 6 μl gel loading dye and were immediately after short vortexing frozen using liquid nitrogen. 0.25 μl papain were added to each sample and an aliquot was treated as mentioned above directly after papain was added (see lanes 2, 6, 10). After 2 min and 5 min incubatione time at room temperature, additional aliquots were taken (lanes 3, 7, 11 for 2 min and 4, 8 and 12 for 5 min). NE biomarker was applied to the SDS-PAGE for size reference (NE M).

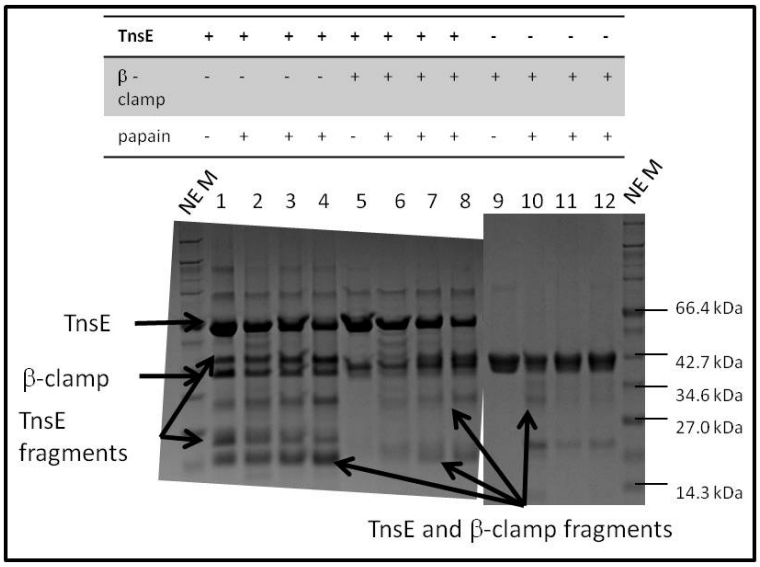

Figure 6.10: Gradient SDS-PAGE stained with coomassie brilliant blue. Samples 1-4 show TnsE, 1 without papain, then papain was added for 0, 2, 5 min. TnsE + β-clamp (lanes 5-8) were treated the same as were samples with β-clamp (lanes 9-12). For each sample, different fractions were found and attributed either to TnsE or β-clamp. It can be noted that even without papain, degradation was obvious.

The β-clamp alone showed two major fragments. When TnsE was co-digested with β-clamp, only two fragments were present wherease the digestion of TnsE lead to six major lanes. In all cases the TnsE band increased in the intensity on the SDS-PAGE, making it feasible to state that papain digested the protein. This might indead prove that TnsE shows a different degradation behavior when β-clamp is bound. All new fragments for TnsE were cut out and sent for amino acid sequencing. However, all these fragments were also found were no papain was present (lane 1). The protein obviously was too old and showed signs of degration. This

was also proven by amino acid sequencing. No new results were revealed by this test. Peters et. al were the first to show that TnsE binds to the β-clamp. [110] They also showed that binding occurs at a specific protein sequence (PQLELERELFL). Since crystalization setups of TnsE+βclamp did not lead to success either, it might be possible that the protein expressed might not have folded correctly. The β-clamp recognition site might not have been accessable and therefore no binding occured. Currently the group of Dr. D. Ronning is using the peptide itself rather the complete TnsE and has succesfully co-crystalized this with the β-clamp. A cell parameter of 3.2 Åwas recieved so far and is under current investigation.

6.6 scFvp53

6.6.1 Introduction

Keeping the genetic information within the human cell intact and working is a complicated process that includes numerous proteins. When the DNA is damaged, the cell integrity is jeapordized. The cell therefore has mechanisms that enable the repair of the corresponding sequence. In this process, the cell should arrest in its current cell cycle to allow time needed for this repair. In addition, if the damage is too big, cells are sacrificed by programmend cell death (apoptosis). Numerous proteins are responsible for the recognition and repair of DNA damage. One protein that has roused very large interest in the last 30 years is the "guardian of the genome" protein p53. [36] This protein can activate a subset of target genes, resulting in either growth arrest, altered DNA repair, altered differentiation or in the worst case, apoptosis. [113] The mechanism when one is preferred over the other is only partially understood and depends on the p53 conformation, localization, activity and stability status (p53 CLASS) as well as the cell type. It was shown that lymphocytes undergo apoptosis whereas fibroblasts and epithelial cells undergo senescence.
The genetic sequence of p53 is known, the protein has three domains that all feature specific responsibilities. The N-terminal domain features phosphorylation sites, a nuclear export signal is proline rich and is responsible for Mdm2 binding. The central domain can bind sequence specific to DNA and features the Blc2 family binding site. Approximatly 90 $\%$ of all mutations of p53 occur at this site. [34] The C-terminal domain features a number of sites that can be functionalized, e.g. by phosphorylation, acetylation or ubiquitylation. It further is responsible for the oligomerization and contains a nuclear export signal as well as a nuclear localization signal. [114] The more of p53 is revealed, the more it is obvious that its role is much more complicated than expected. So far it is known that p53 is active in the cell nucleus by directly binding to its target genes, but also in the cytoplasma and the mitochondria. [114] p53 can directly and indirectly activate genes that are involved in the apoptosis. It thereby influences PUMA, NOXA, members of the Bcl2 family and numerous others. p53 is also active in the mitochondria by releasing directly or indirectly cytochrome C which will also lead to cell death. [36] Post-transcriptional modifications of p53 play an important role of the signal that is then passed on, finally deciding whether a cell shall live or die. p53 thereby features at least 18 phoshporylation sites, and most of them are phosphorylated in response to stress or DNA damage. [113] This ability of phosphorylation on different sites does not only influence the protein itself, changes in the conformation of p53 will influence its association behavior with its regulatory proteins such as p300, Mdm2 or JNK. The phosphorylation pattern can

thereby be completely different to normally functional cells and cells that are under stress or reveal DNA damage. p53 can also be modified by acetylicatin and ubiquitination. The latter one plays an important role in controlling p53. The protein is not activated when it is bound to its most important inhibitor, Mdm2. This protein binds to the N-terminal of p53 that also contains the transcriptional active domain, thereby succesfully blocking gene transcription of the p53 target genes. When DNA damage occurs, Mdm2 releases p53, the protein now has a more stable conformation and the p53 concentration within the cell rises. But Mdm2 also plays a second important role. As a ubiquitin ligase, it has the ability to ubiquitinate p53. This is important for p53 regulation. It has been shown that mono-ubiquitination results in nuclear export of the Mdm2-p53 complex, whereas poly-ubiquitination leads to degradation of p53 by targeting it to the proteasome. p53 proteins found in the mitochondria also carry ubiquitine groups. Detailed pathways of p53 will not be discussed here but are given elsewere. [113, 114, 35, 36, 115]. A small overview of the many responsibilities of p53 is given in figure 6.11.

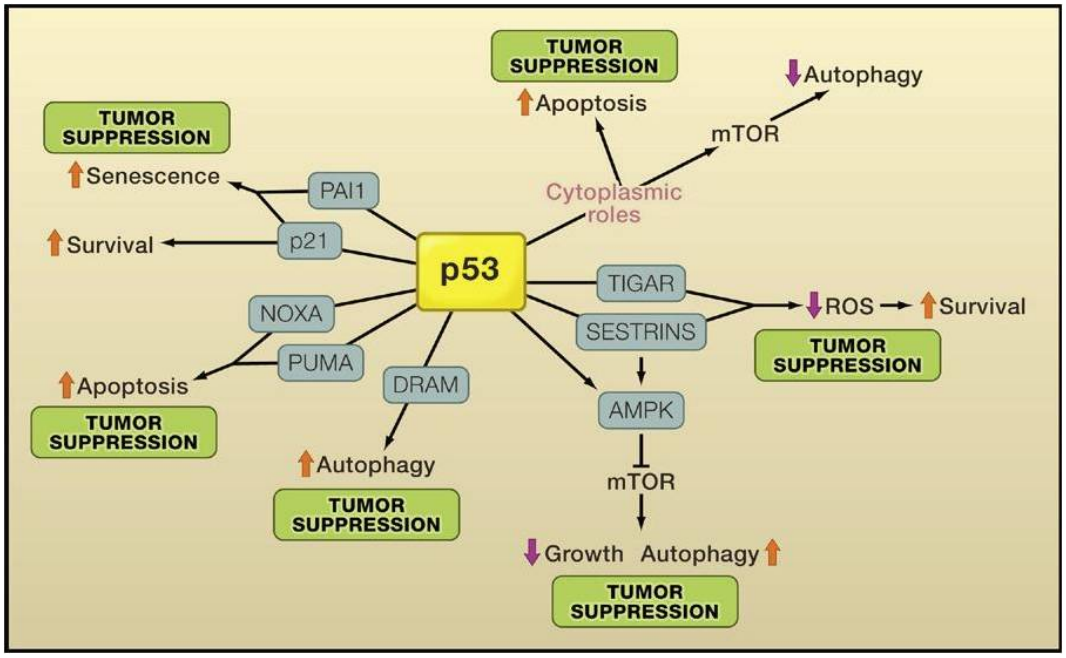

Figure 6.11: **Regulation pathways of p53:** p53 activates and regulated a number of proliferation and death signals within the human cell. It thereby target the corresponding genes within the cell core and features transcriptionally independent cytoplasmic functions. p53 is attributed as a tumor suppressor. [115]

One reason for current high interest in p53 is so high is that in roughly 50 % of all cancer

cell p53 is mutated. As already mentioned, the majority of mutations occur in the region of the central domain. As a result, a conformational change occurs resulting in the exposure of an epitope with the sequence FRHSVV. [34] This epitope can be recognized by antibodies such as PAb240. PAb 421 is an antibody against p53 that has been known for some time now. [116] This single chain antibody fragment (scFv) has proven to be rather helpful in restoring the p53 activity. [37] A monoclonal antibody 11D3 exhibits very comparable properties to that of PAb421 and has also the ability to restore the transcriptional activity of p53 mutants. Based on the sequence of this single chain antibody, a DNA construct was created that encodes the V_L and the V_K region of 11D3, both linked with a linker. Additionally a cut site for the restriction enzymes Nde1 and BamH1 were introduced. Finally a sequence encoding for six histidines was introduced. This was done for purification of the final protein from other *E. coli* proteins but also for the final purification step after binding to nanoparticles. The motivation of this project was to establish a method for easier purification of nanoparticles with and without bound proteins and to fuse the properties of MnO as contrasting agent with the restoring abilities for p53 antibody 11D3. Since the sequence was altered, the antibody construct is abbreviated with scFvp53.

6.6.2 Results and Discussion

When biological active groups shall bind to nanoparticles there is a number of obsticals that need to be overcome. First, it has to be decided whether the linkage shall be covalently or ionical bonding or a weaker chemical bonding such as dipole-dipole interactions or hydrogen bondings. For this thesis a covalent bond was chosen. Secondly, an anchouring group is necessary to link both, the nanoparticles and the bioactive group. The polymer that protects and solubilized the metal core was already designed in such a way that binding is possible via an amide bond between the amine group the polymer and a carboxylic group at the protein which shall bind. A third obstacle is to purify the respective nanoparticles from unbound bioactive groups. As already mentioned in 3, this turned out rather difficult when poly (ethylene glycol) was used as detergent for solubilizing nanoparticles in aqueous solutions. The 11D3 derived antibody against p53 was chosen to be bound to MnO nanoparticles. The construct was designed from the DNA level on and the final protein was designed to allow for specific attributes that are of desired. An single steps for this protein construction are described here. For purification from other *E.coli* proteins as well as after binding to the nanoparticles the DNA sequence that encodes fo scFvp53 was modified to express a final protein with a polyHis-tag and a prescission protease cut site. Finally the amino acid cystein was introduced. The sulfur group can the be used to bind to either Au as described in 4, or to form sulfide bondings between the peptide and the polymer. The resulting DNA sequence was submitted to the company Geneart (Germany) and was designed and delivered ligated in a plasmid provided by the company. This named plasmid however did not feature the lac-operon which allows the activation of protein expression at a dinstinct time and might result in leaky expression which influences the growth of the bacteria. Therefore the sequence for scFvp53 was cut out of the delivered plasmid using restriction enzymes. pET32 was chosen as plasmid for taking up the scFvp53 insert DNA and was therefore also incubated with the restriction enzymes Nde1 and BamH1. After incubating both samples at 37 °C for 1.5 h they were completely loaded on a 1 % agarose gel which is shown in figure 6.12. The pockets of the agarose gel were not big enough to hold the complete sample that was set up for digestion. Therefore the sample was split on two pockets. Therefore two identical patterns could be seen. pET32 was digested in previous work, the region that was cut out was therefore too weak to be seen. The plasmid itself however was visible and due to its size (5900 bp) it did run high on the gel. For scFvp53 two bands were separated. The higher molecular band could be attributed to the plasmid that was provided by the company. The lower one did run at approximately 800 kDa and could be therefore attributed to scFvp53 which was referred to as insert or insert DNA. The insert and pET32 was cut out of the gel and purified using the Quiagen gel extraction kit according to

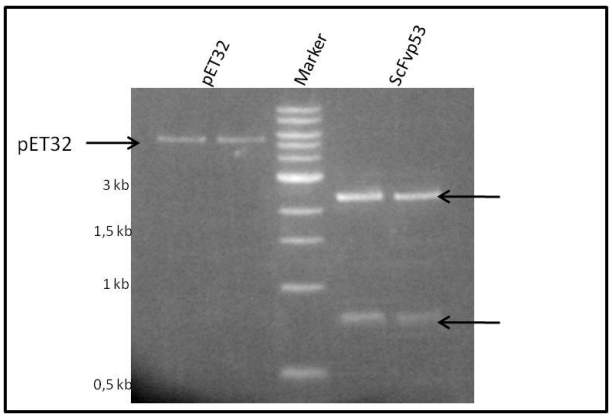

Figure 6.12: **Results of double digest of pscFvp53 and pET32 with Nde1 and BamH1:** Samples were loaded on a 1 % agarosegel and were made visible using SYBR-gel stain. The band at about 800 bp represents the insert scFvp53, the other bands visible belong to the corresponding plasmids.

the supplier. pET32 and insert DNA were then ligated in several attempts and with the help of different ligases. However, in no case did a positive ligation occur. All ligations tested were loaded again on an agarosegel. As can be seen in figure 6.13, nicely separated bands were not found. More than that, a smear could be observed. A band of the size of pET32 was missing completely. It seems like the overall DNA concentration in the sample was too low for a succescfull ligation. Concentrating the insert DNA using a vaccum centrifuge showed no improvment so that it became clear that the DNA concentration needed to be increased. The easiest way to amplify DNA is using polymerase chain reaction (PCR). This method was applied using company plasmid that still featured the insert DNA as well as the insert DNA itself as template. Each template was mixed with dNTP's, polymerase and the corresponding primers and was applied to a thermo-cycler. After the PCR run, both samples were loaded on an agarosegel. Again the pockets were too small to hold one samples completely. Both template samples showed the same pattern with the brightest lane at around 800 kbp (see figure 6.14). It was feasible to attribute this to scFvp53. The low molecular weight lane at around 0.1 kbp was probably formed by so called primer dimers. These can form easily during PCR. The two major additional lanes were side products and were not noticed further. scFvp53 was cut out, purified and digested again to allow ligation with pET32. Four different ligation conditions were chosen, one lead to colonies after 24 h (ligation 4) and a second one lead to colonys after 48 h (ligation 1). All four conditions are shown in table 6.4. The presence of colonies alone already gave a good hint of whether the ligation worked since only colonies could be formed for intact pET32 since only then was the antibiotic restistance is granted al-

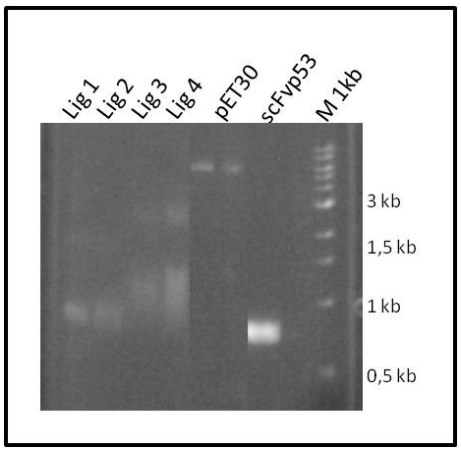

Figure 6.13: **Ligation of pET32 and scFvp53:** 1 % agarosegel of different ligation experiments for pET2 and scFvp53 using different ligases and setups. Staining was done using SYBR-gel stain. The absence of disctinct bands support the suspicion that not enough overall DNA was present.In comparison, pET32 and ScFvp53 were also loaded on this gel.

lowing growth on agar plates supplemented with, in this case, ampicillin. Additionally pET32 was isolated and digested again. As can be seen in figure 6.15 two major lanes did occur for each positive ligation. The higher one represents pET32, the rather light one at roughly 800 bp scFvp53.

Since in both cases the lane was rather weak, both ligated plasmids were sequenced by the company Genterprise (Mainz, Germany). For both samples the result, which is given in the appendix representing ligation 1, was the same clearly indicating that the plasmid DNA was susccesfully inserted and also had the correct orientation.

As a next step, *E. coli* cells were incubated with pET32+scFvp53 and were grown at 37 °C. Protein expression was induced by adding IPTG. The expression temperature was set to 37 °C, 16 °C and 12 °C. The bacteria were collected by centrifugation and were either sonicated or incubated with DNase and lysozyme. An aoliquot of the induced sample, of the pellet fraction and the supernatant fraction after sonication or DNase/ lysozyme treatment were concentrated using SDS-PAGE. However, an overexpression of scFvp53 could not be observed (see figure 6.16 a) neither could a band be attributed for scFvp53 be seen in the soluble fraction. scFvp53 was exprected to run at around 26 kDa. Further studies with this cell type did not follow. pET32+scFvp53 was next transferred to TOP10 cells, an improvment after incubation with IPTG at 37 °C and DNase and lysozyme treatment did not follow (data not shown). Additional studies were done in the group of Prof. Dr. H. Paulsen (Deparment

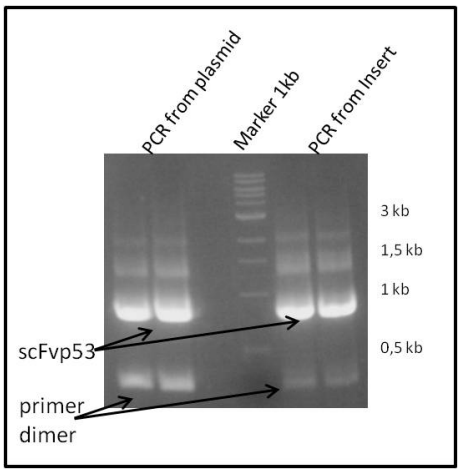

Figure 6.14: **Results of PCR of pscFvp53 and pET32:** Samples were loaded on a 1 % agarosegel and were made visible using SYBR-gel stain. The band at about 800 bp represents the insert scFvp53. In addition side products and primer-dimers were amplified using these conditions.

for Botany, Johannes-Gutenberg Universität, Mainz, Germany). Two strands were tested, one being JM101, a strand that was established in this group and is not commercially availabe anymore. This strand does not recognize every stop codon in the plasmid DNA and the growth is stopped after protein expression is induced. The second one was the strand M15, provided by Qiagen (Germany). This *E. coli* strand additionally features a plasmid that encodes for kanamycin resistance and the inhibitor of the lac operon. Latter one prevents any leaky expression. Additionally the growth is not stopped after protein expression is induced and every stopp-codon within the plasmid is recognized. The protein expression was tested at 37 °C and 18 °C and an aliquot of each strand was taken after 1 h and 3 h. These aliquots were centrifuged and the pellets were resuspended in 3-4 x sparmix and loaded on a 10 % SDS-PAGE (see figure fig:ScFvp53-image5 b and c). However, all *E. coli* strands and all conditions did not lead to an over expression of scFvp53. The *E.coli* proteins were expressed with increasing growth time as was especially be observed for JM101 and M15. All bands that appear on the SDS-PAGE were getting denser with time, clearly showing that more proteins were expressed. However, all proteins did increase in about the same ratio, a favourism of a single protein could not be observed. After testing 4 different cell types and different expression temperatures it became clear that the protein itself could be expressed under the current conditions. It has been shown that some single-chain antibody genes are difficult to express in *E. coli*. The reasons for this might be the toxicity for the host, conformationaly instability proteolytic degradation or other reasons. [34] This obstacle can be overcome by introducing fusion proteins such as

Table 6.4: Different ligation setups for ligating scFvp53 and pET32

Ligation 1	**Ligation 2**
1 μl DNA dilution buffer 5 x	1 μl DNA dilution buffer 5 x
2 μl insert	0.75 μl insert
2 μl pET32	3.75 μl pET32
5 μl T_4 DNA ligation buffer	5 μl T_4 DNA ligation buffer
0.5 μl T_4 ligase	0.5 μl T_4 ligase
5 min room temperature	5 min room temperature
Ligation 3	**Ligation 4**
1 μl DNA dilution buffer 5 x	1 μl DNA dilution buffer 5 x
2 μl insert	0.75 μl insert
2 μl pET32	3.75 μl pET32
5 μl T_4 DNA ligation buffer	5 μl T_4 DNA ligation buffer
0.5 μl T_4 ligase	0.5 μl T_4 ligase
20 min room temperature	20 min room temperature

maltose-binding protein (MBP), thioredoxin or glutahion-S-transferase which are also used to increase the solubility of proteins within the cytosol. [38] In additon the reducing milieu of the cytosol can destabilize the antibody fragments, resulting in very little amounts of functional antibodies. This can be overcome by introducing a sequence that will lead to secretion of the scFv into the periplasm of *E. coli*. [37] For either way, the construct for scFvp53 needs to be changed on the DNA basis. Therefore the corrsponding DNA needs to be isolated and the newly needed DNA sequence can then be introduced using the corresponding primers that encode for the fusion protein or the secretion sequence in a newly PCR. This amplified DNA can then again be isolated, inserted into a plasmid, transferred into bacterial cells and the protein can be expressed using IPTG.

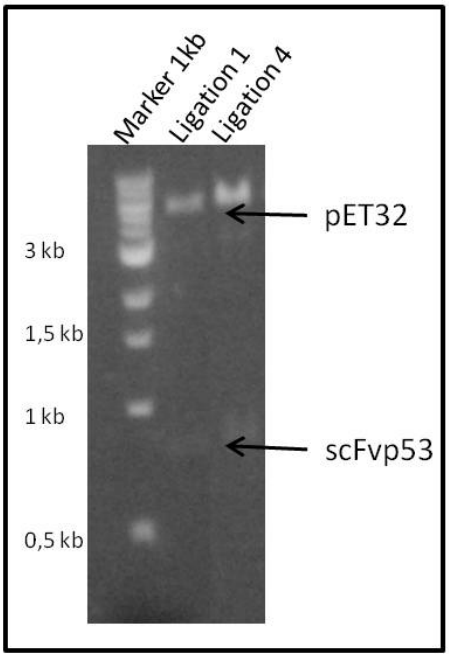

Figure 6.15: **Results for the restriction digest of pET32+scFvp53 construct:** Isolated plasmid from ampicillin resistant XL10 cells were incubated with the restriction digest enzymes Nde1 and BamH1. The insert DNA can be seen as weak band at roughly 800 bp.

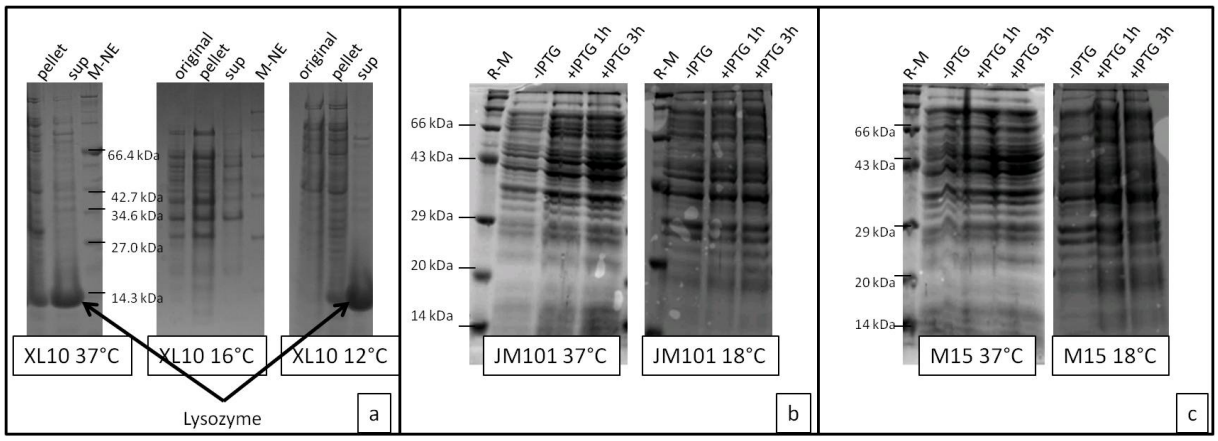

Figure 6.16: **scFvp53 expression at different temperatures:** The original sample, supernatant (sup) and pellet fractions (pellet or Pel) of XL10 competent cells (a) attributed with pET32+scFvp53 were incubated with gel loading dye and were characterized on a gradient SDS-PAGE, stained with coomassie brilliant blue. All original samples were incubated with lysozyme and DNase prior separation via centrifugation and loading. NE biomarker allowed the characterization according to the size of the proteins. Additionally JM101 (b) and M15 (c) cells were tested. Aliquots were taken before (-IPTG) after one (+IPTG 1h) and three hours (+IPTG 3h) after IPTG was added. A distinct band at 26 kDa kDa however was missing.

6.7 Summary and Outlook

Protein crystalization was and still is a time consuming undertaking. The limiting factor, the protein itself, can nowadays be controlled and the protein can be expressed, isolated and purified rather easily once a working expression construct has been made. However, creating such a construct can take as much time as the protein expression itself. Numerous obstacles have to be taken in account. This was especially true for the scFvp53 construct. Although the tripletts that encode for each amino acid of the resulting protein were designed in such a way that rare codons of *E. coli* were excluded, a positive expression was not observed. The expression temperature also plays a significant role. Many protein constructs needed a lower temperature to circumvent degration by the host as was shown for Lsr2 (expression temperature 16 °C) or TnsB (16 °C). In some cases, the temperature can even be lowered further and co-expression of either a fusion protein (Trx-Lsr2) or another protein that forms a protein-protein dimer can help (TnsA + TnsC, expression temperature 12 °C). With decreasing temperature the E. coli metabolism is slowed considerably, the expression time thereby needs to be increased (e.g. Lsr2 up to 42 h). But even if all this is taken into account, protein expression might still not occur or the protein might be degraded. In some cases this can be attributed to the protein itself. This seems to hold true for single chain antibody fragments. But even if the protein is expressed and can be isolated, the crystalization might not occur. This could be due to degration as was seen for TnsB or low concentration (TnsE+β-clamp).
So far, the expression of scFvp53 did not show any promising results, however, literature described the succesful expression in *E. coli*, so that changing the DNA construct should result in soluble protein that can then easily be isolated. For TnsE+β-clamp new insight resulted in a crystal structure of the β-clamp and the β-clamp binding peptide of TnsE.

Appendix

Amino-acid sequence for Lsr2 (H37Rv|Rv3597c):

1-
MSDKIIHLTD DSFDTDVLKA DGAILVDFWA EWCGPCKMIA PILDEIADEY
51-
QGKLTVAKLN IDQNPGTAPK YGIRGIPTLL LFKNGEVAAT KVGALSKGQL
101-
KEFLDANLA G SGSGHM HHHH HH SSG LEVLF QGP AMAKKVT VTLVDDFDGS
151-
GAADETVEFG LDGVTYEIDL STKNATKLRG DLKQWVAAGR RVGGRRRGRS
201-
GSGRGRGAID REQSAAIREW ARRNGHNVST RGRIPADVID AYHAAT

Yellow: aminoacid sequence for thioredoxin, trunkated version (first 19 amino acids missing since not necessary for correct folding)
Red: polyHis-tag and prescission protease cut site, respecitvely
Green: amino acid sequence for Lsr2
Protein size: 12.2kDa
Theoretical pI: 10.08 Extinction coefficient 13980(assuming all Cys residues are reduced): A = 1.149 equals 1 g/ L
Estimated half-life time in *E. coli*: >10 h

Amino acid sequence for TnsB:

1-
MGSSHHHHHH SSGLEVLFQG PHMAWQINEV VLFDNDPYRI LAIEDGQVVW
51-
MQISADKGVP QARAELLLMQ YLDEGRLVRT DDPYVHLDLE EPSVDSVSFQ
101-
KREEDYRKIL PIINSKDRFD PKVRSELVEH VVQEHKVTKA TVYKLLRRYW
151-
QRGQTPNALI PDYKNSGAPG ERRSATGTAK IGRAREYGKG EGTKVTPEIE
201-
RLFRLTIEKH LLNQKGTKTT VAYRRFVDLF AQYFPRIPQE DYPTLRQFRY
251-
FYDREYPKAQ RLKSRVKAGV YKKDVRPLSS TATSQALGPG SRYEIDATIA
301-
DIYLVDHHDR QKIIGRPTLY IVIDVFSRMI TGFYIGFENP SYVVAMQAFV
351-
NACSDKTAIC AQHDIEISSS DWPCVGLPDV LLADRGELMS HQVEALVSSF
401-
NVRVESAPPR RGDAKGIVES TFRTLQAEFK SFAPGIVEGS RIKSHGETDY
451-
RLDASLSVFE FTQIILRTIL FRNNHLVMDK YDRDADFPTD LPSIPVQLWQ
501-
WGMQHRTGSL RAVEQEQLRV ALLPRRKVSI SSFGVNLWGL YYSGSEILRE
551-
GWLQRSTDIA RPQHLEAAYD PVLVDTIYLF PQVGSRVFWR CNLTERSRQF
601-
KGLSFWEVWD IQAQEKHNKA NAKQDELTKR RELEAFIQQT IQKANKLTPS
651-
TTEPKSTRIK QIKTNKKEAV TSERKKRAEH LKPSSSGDEA KVIPFNAVEA
701-
DDQEDYSLPT YVPELFQDPP EKDES

Protein size: 83.3kDa
Theoretical pI: 8.31 Extinction coefficient 102220 (assuming all Cys residues are reduced):

A = 1.227 equals 1/ g L
Estimated half-life time in *E. coli*: >10 h

Amino acid sequence TnsE

1-
MVRLATFNDN VQVVHIGHLF RNSGHKEWRI FVWFNPMQER KWTRFTHLPL
51-
LSRAKVVNST TKQINKADRV IEFEASDLQR AKIIDFPNLS SFASVRNKDG
101-
AQSSFIYEAE TPYSKTRYHI PQLELARSLF LINSYFCRSC LSSTALQQEF
151-
DVQYEVERDH LEIRILPSSS FPKGALEQSA VVQLLVWLFS DQDVMDSYES
201-
IFRHYQQNRE IKNGVESWCF SFDPPPMQGW KLHVKGRSSN EDKDYLVEEI
251-
VGLEINAMLP STTAISHASF QEKEAGDGST QHIAVSTESV VDDEHLQLDD
301-
EETANIDTDT RVIEAEPTWI SFSRPSRIEK SRRARKSSQT ILEKEEATTS
351-
ENSNLVSTDE PHLGGVLAAA DVGGKQDATN YNSIFANRFA AFDELLSILK
401-
TKFACRVLFE ETLVLPKVGR SRLHLCKDGS PRVIKAVGVQ RNGSEFVLLE
451-
VDASDGVKML STKVLSGVDS ETWRNDFEKI RRGVVKSSLN WPNSLFDQLY
501-
GQDGHRGVNH PKGLGELQVS REDMEGWAER VVREQFTH

Protein size: 61.2kDa
Theoretical pI: 5.74 Extinction coefficient 69900 (assuming all Cys residues are reduced): A = 1.142 equals 1 g L
Estimated half-life time in *E. coli*: $>$10 h

DNA-sequence for scFvp53 based on 11D3

1-
AGGAAGGCCCATGAGGCCAGTTAATTAAGAGGTACCATATGCAGGTTA
AACTGCAGGAAA
61-
GTGGCGCAGAACTGGTTCGTAGCGGTGCAAGCGTTAATCTGAGCTGT
ACCGCAAGCGGCT
121-
TTAATATCAAAGATTATTATATGCATTGGGTGAAACAGCGTCCGGA
AGAGGGTCTGGAAT
181-
GGATTGGTTATATTGATCCGGAAAGCGGTGAAACCGAATATGCACC
GAATTTTCAGGGTA
241-
AAGCAACCGTTACCGCAGATACCAGCAGCAATACCGCATATCTGCA
TCTGAGCAGCCTGA
301-
CCAGCGAAGATACCACCGTGTACTACTGCAATGCCGTGATTTATTA
TGAATATGATGGCT
361-
ATGCCCTGGATTATTGGGGTCAGGGCACCACCGTTACCGTTAGCAG
CGGTGGTGGTGGTA
421-
GCGGTGGTGGCGGTTCAGGTGGTGGTGGCAGTGATATTGAACTGAC
CCAGAGCCCGAGCA
481-
GCCTGGCAGTTAGTGCCGGTGAAAAAGTTGCAATGAGCTGTAAAAG
CAGCCAGAGCCTGT
541-
TTAATAGCCGTACCCGTAAAAATTATCTGGCATGGTATCAGCAGAA
ACCGGGTCAGAGCC
601-
CGAAAGTTCTGATTTATTGGGCAAGCACCCGTGAAAGCGGTGTTCC
GGATCGTTTTACCG
661-

GTAGCGGTAGCGGCACCGATTTTACCCTGACCATTAGCAGCGTTCA
GGCAGAAGATCTGG
721-
CAGTTTATTATTGTAAACAGAGCTATAATCTGCCGACCTTTGGTGG
TGGCACCAAACTGG
781-
AAATTAAACATCATCATCATCATCATGGTGGCTGCTAAGGATCCGA
GCTCATGGCGCGCC
841-
TAGGCCTTGACGGCCTTCCT

Amino acid sequence of scFvp53

1-
QVKLQESGAE LVRSGASVNL SCTASGFNIK DYYMHWVKQR PEEGLEWIGY
51-
IDPESGETEY APNFQGKATV TADTSSNTAY LHLSSLTSED TTVYYCNAVI
101-
YYEYDGYALD YWGQGTTVTV SSGGGGSGGG GSGGGGSDIE LTQSPSSLAV
151-
SAGEKVAMSC KSSQSLFNSR TRKNYLAWYQ QKPGQSPKVL IYWASTRESG
201-
VPDRFTGSGS GTDFTLTISS VQAEDLAVYY CKQSYNLPTF

Protein size: 25.8kDa
Theoretical pI: 4.78 Extinction coefficient 54320 (assuming all Cys residues are reduced): A = 2.102 equals 1 g/ L
Estimated half-life time in *E. coli*: 10 h

Plasmid-map of pET32

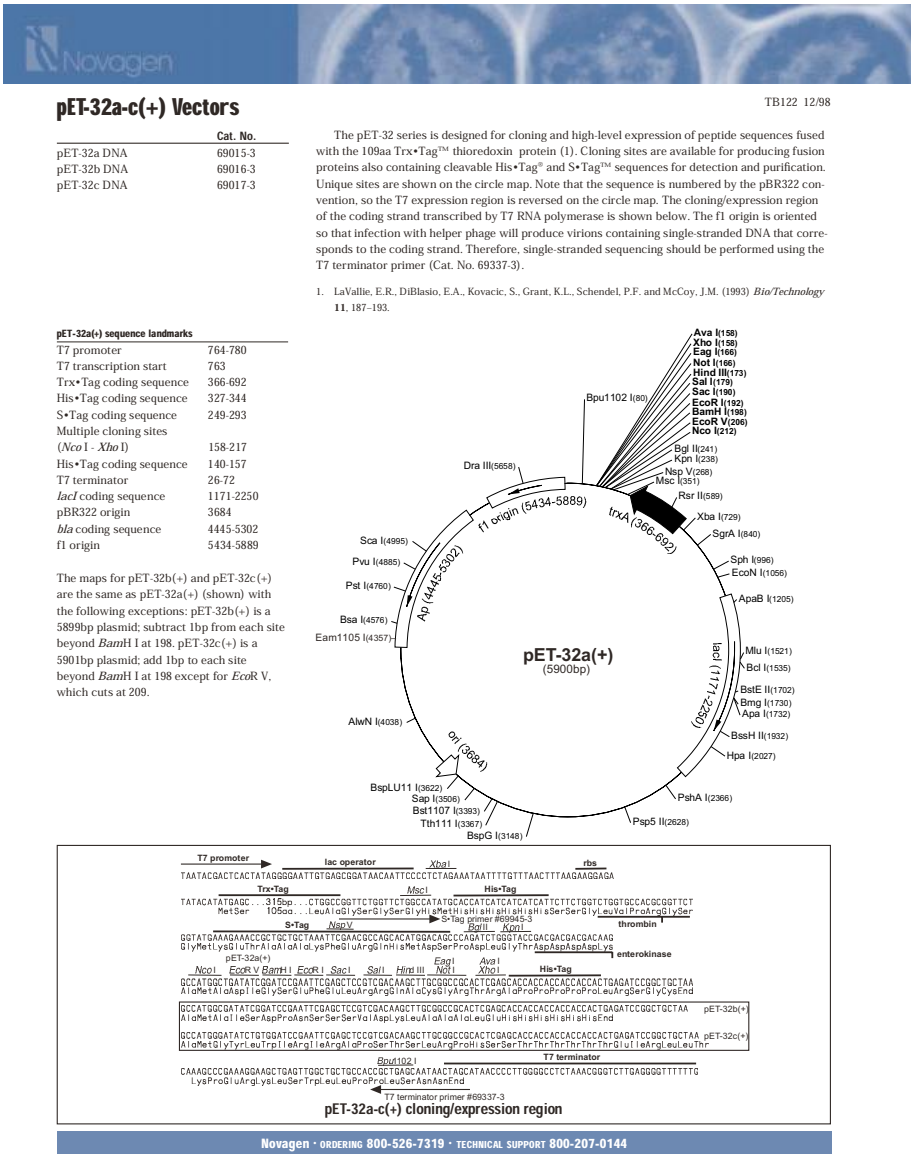

Figure .17: Vector map of pET32 as provided by the supplier (Invitrogen).

pET32 with included scFvp53 as was proofen by DNA sequencing. Vector map characterized with the program SerialCloner 2.1 and was kindly provided by Timo Schüler.

Plasmid-map of pET32

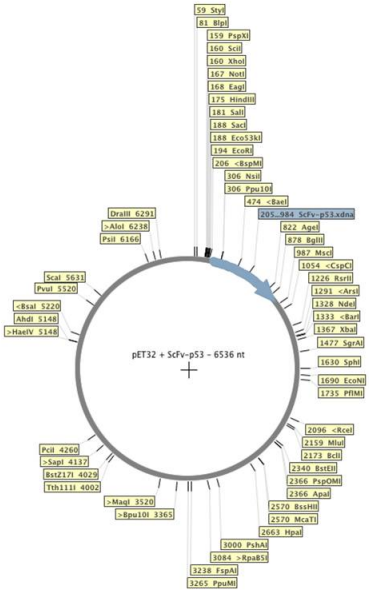

Figure .18: Vector map of pET32+scFvp53 after DNA sequencing. Pictured with the program SerialCloner 2.1 and provided by Timo Schüler.

DNA sequence using T7 forward primer as provided by Geneart, Germany:

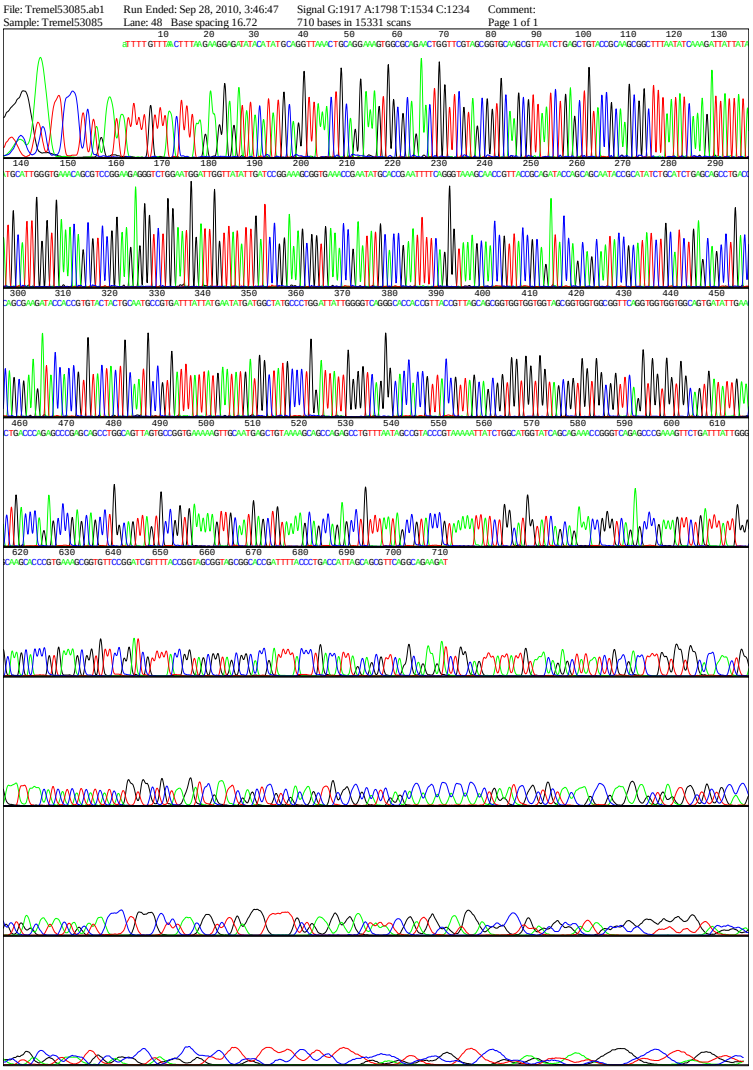

Figure .19: pET32+scFvp53 DNA sequence using the T7 forward primer. Provided by Geneart, Germany

DNA sequence using T7 reversed primer as provided by Geneart, Germany:

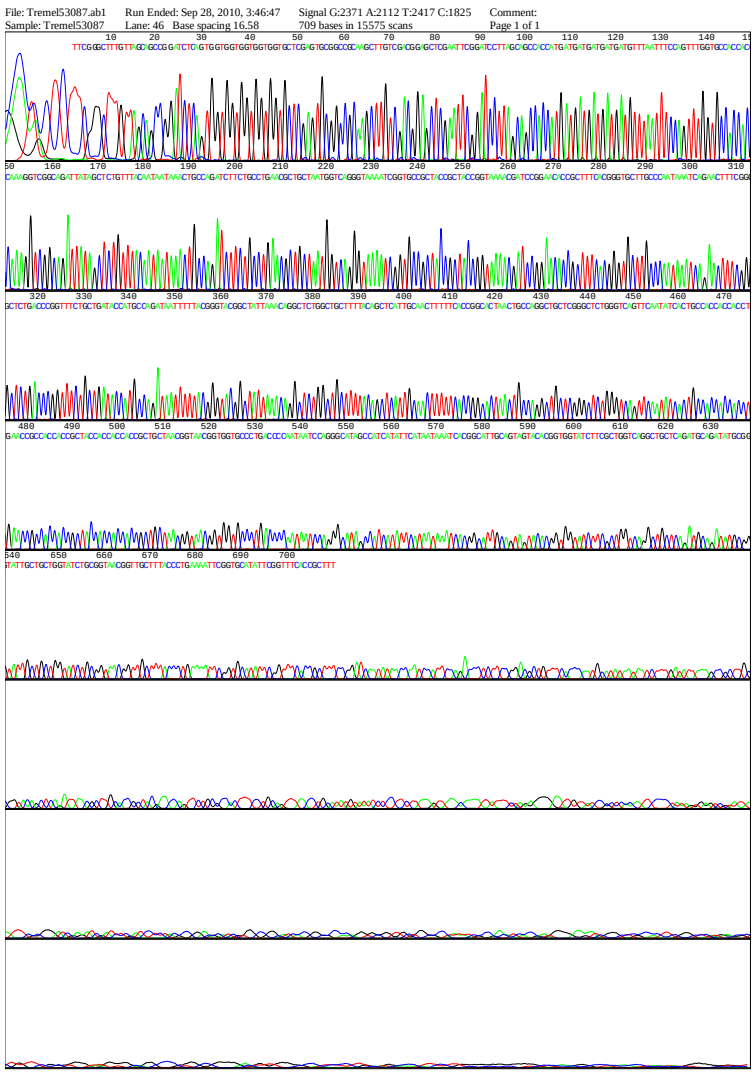

Figure .20: pET32+scFvp53 DNA sequence using the T7 reversed primer. Provided by Geneart, Germany

List of Publications

1. T. D. Schladt, M. I. Shukoor, K. Schneider, M. N. Tahir, F. Natalio, I. Ament, J. Becker, F. D. Jochum, S. Weber, O. Köhler, P. Theato, L. M. Schreiber, C. Sönnichsen, H. C. Schröder, W. E. G. Müller, W. Tremel: "Au@MnO Nanoflowers: Hybrid Nanocomposites for Selective Dual Functionalization and Imaging", *Angewandte Chemie*, **2010**, *122*, 4068-4072; *Angewandte Chemie International Edition*, **2010**, *49*, (23), 3976-3980.

2. T. D. Schladt, K. Schneider, W. Tremel: "Magnetische Nanopartikel als Kontrastmittel in der MRT", *Natur und Geist (Forschungsmagazin der Johannes Gutenberg Universität Mainz)*, **2010**, *26*, 24-27.

3. T. D. Schladt, K. Schneider, M. I. Shukoor, F. Natalio, M. N. Tahir, S. Weber, L. M. Schreiber, H. C. Schröder, W. E. G. Müller, W. Tremel: "Highly Soluble Multifunctional MnO Nanoparticles for Simultaneous Optical and MRI Imaging and Cancer Treatment using Photodynamic Therapy", *Journal of Materials Chemistry*, **2010**, *20*, DOI: 10.1039/c0jm01465f.

4. T. D. Schladt, K. Schneider, H. Schild, W. Tremel: "Engineered Multifunctional Nanotools for Biological and Cancer Applications", *RSC Dalton Transactions*, **2011** DOI: 10.1039/c0dt00689k

5. B. Nakhjavan, M.N. Tahir, F. Natalio, H. Gao, K. Schneider, T Schladt, I. Ament, R. Branscheid, S. Weber, U. Kolb, C. Sónnichsen, L.M. Schreiber and W. Tremel: "Phase separated Cu@Fe3O4 heterodimer nanoparticles from organometallic reactants" *Jouranl of materials chemistry*, **2011**, DOI: 10.1039/c1jm10922g

6. J. Rother, A. Pietuch, T. Schladt, K. Koll, W. Tremel, A. Janshoff: "Enhanced stimulation of Toll-like receptor 9 in alveolar cancer cells using non-toxic multifunctional nanoparticles", *Immunostimulatory Nanocarriers*, textbfsubmitted.

7. F. Natalio, T. D. Schladt, K. Koll, W. Tremel: "MnO Nanoparticles as Superoxide Dismutase (SOD) Biomimetic", *Angewandte Chemie International Edition*, **in preparation**.

8. F. Natalio, K. Koll, T. D. Schladt, S. Weber, J. Brieger, L. M. Schreiber, W. Tremel: "Live Monitoring of the SOD Activity of MnO Nanoparticles in Lymphatic Cells", **in preparation**.

9. T.D. Schladt, K. Schneider, S. Prúfer, H. Bauer, F. Natalio, O. Dumele, R. Raidoo, S. Weber, L.M. Schreiber, M.P. Radsakd, H. Schild and W. Tremel:"Multifunctional Superparamagnetic MnO@SiO_2 Core/Shell Nanoparticles and their Application for Optical and Magnetic Resonance Imaging", **submitted**.

Bibliography

[1] Kunsch, K.; Kunsch, S. *Der Mensch in Zahlen: Eine Datensammlung in Tabellen mit über 20000 Einzelwerten*, 3rd ed.; Spektrum, Akademischer Verl: Heidelberg ; München, 2007.

[2] Murphy, K.; Travers, P.; Walport, M. *Janeway's Immunobiology*, 7th ed.; Garland Science: New York, 2007.

[3] Chatterjee, D. K.; Fong, L. S.; Zhang, Y. *Advanced Drug Delivery Reviews* **2008**, *60*, 1627–1637.

[4] Nie, S.; Xing, Y.; Kim, G. J.; Simons, J. W. *Annual Review of Biomedical Engineering* **2007**, *9*, 257–288.

[5] Duncan, R. *Nature Reviews Cancer* **2006**, *6*, 688–701.

[6] Shubayev, V. I.; Pisanic, T. R.; Jin, S. *Advanced Drug Delivery Reviews* **2009**, *61*, 467–477.

[7] Corr, S. A.; Rakovich, Y. P.; Gun'ko, Y. K. *Nanoscale Research Letters* **2008**, *3*, 87–104.

[8] Liu, Y.; Miyoshi, H.; Nakamura, M. *International Journal of Cancer* **2007**, *120*, 2527–2537.

[9] Simkó, M.; Mattsson, M.-O. *Particle and Fibre Toxicology* **2010**, *7*, 42.

[10] Na, H. B.; Lee, J. H.; Kwangjin,; Park, Y. I.; Park, M.; Lee, S.; Nam, D. H.; Kim, S. T.; Kim, S. H.; Kim, S. W.; Lim, K. H.; Kim, K. S.; Kim, S. O.; Hyeon, T. *Angewandte Chemie International Edition* **2007**, *46*, 5397–5401.

[11] Quarta, A.; Ragusa, A.; Deka, S.; Tortiglione, C.; Tino, A.; Cingolani, R.; Pellegrino, T. *Langmuir* **2009**, *25*, 12614–12622.

[12] Gleeson, O.; Tekoriute, R.; Gun'ko, Y. K.; Connon, S. J. *Chemistry - A European Journal* **2009**, *15*, 5669–5673.

[13] Grancharov, S. G.; Zeng, H.; Sun, S.; Wang, S. X.; O'Brien, S.; Murray, C. B.; Kirtley, J. R.; Held, G. A. *The Journal of Physical Chemistry B* **2005**, *109*, 13030–13035.

[14] Xu, D.; Gu, J.; Wang, W.; Yu, X.; Xi, K.; Jia, X. *Nanotechnology* **2010**, *21*, 375101.

[15] Schladt, T. D.; Schneider, K.; Schild, H.; Tremel, W. *Dalton Transactions* **2011**,

[16] Lu, A.-H.; Salabas, E. L.; Schüth, F. *Angewandte Chemie International Edition* **2007**, *46*, 1222–1244.

[17] Schladt, T. D.; Graf, T.; Tremel, W. *Chemistry of Materials* **2009**, *21*, 3183–3190.

[18] Weishaupt, D.; Köchli, V. D.; Marincek, B. *Wie funktioniert MRI? Eine Einführung in Physik und Funktionsweise der Magnetresonanzbildgebung*, 6th ed.; Springer Berlin Heidelberg: Berlin, Heidelberg, 2009.

[19] Reimer, P.; Vosshenrich, R. *Der Radiologe* **2004**, *44*, 273–283.

[20] Wolf, G. L.; Baum, L. *AJR. American journal of roentgenology* **1983**, *141*, 193–197.

[21] Misselwitz, B.; Mühler, A.; Weinmann, H. J. *Investigative radiology* **1995**, *30*, 611–620.

[22] Shin, J.; Anisur, R. M.; Ko, M. K.; Im, G. H.; Lee, J. H.; Lee, I. S. *Angewandte Chemie International Edition* **2009**, *48*, 321–324.

[23] Gilad, A. A.; Walczak, P.; McMahon, M. T.; Bin Na, H.; Lee, J. H.; An, K.; Hyeon, T.; van Zijl, P. C. M.; Bulte, J. W. M. *Magnetic Resonance in Medicine* **2008**, *60*, 1–7.

[24] Na, H.; Lee, J.; An, K.; Park, Y.; Park, M.; Lee, I.; Nam, D. H.; Kim, S.; Kim, S. H.; Kim, S. W.; Lim, K. H.; Kim, K. S.; Kim, S. O.; Hyeon, T. *Angewandte Chemie* **2007**, *119*, 5341–5341.

[25] Song, H. M.; Kim, Y. J.; Park, J. H. *Journal of Physical Chemistry C* **2008**, *112*, 5397–5404.

[26] Waite, J. H.; Tanzer, M. L. *Science* **1981**, *212*, 1038–1040.

[27] Xu, C. J.; Xu, K. M.; Gu, H. W.; Zhong, X. F.; Guo, Z. H.; Zheng, R. K.; Zhang, X. X.; Xu, B. *Journal of the American Chemical Society* **2004**, *126*, 3392–3393.

[28] Shukoor, M. I.; Natalio, F.; Tahir, M. N.; Ksenofontov, V.; Therese, H. A.; Theato, P.; Schroder, H. C.; Muller, W. E. G.; Tremel, W. *Chemical Communications* **2007**, 4677–4679.

[29] Shukoor, M.; Natalio, F.; Metz, N.; Glube, N.; Tahir, M.; Therese, H.; Ksenofontov, V.; Theato, P.; Langguth, P.; Boissel, J. P.; Schröder, H. C.; Müller, W. E. G.; Tremel, W. *Angewandte Chemie International Edition* **2008**, *47*, 4748–4752.

[30] Shukoor, M. I.; Natalio, F.; Tahir, M. N.; Divekar, M.; Metz, N.; Therese, H. A.; Theato, P.; Ksenofontov, V.; Schröder, H. C.; Müller, W. E. G.; Tremel, W. *Journal of Magnetism and Magnetic Materials* **2008**, *320*, 2339–2344.

[31] Schanen, B. C.; Karakoti, A. S.; Seal, S.; Drake, D. R.; Warren, W. L.; Self, W. T. *ACS Nano* **2009**, *3*, 2523–2532.

[32] Kang, S. J.; Kim, B. M.; Lee, Y. J.; Chung, H. W. *Environmental and Molecular Mutagenesis* **2008**, *49*, 399–405.

[33] Kinsella, T. J.; Colussi, V. C.; Oleinick, N. L.; Sibata, C. H. *Expert Opinion on Pharmacotherapy* **2001**, *2*, 917–927.

[34] Govorko, D.; Cohen, G.; Solomon, B. *Journal of immunological methods* **2001**, *258*, 169–181.

[35] Prives, C.; Hall, P. A. *The Journal of Pathology* **1999**, *187*, 112–126.

[36] Zuckerman, V.; Wolyniec, K.; Sionov, R. V.; Haupt, S.; Haupt, Y. *The Journal of Pathology* **2009**, n/a.

[37] Caron Fromentel, C. d.; Gruel, N.; Venot, C.; Debussche, L.; Conseiller, E.; Dureuil, C.; Teillaud, J. L.; Tocque, B.; Bracco, L. *Oncogene* **1999**, *18*, 551–557.

[38] ORGAD, S.; GOLDFINGER, N.; Cohen, G.; ROTTER, V.; Solomon, B. *FEBS Letters* **2005**,

[39] Petros, R. A.; DeSimone, J. M. *Nature Reviews Drug Discovery* **2010**, *9*, 615–627.

[40] Xie, J.; Lee, S.; Chen, X. *Advanced Drug Delivery Reviews* **2010**, *62*, 1064–1079.

[41] Jun, Y.-w.; Lee, J.-H.; Cheon, J. *Angewandte Chemie International Edition* **2008**, *47*, 5122–5135.

[42] Frullano, L.; Meade, T. *Journal of Biological Inorganic Chemistry* **2007**, *12*, 939–949.

[43] Cheon, J.; Lee, J.-H. *Accounts of Chemical Research* **2008**, *41*, 1630–1640.

[44] Tambalo, S.; Daducci, A.; Fiorini, S.; Boschi, F.; Mariani, M.; Marinone, M.; Sbarbati, A.; Marzola, P. *Magnetic Resonance in Medicine* **2009**, *62*, 1080–1084.

[45] Torchilin, V. P. *Advanced Drug Delivery Reviews* **2006**, *58*, 1532–1555.

[46] Kumar, R.; Ding, H.; Hu, R.; Yong, K.-T.; Roy, I.; Bergey, E. J.; Prasad, P. N. *Chemistry of Materials* **2010**, *22*, 2261–2267.

[47] Yang, H.; Zhuang, Y.; Hu, H.; Du, X.; Zhang, C.; Shi, X.; Wu, H.; Yang, S. *Advanced Functional Materials* **2010**, *20*, 1733–1741.

[48] Otsuka, H.; Nagasaki, Y.; Kataoka, K. *Advanced Drug Delivery Reviews* **2003**, *55*, 403–419.

[49] Tahir, M. N.; Eberhardt, M.; Theato, P.; Faiss, S.; Janshoff, A.; Gorelik, T.; Kolb, U.; Tremel, W. *Angewandte Chemie International Edition* **2006**, *45*, 908–912.

[50] Theato, P. *Journal of Polymer Science Part A: Polymer Chemistry* **2008**, *46*, 6677–6687.

[51] Schladt, T. D.; Schneider, K.; Shukoor, M. I.; Natalio, F.; Bauer, H.; Tahir, M. N.; Weber, S.; Schreiber, L. M.; Schröder, H. C.; Müller, W. E. G.; Tremel, W. *Journal of Materials Chemistry* **2010**, *20*, 8297–8904.

[52] Shukoor, M. I. et al. *Advanced Functional Materials* **2009**, *19*, 3717–3725.

[53] Nie, S.; Xing, Y.; Kim, G. J.; Simons, J. W. *Annual Review of Biomedical Engineering* **2007**, *9*, 257–288.

[54] Sinha, R. *Molecular Cancer Therapeutics* **2006**, *5*, 1909–1917.

[55] Chiron, D.; Jego, G.; Pellat-Deuceunynck, C. *Leukemia Research* **2010**, *34*, 1545–1550.

[56] Kaisho, T. *Biochimica et Biophysica Acta (BBA) - Molecular Cell Research* **2002**, *1589*, 1–13.

[57] Takeda, K.; Kaisho, T.; Akira, S. *Annual Review of Immunology* **2003**, *21*, 335–376.

[58] Hemmi, H.; Akira, S. *Chemical immunology and allergy* **2005**, *86*, 120–135.

[59] Falk, K.; Rötzschke, O.; Stevanović, S.; Jung, G.; Rammensee, H.-G. *Nature* **1991**, *351*, 290–296.

[60] Rötzschke, O.; Falk, K.; Stevanovic, S.; Jung, G.; Walden, P.; Rammensee, H.-G. *European Journal of Immunology* **1991**, *21*, 2891–2894.

[61] Hamdy, S.; Elamanchili, P.; Alshamsan, A.; Molavi, O.; Satou, T.; Samuel, J. *Journal of biomedical materials research. Part A* **2007**, *81*, 652–662.

[62] GRABAREK, Z. *Analytical Biochemistry* **1990**, *185*, 131–135.

[63] Bruce, I. J.; Sen, T. *Langmuir* **2005**, *21*, 7029–7035.

[64] Weng, Y.; Hou, R.; Li, G.; Wang, J.; Huang, N.; Liu, H. *Applied Surface Science* **2008**, *254*, 2712–2719.

[65] Welser, K.; Perera, M. D. A.; Aylott, J. W.; Chan, W. C. *Chemical Communications* **2009**, 6601.

[66] Pease, L.; Tsai, D.-H.; Zangmeister, R.; Zachariah, M.; Tarlov, M. *Journal of Physical Chemistry C* **2007**, *111*, 17155–17157.

[67] Qin, W. J.; Yung, L. Y. L. *Langmuir* **2005**, *21*, 11330–11334.

[68] Kerkmann, M.; Lochmann, D.; Weyermann, J.; Marschner, A.; Poeck, H.; Wagner, M.; Battiany, J.; Zimmer, A.; Endres, S.; Hartmann, G. *Oligonucleotides* **2006**, *16*, 313–322.

[69] Kim, E.-Y. *Nucleic Acids Research* **2006**, *34*, e54.

[70] Fako, V. E.; Furgeson, D. Y. *Advanced Drug Delivery Reviews* **2009**, *61*, 478–486.

[71] Karlsson, H. L.; Cronholm, P.; Gustafsson, J.; Mueller, L. *Chemical Research in Toxicology* **2008**, *21*, 1726–1732.

[72] Schanen, B. C.; Karakoti, A. S.; Seal, S.; Drake III, D. R.; Warren, W. L.; Self, W. T. *ACS Nano* **2009**, *3*, 2523–2532.

[73] Magrez, A.; Horvaith, L.; Samjda, R.; Salicio, V.; Pasquier, N.; Forroi, L.; Schwaller, B. *ACS Nano* **2009**, *3*, 2274–2280.

[74] Jain, T. K.; Reddy, M. K.; Morales, M. A.; Leslie-Pelecky, D. L.; Labhasetwar, V. *Molecular Pharmaceutics* **2008**, *5*, 316–327.

[75] Sárközi, L.; Horváth, E.; Kónya, Z.; Kiricsi, I.; Szalay, B.; Vezér, T.; Papp, A. *Inhalation Toxicology* **2009**, *21*, 83–91.

[76] Oszlánczi, G.; Vezér, T.; Sárközi, L.; Horváth, E.; Kónya, Z.; Papp, A. *Ecotoxicology and Environmental Safety* **2010**, *73*, 2004–2009.

[77] Schmitz, S. *Zellkultur*, 1st ed.; Elsevier Spektrum Akad. Verl.: München, 2007.

[78] Pujalté, I.; Passagne, I.; Brouillaud, B.; Tréguer, M.; Durand, E.; Ohayon-Courtès, C.; L'Azou, B. *Particle and Fibre Toxicology* **2011**, *8*, 10.

[79] Shultz, M. D.; Reveles, J. U.; Khanna, S. N.; Carpenter, E. E. *Journal of the American Chemical Society* **2007**, *129*, 2482–2487.

[80] Choi, J. Y.; Lee, S. H.; Na, H. B.; An, K.; Hyeon, T.; Seo, T. S. *Bioprocess and Biosystems Engineering* **2010**, *33*, 21–30.

[81] Li, F.; Zhou, X.; Zhu, J.; Ma, J.; Huang, X.; Wong, S. T. C. *BMC Biotechnology* **2007**, *7*, 66.

[82] Murphy, C. J.; Gole, A. M.; Stone, J. W.; Sisco, P. N.; Alkilany, A. M.; Goldsmith, E. C.; Baxter, S. C. *Accounts of Chemical Research* **2008**, *41*, 1721–1730.

[83] Shukla, R.; Bansal, V.; Chaudhary, M.; Basu, A.; Bhonde, R. R.; Sastry, M. *Langmuir* **2005**, *21*, 10644–10654.

[84] Chen, Y.-S.; Hung, Y.-C.; Liau, I.; Huang, G. S. *Nanoscale Research Letters* **2009**, *4*, 858–864.

[85] Schaeublin, N. M.; Braydich-Stolle, L. K.; Schrand, A. M.; Miller, J. M.; Hutchison, J.; Schlager, J. J.; Hussain, S. M. *Nanoscale* **2011**, *3*, 410.

[86] Dobrovolskaia, M. A.; Aggarwal, P.; Hall, J. B.; McNeil, S. E. *Molecular Pharmaceutics* **2008**, *5*, 487–495.

[87] Hackenberg, S.; Friehs, G.; Kessler, M.; Froelich, K.; Ginzkey, C.; Koehler, C.; Scherzed, A.; Burghartz, M.; Kleinsasser, N. *Environmental and Molecular Mutagenesis* **2011**, *52*, 264–268.

[88] Choi, J.; Lee, S.; Na, H.; Kwangjin,; Hyeon, T.; Seo, T. *Bioprocess and Biosystems Engineering* **2010**, *33*, 21–30.

[89] Jain, T. K.; Reddy, M. K.; Morales, M. A.; Leslie-Pelecky, D. L.; Labhasetwar, V. *Molecular Pharmaceutics* **2008**, *5*, 316–327.

[90] Lewinski, N.; Colvin, V.; Drezek, R. *Small (Weinheim an der Bergstrasse, Germany)* **2008**, *4*, 26–49.

[91] Xie, J.; Xu, C.; Kohler, N.; Hou, Y.; Sun, S. *Advanced Materials* **2007**, *19*, 3163–3166.

[92] Bertin, A.; Steibel, J.; Michou-Gallani, A.-I.; Gallani, J.-L.; Felder-Flesch, D. *Bioconjugate Chemistry* **2009**, *20*, 760–767.

[93] Issa, M. C. A.; Manela-Azulay, M. *Anais Brasileiros de Dermatologia* **2010**, *85*, 501–511.

[94] KONAN, Y.; GURNY, R.; ALLEMANN, E. *Journal of Photochemistry and Photobiology B: Biology* **2002**, *66*, 89–106.

[95] Couleaud, P.; Morosini, V.; Frochot, C.; Richeter, S.; Raehm, L.; Durand, J.-O. *Nanoscale* **2010**, *2*, 1083.

[96] Roy, I.; Ohulchanskyy, T. Y.; Pudavar, H. E.; Bergey, E. J.; Oseroff, A. R.; Morgan, J.; Dougherty, T. J.; Prasad, P. N. *Journal of the American Chemical Society* **2003**, *125*, 7860–7865.

[97] Wieder, M. E.; Hone, D. C.; Cook, M. J.; Handsley, M. M.; Gavrilovic, J.; Russell, D. A. *Photochemical & Photobiological Sciences* **2006**, *5*, 727.

[98] Wong, D. K.; Lee, B. Y.; Horwitz, M. A.; Gibson, B. W. *Infection and immunity* **1999**, *67*, 327–336.

[99] Laal, S.; Sharma, Y. D.; Prasad, H. K.; Murtaza, A.; Singh, S.; Tangri, S.; Misra, R. S.; Nath, I. *Proceedings of the National Academy of Sciences of the United States of America* **1991**, *88*, 1054–1058.

[100] Colangeli, R.; Helb, D.; Vilchèze, C.; Hazbón, M. H.; Lee, C.-G.; Safi, H.; Sayers, B.; Sardone, I.; Jones, M. B.; Fleischmann, R. D.; Peterson, S. N.; Jacobs, W. R.; Alland, D. *PLoS Pathogens* **2007**, *3*, e87.

[101] Colangeli, R.; Haq, A.; Arcus, V. L.; Summers, E.; Magliozzo, R. S.; McBride, A.; Mitra, A. K.; Radjainia, M.; Khajo, A.; Jacobs, W. R.; Salgame, P.; Alland, D. *Proceedings of the National Academy of Sciences of the United States of America* **2009**, *106*, 4414–4418.

[102] Arora, K.; Whiteford, D. C.; Lau-Bonilla, D.; Davitt, C. M.; Dahl, J. L. *Journal of Bacteriology* **2008**, *190*, 4291–4300.

[103] Gordon, B. R. G.; Imperial, R.; Wang, L.; Navarre, W. W.; Liu, J. *Journal of Bacteriology* **2008**, *190*, 7052–7059.

[104] Gordon, B. R. G.; Li, Y.; Wang, L.; Sintsova, A.; van Bakel, H.; Tian, S.; Navarre, W. W.; Xia, B.; Liu, J. *Proceedings of the National Academy of Sciences of the United States of America* **2010**, *107*, 5154–5159.

[105] Westermeier, R. *Proteomics* **2007**, *7 Suppl 1*, 60–63.

[106] Chen, J. M.; Ren, H.; Shaw, J. E.; Wang, Y. J.; Li, M.; Leung, A. S.; Tran, V.; Berbenetz, N. M.; Kocincova, D.; Yip, C. M.; Reyrat, J.-M.; Liu, J. *Nucleic Acids Research* **2008**, *36*, 2123–2135.

[107] Peters, J. E.; Craig, N. L. *Nature reviews. Molecular cell biology* **2001**, *2*, 806–814.

[108] Barth, P. T.; Datta, N.; Hedges, R. W.; Grinter, N. J. *Journal of bacteriology* **1976**, *125*, 800–810.

[109] Ronning, D. R.; Li, Y.; Perez, Z. N.; Ross, P. D.; Hickman, A. B.; Craig, N. L.; Dyda, F. *The EMBO Journal* **2004**, *23*, 2972–2981.

[110] Parks, A. R.; Li, Z.; Shi, Q.; Owens, R. M.; Jin, M. M.; Peters, J. E. *Cell* **2009**, *138*, 685–695.

[111] Stellwagen, A. E.; Craig, N. L. *Journal of Molecular Biology* **2001**, *305*, 633–642.

[112] Chandler, M. *Cell* **2009**, *138*, 621–623.

[113] Alarcon-Vargas, D.; Ronai, Z. *Carcinogenesis* **2002**, *23*, 541–547.

[114] Yee, K. S. *Carcinogenesis* **2005**, *26*, 1317–1322.

[115] Vousden, K. H.; Prives, C. *Cell* **2009**, *137*, 413–431.

[116] Harlow, E.; Crawford, L. V.; Pim, D. C.; Williamson, N. M. *Journal of virology* **1981**, *39*, 861–869.